

**SJCE**  
SCIENTIFIC  
JOURNAL  
OF CIVIL  
ENGINEERING

 SS CYRIL AND METHODIUS UNIVERSITY  
FACULTY OF CIVIL ENGINEERING

Volume 8  
Issue 2  
December 2019

ISSN - 1857 - 839X

**SJCE** FORM 15  
SCIENTIFIC JOURNAL OF CIVIL ENGINEERING FORM 15  
SEE FORM 15  
SEE FORM 15  
SEE FORM 15  
SEE FORM 15  
SEE FORM 15  
SEE FORM 15  
SEE FORM 15

 SS CYRIL AND METHODIUS UNIVERSITY  
FACULTY OF CIVIL ENGINEERING

### FOUNDER AND PUBLISHER

Faculty of Civil Engineering -  
Skopje Partizanski odredi 24,  
1000 Skopje

### EDITORIAL OFFICE

Faculty of Civil Engineering -  
Skopje Partizanski odredi 24,  
1000 Skopje Rep. of  
Macedonia tel. +389 2 3116  
066; fax. +389 2 3118 834  
email:  
prodekan.nauka@gf.ukim.edu.  
mk

### EDITOR IN CHIEF

Prof. Dr. Sc. **Marijana  
Lazarevska**

University Ss. Cyril and  
Methodius Faculty of Civil  
Engineering -Skopje  
Partizanski odredi 24, 1000  
Skopje Republic of  
MACEDONIA  
email:  
marijana@gf.ukim.edu.mk

**ISSN: 1857-839X**

### EDITORIAL BOARD

Prof. PhD **Darko Moslavac**  
University Ss. Cyril and  
Methodius, Rep. of Macedonia

Prof. Dr. **Ibrahim Gurer**  
Gazi University, Turkey

Prof. Dr **Miodrag Jovanovic**  
University of Belgrade, R  
Serbia

Em.O.Univ.Prof. Dipl.-Ing.  
Dr.h.c.mult. Dr.techn. **Heinz  
Brandl** Vienna University of  
Technology, Austria

Prof. Dr. sc. **Zalika Črepinšek**  
University of Ljubljana,  
Slovenia

Prof. Dr.ir. **J.C. Walraven**  
Delft University of Technology,  
Netherlands

univ.dipl.ing.gradb. **Viktor  
Markelj** University of Maribor,  
Slovenia

PhD, Assoc. Prof. **Jakob Likar**  
University of Ljubljana,  
Slovenia

PhD, PE, CE **Davorin Kolic**  
ITA Croatia

Prof. Dr. Sc. **Stjepan Lakušić**  
University of Zagreb, Croatia

**Marc Morell**  
Institute des Sciences de  
l'Ingénieur de Montpellier,  
France

Prof. PhD **Milos Knezevic**  
University of Montenegro

Prof. PhD **Biljana Scepanovic**  
University of Montenegro

Prof. PhD **Cvetanka Popovska**  
University Ss. Cyril and  
Methodius, Rep. of Macedonia

Prof. PhD **Ljupco Lazarov**  
University Ss. Cyril and  
Methodius, Rep. of Macedonia

Prof. PhD **Milorad Jovanovski**  
University Ss. Cyril and  
Methodius, Rep. of Macedonia

Prof. PhD **Todorka  
Samardzioska** University Ss.  
Cyril and Methodius, Rep. of  
Macedonia

Prof. PhD **Zlatko Srbinoski**  
University Ss. Cyril and  
Methodius, Rep. of Macedonia

Prof. PhD **Elena Dumova  
Jovanoska**  
University Ss. Cyril and  
Methodius, Rep. of Macedonia

### ORDERING INFO

**SJCE** is published  
semiannually. All articles  
published in the journal have  
been reviewed.

Edition: 100 copies

### SUBSCRIPTIONS

Price of a single copy: for  
Macedonia (500 den); for  
abroad (10 EUR + shipping  
cost).

**BANKING DETAILS  
(MACEDONIA)**

Narodna banka na RM

Account number:  
160010421978815

Prihodno konto 723219

Programa 41

**BANKING DETAILS  
(INTERNATIONAL)**

Correspond bank details:  
Deutsche Bundesbank Zentrale

Address: Wilhelm Epstein  
strasse 14 Frankfurt am Main,  
Germany

SWIFT BIC: MARK DE FF

Bank details:

National Bank of the Republic  
of Macedonia

Address: Kompleks banki bb  
1000 Skopje Macedonia

SWIFT BIC: NBRM MK 2X

IBAN: MK 07 1007 0100 0036  
254

Name: Gradezen fakultet  
Skopje

## CONTENTS

---

E. Dumova-Jovanoska, G. Schmid, R. Hoeffler, M. Petronijevic 15 YEARS SEEFORM	5
T. Arangjelovski CRACKING IN FLEXURAL HIGH-STRENGTH CONCRETE ELEMENTS SUBJECTED TO VARIABLE LOAD	11
F. Grajcevci, E. Dumova-Jovanoska VULNERABILITY OF EXISTING MASONRY BUILDINGS, IN FUNCTION OF THEIR HEIGHTS	17
M Sahinagic-Isovic, A. Spago COMPOSITES MATERIALS WITH INDUSTRIAL BY-PRODUCTS	23
S. Churilov, E. Dumova-Jovanoska OVERVIEW OF RESEARCH PROJECTS: PROJECT STREP AND PROJECT MPC	27
S. Coric NUMERICAL PROCEDURE FOR STABILITY CALCULATION IN INELASTIC DOMAIN	33
D. Djuric Mijovic, A. Cilic, D. Kostic LATERAL-TORSIONAL BUCKLING OF ALUMINUM MULLION IN CURTAIN WALL	37
M. Vitanova, K. Edip, V. Hristovski, R. Salic SEISMIC RESPONSE OF ISOLATED BRIDGES INCLUDING SOIL-STRUCTURE INTERACTION (SSI) EFFECTS	43
E. Zlatanovic, V. Sheshov, D. Lukic, Z. Bonic, N. Davidovic SEISMIC DESIGN CODES FOR TUNNELS AND UNDERGROUND STRUCTURES	49
V. Sheshov, M. Vitanova, R. Salic, K. Edip, S. Micajkov, B. Petreski SAFETY ASSESSMENT OF BRIDGE STRUCTURES EXPOSED TO EARTHQUAKE HAZARD	55
K. Todorov, Lj. Lazarov DISPLACEMENT DISTRIBUTION INDEX AS A TOOL FOR IDENTIFICATION OF VERTICAL IRREGULARITY OF STRUCTURES	61

S. Bogoevska, E. Chatzi, E. Dumova-Jovanoska, R. Hoeffler	65
DATA-DRIVEN TOOL FOR STRUCTURAL HEALTH MONITORING OF OPERATING WIND TURBINES	
M. Marjanovic, M. Nefovska-Danilovic, M. Petronijevic	69
DEVELOPMENT OF DYNAMIC STIFFNESS METHOD FOR FREE VIBRATION ANALYSIS OF PLATE STRUCTURES	
N. Markovic, D. Stojic, T. Nestorovic	75
NUMERICAL MODELING OF PIEZOELECTRIC SMART AGGREGATES	
M. Radisic, M. Petronijevic, G. Muller	81
VERTICAL VIBRATIONS OF RECTANGULAR FLEXIBLE FOUNDATION ON VISCOELASTIC HALFSPACE	
M. Jovanoska, T. Samardzioska	87
CLASSROOM ACOUSTICS ASSESSMENT	
K. Milkova, E. Dumova-Jovanoska, F. Vaccari, F. Romanelli, G.F. Panza	91
APPLICATION OF NEO-DETERMINISTIC ANALYSIS FOR NORTH MACEDONIA	
M. Docevska, G. Markovski, P. Mark	95
CREEPING EFFECTS OF CONCRETE UNDER TIME-VARYING STRESS HISTORIES	
M. Partikov, P. Cvetanovski	101
MODEL CALIBRATION OF WELDED SHS-TO-SHS T-JOINTS UNDER MOMENT LOADING	
A. Grupcheva, G. Taseski	107
HYDRAULIC MODEL OF STORMWATER DRAINAGE SYSTEM USING DIFFERENT METHODS FOR DEFINING THE CATCHMENT AREA	



# 15 YEARS SEEFORM



## Elena Dumova-Jovanoska

PhD, Full Professor

University “Ss. Cyril and Methodius”

Faculty of Civil Engineering – Skopje

dumova@gf.ukim.edu.mk

We proudly honor and celebrate 15 years since the **S**outh **E**astern **E**uropean School for Master and PhD **F**ORMation in Engineering – **SEEFORM** was established.

Turbulent times and circumstances have challenged our own determination and dedication, not less the persistence and truthfulness of our advocates and allies. A persistent motivation emerged from our young scholars for whom SEEFORM represented a unique opportunity for high-end research support, international working environment, and perfect settings for building



Figure 1: : On-site SEEFORM Lectures, Skopje, December 2016

SEEFORM had to withstand changes not only in the region, but also in Europe, and today it represents a fully established and matured network that successfully channeled strong collaboration between universities, resulting in fresh and improved concepts. A successive double supervision model for our doctoral students is now granted by the Ruhr University in Bochum (RUB), represented by Prof. Peter Mark from the Institute of Concrete Structures, Prof. Ruediger Hoeffler from the Institute of Wind Engineering and Fluid Dynamics and the RUB Research School, and supported by the University of Ss. Cyril and Methodius, represented by Prof. Goran Markovski from the Chair of Concrete Structures and Prof. Elena Dumova-Jovanoska from the Chair of Theory of Structures and Computational Analysis.



Prof. Peter Mark  
Institute of Concrete Structures

and

Prof. Rüdiger Höffer  
Wind Engineering and Fluid Dynamics

Figure 2: Continuing cooperation  
(Adopted from RUB Research School website)

In retrospect, many individuals, in unique ways, have contributed to the success of SEEFORM. However, without the creative spirit of Prof. Guenter Schmid, the motivated and persistent work of Prof. Ruediger Hoeffler and the unconditional trust of Prof. Mira Petronijevic the cultivation and conservation of this initiative would not have been possible.

What follows next are their reflections on 15 years of SEEFORM ideas, activities and results.



### Guenter Schmid

PhD, Full Professor (retired)  
Ruhr University Bochum, Bochum, Germany  
Faculty of Civil and Environmental Engineering

### OVERVIEW

Ruhr University Bochum had from the early 1970-years a University Partnership with Nish University to which I, as a young professor, was elected as the Rector's representative of my university. At The World conference on Earthquake engineering in San Francisco in 1984 I met colleagues from the Institute for Earthquake Engineering and Engineering Seismology - IZIS at "Ss.Cyril and Methodius" University, Skopje. We agreed to extent the university partnership Bochum-Skopje to include IZIS. Later, shortly before the wars on territory of Former Yugoslavia started, I met at a conference on Earthquake Engineering in Karlsruhe a colleague from Sarajevo, Branko Verbic. He presented in his talk results, performed in IZIS: experiments related to vibrations of block-foundations. These experiments corresponded to my theoretical investigations on Soil-Foundation-Vibration due to soil waves and we decided to cooperate to compare our results.

The wars prevented this plan and also all other cooperation with the Balkan until the restart with SEE-project in the late 1990-years. In the year 2000 the EU started to introduce in Engineering the American or English Degrees Bachelor and Master, instead of the degree Dipl.-Ing. This allowed me to introduce in my faculty the international peer review Master course ComP-Eng (Computational Engineering) and combine it with our SEE program which I called DYNET (Standing for dynamically extending network in the field of Dynamics). We recruited for our international Master Course „Computational Engineering” in Bochum English speaking students worldwide and also students from the universities Belgrade, Skopje, and Sarajevo, to which I had, as mentioned above personal

relations. This allowed me to obtain Scholarships for Comp-Eng students from the SEE-project but only for students from the Balkans, the other students had to pay fees at that time.

After the first Section of DYNET, DAAD proposed to proceed further and in our cooperation. At a meeting in Bonn I proposed to create something like the „Graduate School” and suggested later the name SEEFORM (South East-European Formation of Master- and PhD- Degrees.) It was decided that the headquarter of SEEFORM should be located at the Faculty of Civil Engineering of the Cyril and Methodius University in Skopje; but with close connection to IZIS. The responsible person for SEEFOM was agreed to be Elena Dumova-Jovanoska. The opening ceremony and start of the first lectures were organized on 6<sup>th</sup> December, 2004.

### EXPECTATIONS AND RESULTS

Our ideas for SEEFORM were:

- ✓ To create in the Balkans together with German universities a network of cooperation.
- ✓ To invite speakers from SEE- and German Universities for seminars and workshops.
- ✓ Each PhD candidate would have a German and a local adviser.
- ✓ The M.Sc. and Ph.D. degrees would be recognized in the partner universities, in Germany and the Balkans.
- ✓ Common research projects would be defined (e.g. vibration due high speed train traffic; wind engineering; masonry structures).



Figure 3: Welcome reception on occasion of the opening ceremony of SEEFORM, Skopje, December 2004

Each of these expectations has been realized with higher or lower level of success. SEEFORM outcomes may be seen in many different types of contributions, but most of all I

clearly have to mention the successful results of the former students, who are now active on academic, or other professional, position.

### **PERSONAL EXPECTATIONS AND RESULTS**

My stay in the Balkans was much more exciting than I had ever expected. I found great hospitality and long-lasting friendship. I saw beautiful landscape, climbed mountains in winter and summer, and enjoyed wonderful food and wine. I tried to see all the monasteries in Macedonia and Serbia, but to do that I should have stayed probably for a lifetime.

I tried do learn Macedonian and Serbian language; but for this I should have come much earlier. I liked to see the different regions in the Balkans and I am thankful to DAAD and HRK that I could teach and stay there for so long.

### **ACKNOWLEDGEMENTS:**

SEEFORM to be successful for 15 years could definitely not have been possible without Elena Dumova-Jovanoska, Branko Verbic, Mira Petronijevic, Rüdiger Höffer, Peter Mark, Christoph Butenweg; and many others who are not mentioned here.



Figure 4: Coordination meeting, Bochum, February 2010



### **Ruediger Hoeffler**

PhD, Full Professor

Ruhr University Bochum, Bochum, Germany

Dean of Faculty of Civil and Environmental Engineering

ruediger.hoeffler@rub.de

### **INTRODUCTION**

The DYNET network was established in 2000 as part of a bilateral program for the higher education of students of civil engineering and the integration of doctoral students in a structured, international teaching program. The name DYNET stands for "Dynamic Networking" and originates from an initiative of the Faculty of Civil Engineering at the Ruhr University Bochum.

The South East European Graduate School for Master and PhD Formation (SEEFORM) is a project inside the DYNET network, established in 2004. It is supported by the DAAD (German Academic Exchange Service) and the (former) European Stability Pact for South Eastern Europe. The SEEFORM project offered a structured doctoral program for doctoral students of all participating regional universities, through which qualified doctoral students were supported in their research by advisors in their home universities in South East Europe, as well as by the co-advisors from one of the German universities. Doctoral students also obtain financial support for their research stay in Germany for duration of several months per year. DAAD has recognized the significance of the existence of SEEFORM project and supported it financially since its foundation with the total amount of approximately 1.6 Million Euros. The open network was formed by the civil engineering faculties of seven universities in Germany, coordinated by Ruhr University Bochum, and twelve universities in South Eastern Europe with its regional center at the University St Cyril & Methodius at Skopje. Ultimately, however, the network was and is supported by the personal commitment of many colleagues.

Today and from the very beginning, the network was able to rely on the continuous contribution and cooperation of the Faculty of Civil Engineering at the University St Cyril & Methodius.

### **BACKGROUND**

In the decade of devastating conflicts in the former Yugoslavia, an exodus of the elites from the disintegrating Yugoslavia had to be determined. During and immediately after the wars in the region, many university teachers and scientists also left their universities and institutes. The European public hoped for a rapid improvement in the situation in the countries of the former Yugoslavia. It was easy to see that reforms in university education and the expansion of job opportunities at regional universities could reduce the emigration of the best students and their teachers. To this end, it was regarded as crucial to consolidate academic reconstruction through the targeted promotion of young scientists on the ground and to transfer studies into comparable European structures through integration into the so-called Bologna Process.

The German Academic Exchange Service (DAAD) has been supporting networks since 2000 with special funds from the German Ministry of Education and the Federal Foreign Office within the framework of the Stability Pact for South Eastern Europe and from its own programs. The self-imposed task of the networks was to support the academic reconstruction in the Southeast European region and the promotion of research excellence as well as the integration into the European context through cooperation in research and teaching. More than 10.8 million euros flowed into the entire special program between 2000 and 2003.



Figure 5: Opening Ceremony of SEEFORM, Skopje, December 2004



The particular aim of the program was to rapidly and sustainably improve the quality of teaching at universities and secondary schools in South Eastern Europe, to establish research and teaching networks and to promote highly qualified young scientists in the region. Specialist areas were selected which are considered to be particularly relevant for the reconstruction of the region: Engineering, information technologies, agriculture and forestry, health and social sciences, law and economics.

## DYNET/SEEFORM ACTIVITIES

DYNET/SEEFORM was supported from 2000 to 2016. At the beginning of the funding by the Stability Pact for South-Eastern Europe in 2000, the DAAD supported about 12 students per year from the Balkan region, mostly from the universities at Belgrade, Nis and Skopje, who obtained their master's degree in Computational Engineering at the Faculty of Civil Engineering of the Ruhr University Bochum. The first graduates from the Southeast European countries completed their studies on schedule in 2002 and came back home as doctoral students and assistants or were employed in industry there, thus contributing to the development of the region. Some of the graduates received their doctorates at chairs of the Ruhr-Universität in order to acquire further qualifications in Germany.

In October 2004, again with the generous support of the DAAD, the new international doctoral program "South Eastern European Graduate School for Master and PhD Formation in Engineering" SEEFORM could start its work with selected doctoral students from the entire region.



Figure 6: First SEEFORM lectures, Skopje, December 2004.



Figure 7: Welcoming Ceremony for second generation of doctoral students, Skopje, April 2008

In the first cycle from 2004 to 2007, five scholarship holders from North-Macedonia, three from Bosnia & Herzegovina and two from Serbia took part, and one doctoral student from Kosovo also participated in the program. Further three doctoral students from North-Macedonia were released for doctoral studies by their employer, a major regional construction company. One university professor each from Southeast Europe and Germany supervised one doctoral student. Each doctoral student visited the German supervisor's university during a research stay over several months. To date, more than 25 doctorates have been successfully completed, several of them at German universities. Almost all PhDs have embarked on an academic career, so that a noticeable proportion of the young professors in Skopje, Belgrade, Nis and other regional universities have come into intensive contact with DYNET/SEEFORM and are internationally positioned via our network.

## ACKNOWLEDGEMENTS

The SEEFORM Centre is still and will surely also be in future located at the Faculty of Civil Engineering at the University St Cyril & Methodius at Skopje, the local coordination is in the hands of Professor Elena Dumova-Jovanoska. The described teaching and research activities have only been possible through the targeted, international cooperation of our universities in Germany and the South East European region. However, the long-term support of the German Academic Exchange Service DAAD, of the Johann-Gottfried-Herder Foundation Initiative, of the German Rectors' Conference HRK, of the German Embassies in Skopje and Belgrade, and especially through the commitment of so many university teachers, junior researchers, students, administrators and technicians involved, is the indispensable and vital basis of our work.



**Mira Petronijevic**

PhD, Professor (retired)  
University of Belgrade  
Faculty of Civil Engineering  
pmira@grf.bg.ac.rs

The Faculty of Civil Engineering, University of Belgrade, (FCE) participated actively in the DYNET program from 2004 to 2016. Within the project, in 2005 an international Master Course “Computational Engineering”, concerned with the simulation of advanced engineering problems using the finite element modeling techniques and computer implementation was established. In two generations, 15 students from Serbia and the region were awarded scholarships. Among them, 9 students finished master thesis at FCE (plus 2 of them abroad). Besides the professors from FCE, lecturers from Universities in Aachen, Bochum, Ljubljana, Nish and Okayama participated. According to the new law and Bologna recommendations in 2006 doctoral studies started at the FCE.

SEEFORM provided scholarships and co-mentors to PhD students from the German universities in Bochum, Aachen and Munich. At FCE, six out of eight SEEFORM scholars received doctoral degrees, while 2 of them are in the final stage and are still supported by SEEFORM. During all these years a number of workshops, lecture seminars and summer schools were organized as well. Bearing in mind that during the 1990s the master studies were almost extinguished at FCE, that the faculty was left without teaching assistants, and the scientific work had almost ceased, it is quite clear what great significance the SEEFORM project had for our faculty.

Thanks to the activities within the project, the level of master and doctoral studies at FCE was raised, as well as the level of doctoral dissertations, especially processing of scientific papers and the way of presenting them. The number of papers published in reference journals on the SCI list has increased significantly.

All above mentioned contributed to the formation of young, professional teaching staff, especially in the field of Theory of structures, focused on scientific research and able to collaborate within European projects with other participants. In this way, FCE has become internationally recognized. That is why I must point out that SEEFORM has completely fulfilled its task in the renewal of the Master studies, as well as in establishing of quality doctoral studies in the field of Theory of structures at FCE.



Figure 8: SEEFORM Lectures, Faculty of Civil Engineering, Belgrade, June 2014

AUTHOR

**Toni Arangjelovski**

Associate professor,  
University “Ss. Cyril and Methodius”  
Faculty of Civil Engineering – Skopje  
Partizanski Odredi 24, 1000 Skopje  
arangjelovskitoni@gf.ukim.edu.mk

## **CRACKING IN FLEXURAL HIGH-STRENGTH CONCRETE ELEMENTS SUBJECTED TO VARIABLE LOAD**

In this paper the influence of loading histories, including variable (imposed) actions, on the behavior of high-strength reinforced concrete beams were analyzed especially the crack parameters: crack width and crack distance. For the evaluation of long-term effects (effects due to creep and shrinkage in concrete structures), quasi-permanent combination of actions was used to verify the serviceability reversible limit state. Extensive experimental program was performed in order to define the factor  $\psi_2$  for the evaluation of serviceability reversible limit state for crack control with two specific loading histories. Loading histories are consisted of sustained permanent action G and repeated variable load Q applied in cycles loading and unloading for 24 and 48 hours respectively for the beams series D and E. A total of four reinforced concrete beams, dimensions 15/28/300cm were tested. The beams were made of concrete class C60/75. Experimental results obtained during testing of the beams, from measured maximum crack spacing and crack width, were analyzed by the crack control models given in EN1992-1-1 Eurocode 2 and in the fib Model Code for Concrete Structures 2010.

**Keywords:** high-strength concrete, crack width, crack spacing, variable load,  $\psi_2$  quasi permanent coefficient.

### **1. INTRODUCTION**

Cracks can be usually observed on the concrete surface during service life of concrete structures and causes nonlinear behavior of concrete structures exceeding the tensile strength of concrete. Beside their great influence on serviceability, cracks are also associated to durability, permeability and aesthetics issues.

There are various types of cracks, essentially defined by the principal cause or mechanism, but a few of them can be controlled by the designer. Usually restrained deformations from shrinkage or temperature movements and loading can be treated by the designer [6].

Variable actions such as imposed loads for buildings are those arising from occupancy. Because of nature of variable loads, they have phenomenon of appearance in different time intervals that cannot be predicted and that are acting like random variables during the service life of structure [1]. Repeated variable actions cause significant increase in concrete and reinforcement strain, increase in crack width and deflections, reduction of tension stiffening and increase in bond-slip [8].

The quasi-permanent combination of actions is normally used for long term effects and the appearance of the structure, and usually can be expressed as [11]:

$$\sum_{j \geq 1} G_{k,j} + P + \sum_{i > 1} \psi_{2,i} Q_{k,i} \quad (1)$$

Where:  $G_{k,j}$ -permanent actions;  $P$ -prestressing action;  $Q_{k,i}$ -accompanying variable actions and  $\psi_{2,i}$ -quasi permanent factor depending on the type of action.

## 2. MODELS FOR CALCULATION OF CRACK WIDTH

### 2.1 MODEL OF EUROCODE 2

For the calculation of crack width in reinforced concrete elements following expression may be used [6]:

$$w_k = S_{r,max} (\varepsilon_{sm} - \varepsilon_{cm}) \quad (2)$$

Where:  $S_{r,max}$ -maximum crack spacing;  $\varepsilon_{sm}$ -mean strain in the reinforcement under the relevant combinations of loads, including the effect of imposed deformations and taking into account the effects of tension stiffening and  $\varepsilon_{cm}$ -mean concrete strain between cracks.

The difference of the main strains in the reinforcement and concrete  $\varepsilon_{sm} - \varepsilon_{cm}$  may be calculated from the expression [6]:

$$\varepsilon_{sm} - \varepsilon_{cm} = \frac{\sigma_s - k_t \frac{f_{ct,eff}}{\rho_{p,eff}} (1 + \alpha_e \rho_{p,eff})}{E_s} \geq 0.6 \frac{\sigma_s}{E_s} \quad (3)$$

Where:  $\sigma_s$  -stress in the tension reinforcement assuming a cracked section;  $\alpha_e$  -ratio of  $E_s/E_c$ ;  $\rho_{p,eff}$  - $A_s/A_{c,eff}$  and  $k_t$  -factor dependent on the duration of load ( $k_t = 0.6$  for short term loading and  $k_t = 0.4$  for long term loading).

For the calculation of maximum crack spacing the following expression may be used [6]:

$$S_{r,max} = k_3 c + k_1 k_2 k_4 \phi / \rho_{p,eff} \quad (4)$$

Where:  $\phi$ -bar diameter,  $c$ -cover to the longitudinal reinforcement;  $k_1$ -coefficient which takes account the bond properties of the bonded reinforcement ( $k_1=0.8$  for high bond bars and  $k_1=1.6$  for bars with an effectively plain surface),  $k_2$ -coefficient which takes account of the distribution of strains ( $k_2=0.5$  for bending and  $k_2=1.0$  for pure tension),  $k_3 = 3.4$  and  $k_4 = 0.425$ .

### 2.2 FIB MODEL CODE FOR CONCRETE STRUCTURES 2010

For all stages of cracking, the design crack width  $w_d$  may be calculated as [9]:

$$w_d = 2l_{s,max} (\varepsilon_{sm} - \varepsilon_{cm} - \varepsilon_{cs}) \quad (5)$$

Where:  $l_{s,max}$ -is the length over which slip among concrete and steel occurs;  $\varepsilon_{sm}$ -average steel strain over the length  $l_{s,max}$ ;  $\varepsilon_{cm}$ -average concrete strain over the length  $l_{s,max}$ ; and  $\varepsilon_{cs}$ -strain of concrete due to shrinkage.

For the length  $l_{s,max}$  the following expression applies [9]:

$$l_{s,max} = k \cdot c + \frac{1}{4} \cdot \frac{f_{ctm}}{\tau_{bms}} \cdot \frac{\varphi_s}{\rho_{s,ef}} \quad (6)$$

Where  $k$ -empirical parameter to take the effect of the concrete cover into consideration ( $k=1$ );  $c$ -concrete cover; and  $\tau_{bm}$ -mean bond strength between steel and concrete.

The relative mean strain  $\varepsilon_{sm} - \varepsilon_{cm} - \varepsilon_{sh}$  is [9]:

$$\varepsilon_{sm} - \varepsilon_{cm} - \varepsilon_{cs} = \frac{\sigma_s - \beta \cdot \sigma_{sr}}{E_s} - \eta_r \cdot \varepsilon_{sh} \quad (7)$$

Where:  $\sigma_s$ -steel stress in a crack;  $\sigma_{sr}$ -maximum steel stress in a crack in the crack formation stage, which for pure tension is:

$$\sigma_{sr} = \frac{f_{ctm}}{\rho_{s,ef}} (1 + \alpha_e \rho_{s,ef}) \quad (8)$$

$$\rho_{s,ef} = \frac{A_s}{A_{c,ef}} \quad (9)$$

Where:  $A_{c,ef}$ -effective area of concrete in tension;  $\alpha_e$ -modular ratio  $E_s/E_c$ ;  $\beta$ -an empirical coefficient to assess the mean strain over  $l_{s,max}$



depending on the type of loading;  $\eta_r$ -coefficient for considering the shrinkage contribution; and  $\epsilon_{shr}$ -shrinkage strain.

The value for  $\tau_{bm}$  and coefficients  $\beta$  and  $\eta_r$  are given in fib Model Code 2010 for Concrete Structures [9].

### 3. EXPERIMENTAL PROGRAM

#### 3.1 DESCRIPTION

An experimental program was proposed to analyze long-term behavior of reinforced concrete elements under the action of different types of loading histories. In this paper experimental results from testing of 6 beams were given for the series of beams *D*, *E* and *F*. This part of the experimental program is given in Table 1.

Table 1 Experimental program

	Type of load	Loading cycle
D	Permanent load "G" and variable load "Q"	Loading/unloading for $\Delta t_1=24$ hours.
E	Permanent load "G" and variable load "Q"	Loading/unloading for $\Delta t_2=48$ hours.
F	Shrinkage	/

Series of beams *D* and *E* were consisting of combination of action of long-term permanent load with intensity *G* and repeated variable load *Q* which was applied in cycles of loading/unloading for 24/48 hours respectively for a period of 330 days.

Beams from series *F* were used for measuring free shrinkage of reinforced concrete in same period of 330 days.

Design characteristics of actions are given in Table 2. The self-weight of the beam is uniformly distributed load of 1kN/m.

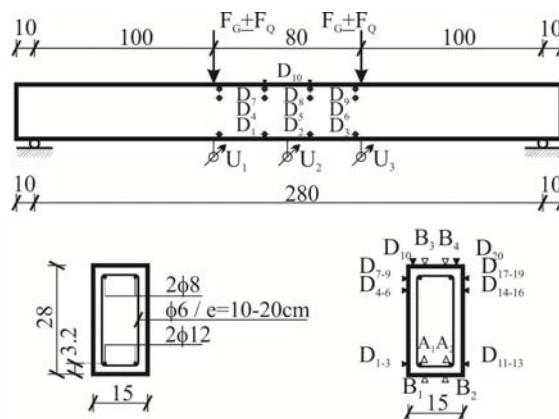
Table 2. Design values of actions

Actions		Intensity [kN]
Permanent action	"G"	2x4
Variable action	"Q"	2x7.6
Service load	"G+Q"	2x11.6

In each series of reinforced concrete beams, the dimensions were width/height/length = 15/28/300cm. Series of beams *D* were divided in *D1* and *D2* made from ordinary concrete class C30/37 and *D3* and *D4* were made of high-strength concrete class C60/75.

This was also applied and for series *E* and *F*.

Details of the beams and test set up for the experiment are provided on Figure 1. All specimens were cast from the same batch of concrete and all specimens were tested at concrete age of 40 days and at concrete age of 370 days.



\*D-mechanical deform-meter, A-strain gauge for reinforcement, B-strain gauge for concrete, U-deflection-meter

Figure 1. Reinforced concrete beams, dimensions, detail of reinforcement and test set up.

The measured compressive strength, tensile splitting strength and elastic modulus of concrete class C60/75 at the age of loading at 40 days were:  $f_{ck}=66.4$ MPa,  $f_{ct,sp}=5.3$ MPa and  $E_{cm}=39470$ MPa. Measured values of concrete properties at age of 370-day for concrete C60/75 were  $f_{ck}=75.5$ MPa,  $f_{ct,sp}=5.3$ MPa and  $E_{cm}=41230$ MPa, total shrinkage (as a sum of autogenous and drying shrinkage)  $\epsilon_c=683 \times 10^{-6}$  and creep coefficient  $\phi_c=0.703$ .

Deformed reinforcement, diameter of 12mm, was used with yield strength of  $f_{0.2}=400$ MPa and modulus of elasticity  $E_{sm}=200200$ MPa.

Throughout the period of 330 days the beams were carefully monitored in the middle of the span to record: deflections *a*, development of cracks, number of cracks,  $l_{smax}$ -maximum crack spacing,  $w_k$ -characteristic crack width and for  $\sigma_s$ -steel stress in a crack.

The tests were performed at the Laboratory of Faculty of Civil Engineering, University "Ss. Cyril and Methodius" in Skopje. The environmental conditions in the laboratory were relative constant value of humidity RH=63% and temperature T=17°C.

More details of the experimental program, mix design and results are given in the doctoral thesis of Arangelovski [1] and in the papers from Arangelovski, Markovski & Mark [2] and [3].

### 3.2 RESULTS FROM MEASURED CRACK PARAMETERS

At the start of the experiment at concrete age of  $t=40$  days, first the beams were loaded by the permanent load  $G$  which does not caused cracks in the section, then the variable load  $Q$  was applied and the load  $G+Q$  causes cracks in the beams. First the crack width  $w_{G+Q}$  ( $t=40$ ) was measured approximately in the middle of the span, and then after unloading at the level of permanent load  $G$  crack width  $w_G$  ( $t=40$ ) was measured.

The values of initial crack width, obtained at loading at age of concrete of  $t=40$  days and final crack width measured at concrete age of  $t=370$  days for series  $D$  are given in Table 3, and for series  $E$  in Table 4.

Table 3. Experimentally measured crack width  $w$  for series "D" beams

Level of actions	Crack width $w$	
	D3- C60/75 [mm]	D4- C60/75 [mm]
$w_G$ ( $t_0=40$ )	0.050	0.040
$w_G$ ( $t=370$ )	0.055	0.045
$w_{G+Q}$ ( $t_0=40$ )	0.100	0.070
$w_{G+Q}$ ( $t=370$ )	0.120	0.080

Table 4. Experimentally measured crack width  $w$  for series "E" beams

Level of actions	Crack width $w$	
	E3- C60/75 mm	E4- C60/75 mm
$w_G$ ( $t_0=40$ )	0.06	0.05
$w_G$ ( $t=370$ )	0.09	0.08
$w_{G+Q}$ ( $t_0=40$ )	0.08	0.07
$w_{G+Q}$ ( $t=370$ )	0.12	0.12

One representative diagram of relation crack width  $w$  versus time  $t$  was given in Figure 2, for the beam D3 made of high-strength concrete C60/75.

The same was done and for the beam E3 made of high-strength concrete C60/75, a typical diagram of relation between crack width  $w$  and time  $t$  is given in Figure 3.

Because of the type of loading histories (repeated loading and unloading) the diagram of the measured crack  $w$  during time  $t$  has a form of an area defined by the limits of permanent load  $G$  and by the sum of the permanent load  $G$  and variable load  $Q$ .

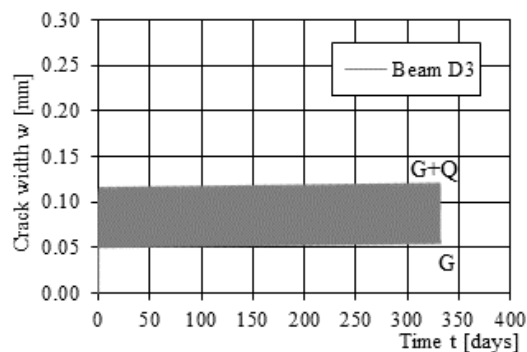


Figure 2. Diagram crack width  $w$  - time  $t$  for beam D3 concrete class C60/75

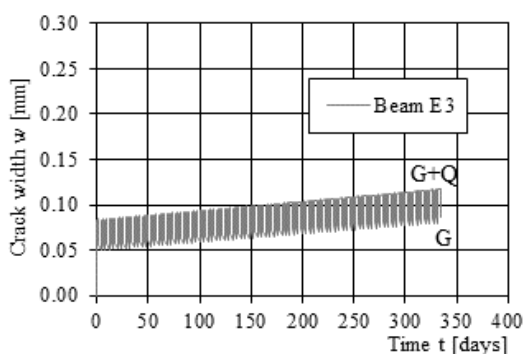


Figure 3. Diagram crack width  $w$  - time  $t$  for beam E3 concrete class C60/75

Experimental results from measuring the  $n$ -number of cracks and  $S_{r,max}$  maximum crack spacing is given in Table 5 and Table 6 for series of beams D and E respectively.

Table 5. Experimentally measured maximum crack spacing  $S_{r,max}$  for series "D" beams

Beams	No. of crack $n$	Maximum crack spacing $S_{r,max}$	
		D3- C60/75 [mm]	D4- C60/75 [mm]
D3	3	194	238
D4	3	182	180
		182	178
Mean value:		186	199

Table 6. Experimentally measured maximum crack spacing  $S_{r,max}$  for series "E" beams

Beams	No. of crack $n$	Maximum crack spacing $S_{r,max}$	
		D3- C60/75 [mm]	D4- C60/75 [mm]
E3	3	202	192
E4	3	200	186
		182	194
Mean value:		195	191

For the purpose of using the model for the calculation of the crack width according to fib Model Code for Concrete Structures 2010, also the free shrinkage was investigated in the experimental program on separate series of beams F made from high-strength concrete class C60/75.

The experimental results for the shrinkage deformation  $\epsilon_{cs}$  during the period of  $t=370$  days are given in Table 7.

Table 7. Experimentally measured shrinkage  $\epsilon_{cs}$  for series "F" beams

Days	Shrinkage $\epsilon_{cs}$	
	F3- C60/75	F4- C60/75
	[10 <sup>-3</sup> ]	[10 <sup>-3</sup> ]
$t_0=40$	0.070	0.080
$t=370$	0.160	0.116

#### 4. ANALYTICAL ANALYSIS

To compare the experimental results with the results obtained from analytical analysis, evaluation of the serviceability limit state was performed using the crack control model of the EN1992-1-1 Eurocode 2 Design of concrete structures – Part 1-1: General rules and rules for buildings 2004 and fib Model Code for Concrete Structures 2010.

In both models, for the serviceability limit states design, combination of actions was used to verify the serviceability reversible limit state including time effects from shrinkage and creep of concrete, using the quasi-permanent combination of action to verify time-dependent final crack width at the level of permanent load G, which is of interest to define the quasi-permanent coefficient  $\psi_2$ .

For the calculation of stresses in the cross section the AAEM method and principle of superposition was used [5].

##### 4.1 ANALYSIS OF RESULTS FOR MAXIMUM CRACK SPACING $S_{r,MAX}$

First, analysis of maximum crack spacing  $S_{r,max}$  was performed to verify the experimental results and analytical results using both crack models. The results of the comparison are given in Table 8.

Using the crack model given in Eurocode 2, calculated maximum crack spacing in the beams made from concrete class C60/75 is similar to the obtained experimental results in range of 5% difference.

Table 8. Experimental and analytical results for maximum crack spacing  $S_{r,max}$

Beams	Maximum crack spacing $S_{r,max}$	
	D3- C60/75	D4- C60/75
	mm	mm
Mean value:	186	199
	E3- C60/75	E4- C60/75
Mean value:	195	191
EN1992-1-1	190	190
fib 2010	207.6	207.6

Using the crack model given in fib Model Code for Concrete Structures 2010 overestimated the results for the beams made from concrete C60/75 in range of 10.4% difference.

##### 4.2 ANALYSIS OF RESULTS FOR MAXIMUM CRACK WIDTH W

Analysis of comparison the experimental results and calculated crack width  $w$  using both models are given in Table 9.

Table 9. Experimental and analytical results for crack width  $w$

Level of actions	Crack width $w$	
	D3- C60/75	D4- C60/75
Experiment	mm	mm
$w_{G+Q}$ ( $t_0=40$ )	0.10	0.07
$w_{G+Q}$ ( $t=370$ )	0.12	0.08
	E3- C60/75	E4- C60/75
$w_{G+Q}$ ( $t_0=40$ )	0.08	0.07
$w_{G+Q}$ ( $t=370$ )	0.12	0.12
EN1992-1-1 EC2		
$w_{G+Q}$ ( $t_0=40$ )	0.11	0.11
$w_{G+Q}$ ( $t=370$ )	0.13	0.13
fib Model Code 2010		
$w_{G+Q}$ ( $t_0=40$ )	/	/
$w_{G+Q}$ ( $t=370$ )	/	/

The crack model given in Eurocode 2, to verify serviceability irreversible limit state, gives proper prediction of the crack width  $w$  for the beams made of concrete C60/75. Calculation of the crack width was performed for the level of load as a sum of permanent load G and variable load Q at the time of loading  $t=40$  days and for  $t=370$  days.

In the analysis using the fib Model Code 2010 crack model the crack width could not be calculated for the beams using concrete class C60/75 because the calculated steel stress in the crack  $\sigma_s$  was lower than  $\sigma_{sr}$ , maximum steel stress at the crack formation stage  $\sigma_s < \sigma_{sr}$ .

One explanation for this problem may be that higher mechanical properties of high-strength concrete enables formation of cracks at the level of combination of actions as a sum of permanent  $G$  and variable load  $Q$ . The service load, flexure moment  $M=12.6\text{kNm}$ , is much too close to cracking moment  $M_{cr}=11.6\text{kNm}$ , which suggest that crack formation stage will last during the whole period of loading.

### 4.3 ANALYSIS OF RESULTS FOR THE QUASI-PERMANENT COEFFICIENT $\psi_2$

For the reversible serviceability limit state, quasi-permanent combination of actions was used to verify the crack width at the level of permanent load  $G$ , which is from prime interest for the designers. Eurocode 2 crack model was used to obtain the same crack width with experimental ones. The results from the analysis are given in the Table 10.

Table 10.  $\psi_2$  factors for series of beams D and E made of high-strength concrete C60/75

No.	G	Q	$\psi_2$	$G+\psi_2Q$	Crack width $w$
	kN	kN		M [kNm]	mm
Beams made from concrete C60/75					
D	4	7.6	0.55	9.2	0.05
E	4	7.6	0.70	10.3	0.08

## 5. CONCLUSIONS

From the experimental and analytical analysis of crack parameters, for beams subjected to permanent load  $G$  and repeated variable load  $Q$  following conclusions can be received:

-Using both crack models, given in the Eurocode 2 and in fib Model Code 2010, give good agreement with experimental results.

-It is very important, especially when we use high-strength concrete for the reinforced concrete elements to ensure that the tensile steel stress in the crack  $\sigma_s$  are greater than maximum steel stress in the crack in the crack formation stage  $\sigma_{sr}$ . This condition was not satisfied using the fib Model Code 2010.

-For the beams made of concrete C60/75, verification of crack width using quasi-permanent combination of actions shows that the quasi-permanent factor is in range of  $\psi_2=0.55-0.70$ . These values are lower than the proposed values in Eurocode 2, which indicates that because of higher mechanical properties we should use higher level of load intensity.

## Acknowledgements

The author would like to express his gratitude and compliments to Ruhr-University of Bochum - Germany, to the DAAD (Deutscher Akademischer Austausch Dienst) - Germany and to SEEFORM Ph.D. School for the scholarship and the financial support during the work on the Ph.D. thesis.

## REFERENCES

- [1] Arangelovski, T. 2011. Time-dependent behavior of reinforced high-strength concrete elements under action of variable loads, *Doctoral dissertation*, Skopje: University "St. Cyril and Methodius" and SEEFORM doctoral studies-DAAD program, English version.
- [2] Arangelovski, T., Markovski, G. & Mark, P. 2012 Influence of repeated variable load on long-term behaviour of concrete elements, *Life-Cycle and Sustainability of Civil Infrastructure Systems, Proceedings of the third international symposium on life-cycle civil engineering Vienna*, pp.1382-1389, London: Taylor&Francis Group.
- [3] Arangelovski, T., Markovski, G. & Mark, P. 2014 Influence of repeated variable load on long-term behaviour of concrete elements, *Journal of Civil Engineering and Architecture* Vol.8, No.3:302-314. New York: David Publishing Company
- [4] Balazs, G.L. et al. 2013. Design for SLS according to fib Model Code 2010, *Structural Concrete Journal of the fib* Vol. 14, No.2:99-123. Berlin: Ernst & Sohn.
- [5] Bazant Z.P. 1972. Prediction of concrete creep effects using age-adjusted effective modulus method, *ACI Journal* 69:212-217. Farmington Hills: ACI.
- [6] Beeby, A.W. & Narayanan, R.S. 1995. *Designers' handbook to Eurocode 2*. London: Thomas Telford.
- [7] Borosnyoi, A. & Balazs, G.L. 2005. Models for flexural cracking in concrete: the state of the art, *Structural Concrete Journal of the fib* Vol.6, No.2:53-62. London: Thomas Telford.
- [8] CEB Bulletin d'information N° 235. 1997. *Serviceability Models-Behaviour and modelling in serviceability limit states including repeated and sustained loads*. G. Balazs (eds). Lausanne.
- [9] Fib, CEB-FIP. 2013. *Fib Model Code for concrete structures 2010*, Berlin: Ernst&Sohn
- [10] Fischer, A., Kramp, M., Prietz, F., & Rosler, M. 2003. *Stahlbeton nach DIN 1045-1*, Berlin: Ernst & Sohn.
- [11] Gulvanessian, H., Calgaro, J.A. & Holicky, M. 2002. *Designers' Guide to EN1990 Eurocode: Basis of structural design*. London: Thomas Telford.

## AUTHORS

### **Florim Grajcevci**

Professor, assistant  
University "Hasan Pristina", in Pristina  
Faculty of Civil Engineering  
florim.grajcevci@uni-pr.edu

### **Elena Dumova-Jovanoska**

PhD, Full Professor  
University "Ss. Cyril and Methodius"  
Faculty of Civil Engineering – Skopje  
dumova@gf.ukim.edu.mk

## **VULNERABILITY OF EXISTING MASONRY BUILDINGS IN FUNCTION OF THEIR HEIGHTS**

Pristina, the Capital of Kosovo, is known by historical monographs as an old town evolving from ancient Ulpiana, built mainly of small dense dwellings. The materials used for construction were mainly stone, wood and clay bricks. Today, Pristina is known as a modern-built city, though there are still blocks of housing and other buildings built in the early 20th century with massive stone wall or clay brick system with lime mortar bricks.

The possibility of earthquakes in our country, more precisely in Pristina, that theoretically, according to available data (from the Kosovo Seismological Report), can be of great intensity. Also, the number of residents in these buildings is not small, so the human loss and economic consequences can be significant. From the above it can be roughly estimated that this existing category of buildings is more vulnerable to possible earthquake shocks, so the need to assess seismic vulnerability for these buildings is necessary.

**Keywords:** Vulnerability, human and economic loss, assessment.

## **1. INTRODUCTION**

The existing methods for assessing the vulnerability of buildings based on result assignments are quite detailed and therefore time consuming. The more sophisticated methods, which imply a more detailed analysis and refined models, take even more time and therefore serve only for the evaluation of individual buildings, perhaps as a further step after a quick examination of the hazardous buildings, possible in a multiphase procedure.

The basic criteria for selecting 15 representative buildings out of a total of 50 stock buildings, which are further analyzed include the consideration of mainly the number of stories, are described in this paper.

In order to provide the best results on the seismic susceptibility of selected buildings, as the seismic movement of the selected entrance are three typical earthquake records:



Ulcinj - Albatros, El-Centro and, Prishtina Synthetic Earthquake Record. To implement a dynamic analysis to increase earthquake intensity, 11 Acceleration of Different Peak Ground Acceleration levels (PGA) from 0.025g to 0.50g have been adopted.

The estimated large number of 990 nonlinear seismic response analysis results for all 15 buildings analyzed are systematically evaluated.

### 1.1 EVALUATION METHODOLOGY FOR EXISTING VULNERABILITY OF MASONRY BUILDINGS

Detailed sophisticated methods for assessing vulnerability include detailed analysis ranging from recording real building conditions, (building inventory, geomechanics investigation, mechanical properties of material, seismic determination hazards or micro zone earthquake maps, etc.) until detailed static or dynamic structural analysis procedures (linear or nonlinear).

For the earthquake scenario project for this paper, the city of Prishtina, Kosovo, was therefore to use an analytical approach with simple building models based on nonlinear dynamic procedures. The method, which is presented in the following, is simple enough to allow the evaluation of a large number of buildings; still, the use of engineering models of the structure allow an understanding of the important parameters.

The key is to determine the vulnerability function (as shown in Figure 1) where it is the relationships which determine the expected damage to a building or a building class as a function of ground motion. The capacity curve of building and seismic demand are key elements to define the vulnerability analysis.

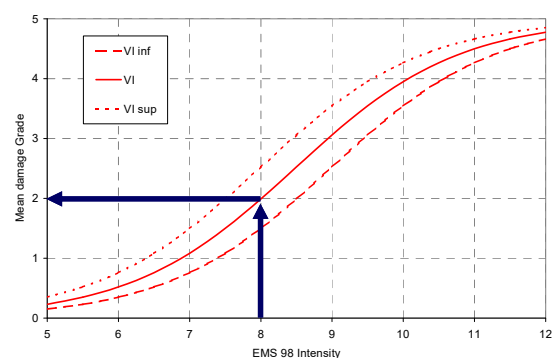


Figure 1. Vulnerability function of the building

In earthquake engineering the capacity of a building to resist seismic action is presented

by a capacity curve which is defined as the base shear  $V_b$  acting on the building as a function of the horizontal displacement at the top of the building  $\Delta$ , also often referred to as a pushover curve. The shear capacity of the building refers to the maximum base shear the building can sustain  $V_{bm}$  and the displacement capacity refers to the ultimate displacement at the top of the building  $\Delta_{bu}$ .

Using a bilinear approximation of the capacity curve of the fictitious example building, the stiffness of the linear elastic part  $k$  corresponds to the sum of the effective stiffnesses of the walls:

$$k = \frac{V_{bm}}{\Delta_{by}} = \sum_j k_{effj} \quad (1)$$

To express the seismic demand, until very recently, the “intensity” was used nearly exclusively. However, information on the real ground movement is lost and empirical relationships between intensity and peak ground acceleration vary a lot. Some methods use the peak ground acceleration as the parameter defining the earthquake. The demand spectrum, respectively the elastic response spectrum ( $S_{ae}$ ) is an extremely useful tool characterizing ground motions demand. It also provides convenient means to summarize the peak responses of all possible linear SDOF or MDOF systems to a particular component of ground motion.

The use of a displacement response spectrum seems therefore more appropriate. Except for very small frequencies ( $f < 0.2\text{Hz}$ ) the following simple formula is used:

$$S_a \approx \omega^2 \cdot S_d \quad (2)$$

$S_a$  and  $S_d$  are the spectral acceleration and the spectral displacement and  $\omega$  is the corresponding circular frequency,  $\omega = 2 \pi f$ .

This vulnerability representative function should describe the overall behavior of the building and hence should be some sort of ‘mean’ of the two vulnerability functions in the two principal directions.

#### 1.1.1 Building structure Identification

In each existing building a distinction must be made between structural and non-structural elements. The mezzanine typologies it has to identify their support direction. The masonry structural system contains the bearing capacity walls and shear walls, and their combination.

Structural elements are those elements of the building that help to support the horizontal and vertical forces acting on a building.

Every wall plane (as it is shown in figure 2) can be considered as a system of coupled walls, the case of interacting cantilever walls being a “limit case” where the stiffness of the spandrels becomes negligible with respect to the stiffness of the walls and hence the coupling effect reduces to zero [1].

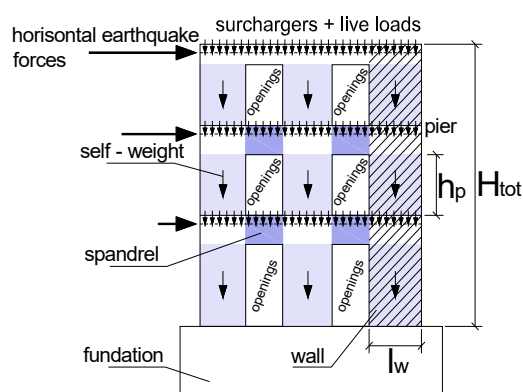


Figure 2. Masonry panel with bearing and shear walls.

## 2. CONCEPT FOR SEISMIC RISK ASSESSMENT BASED VULNERABILITY FUNCTIONS

In many seismically active areas of the world, this type of structure accounts for only a small fraction of the building stock while a large proportion of buildings are older structures made of unreinforced masonry that pose a significant risk during an earthquake.

The integral procedure presently suggested for assessments of the expected vulnerability and seismic risk of the considered region, sub region, city, etc. should involve the following basic steps [3]:

1. identification of the present elements at risk and their distribution;
2. evaluation of the seismic hazard and its distribution;
3. derivation of the appropriate vulnerability functions applicable to the existing elements at risk (classes/level of buildings), describing the interrelation between the specific loss and seismic hazard intensity;
4. evaluation of the specific seismic risk per element at risk and the factor of

participation in the existing volume of properties; and

5. evaluation of the total and/or cumulative seismic risk for the region under consideration.

### 2.1. ANALYSIS OF BUILDING INELASTIC EARTHQUAKE RESPONSE

In general studies, the building response in earthquake is analyzed by applying the dynamic formed inelastic model separately for the longitudinal and transverse direction of the building. The reinstatement of force in building floors the analytical model must be represented by appropriate hysterical relationships. However, the realistic values of the element model parameters are of crucial importance and should be determined based on the available experimental data and the detailed capacity analysis of the respective structural and non-structural components.

To analyze the various aspects of building dynamic behavior under earthquake excitation, in the range of the yielding begin up to the total failure, the intensity of input earthquake ground excitation must be varied in a wide range, starting from very low peak ground accelerations (i.e., PGA = 0.05 g) and then magnifying it in the case of subsequent analysis cases up to defined maximum expected level.

Considering the available statistical data from multiple analyzes of nonlinear earthquake response parameters, which basically relate the respective earthquake input intensity parameters (PGA) and computed structural response parameters (response inter-story drifts ISD), it is possible to obtain the corresponding relationships that represent structural dynamic responses in relation to the increasing intensity of earthquake land excitation in a statistical sense.

### 2.2. DAMAGE CRITERIA OF STRUCTURAL ELEMENTS BASED LOAD BEARING AND DEFORMABILITY CAPACITY

To establish the applicable practical element, the damage criteria which will properly reflect the most important element of the damage characteristics. The following characteristics of phenomenological failure, which characterize its hysterical behavior to the complete collapse of the elements, have been evaluated and considered.

The Figure 3 and 4 shows the range of displacement in force response and specific loss.

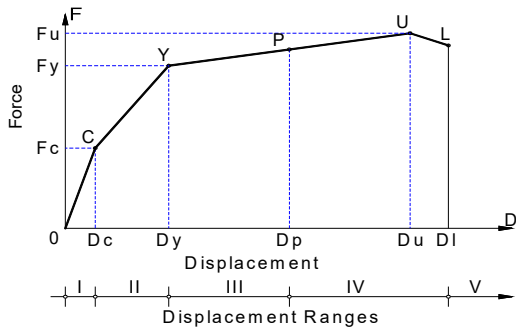


Figure 3. Envelope Curve, Force-Displacement with five ranges.

The specific loss function referring to the five ranges.

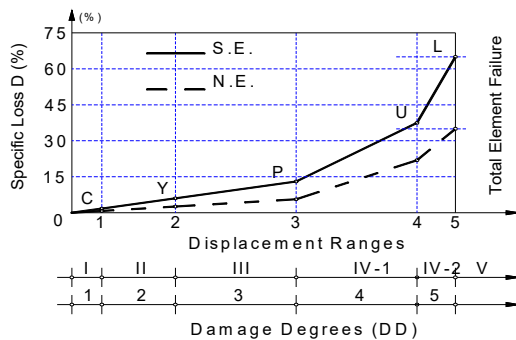


Figure 4. Specific loss functions in Structural and nonstructural elements.

### 3. NONLINEAR ANALYTICAL MODELING FOR DYNAMIC RESPONSE

Often creation of the analytical model for the design of buildings resistant to earthquake seismic impacts considers only stiffness and deformation characteristics of structural elements of the building. This adaptation of the analytical model in many cases does not correspond to reality, where participation of non-structural elements in the overall stiffness and response can be substantial. [5].

All real physical structures, subjected to loads or displacements, behave dynamically. The additional inertia forces, from **Newton's second law**, are equal to the mass times the acceleration. If the loads or displacements are applied very slowly then the inertia forces can be neglected and a static load analysis can be justified [4].

The force equilibrium of a multi-degree-of-freedom lumped mass system as a function of

time can be expressed by the following relationship:

$$[F] + [F]_b + [F]_s = [R] \quad (3)$$

From there, the equation of dynamic equilibrium can be written as:

$$[M]\{\ddot{U}\} + [C]\{\dot{U}\} + [K]\{U\} = -\{M\}\{\ddot{U}_g\} \quad (4)$$

Equation (3) is based on physical laws and is valid for both linear and nonlinear systems, if equilibrium is formulated with respect to the deformed geometry of the structure.

### 4. SELECTED REPRESENTATIVE BUILDINGS

The development of the city, over time, is embryonic, forming the core towards the periphery. Old historic buildings are mainly concentrated in the City Center, including religious cult buildings, museums, public schools, and many residential buildings that are largely of a small footprint and with limited levels [1]. Figure 5 shows the existing typical masonry structure.

In the City Center there are blocks of dwelling areas, mainly built with structural masonry walls. In addition to these blocks, there are insulated buildings built in the same system, with masonry walls. Among the large number of existing buildings in the city, we have listed 55 buildings for analysis. The basic criteria for selecting buildings were the representation of a large number of buildings that can be grouped into a typical structure, the variety of the number of stories.



Figure 5. Residential Buildings, in Pristina



## 5. SEISMIC VULNERABILITY OF ANALYZED MASONRY BUILDINGS

From the calculated results for each building in particular, comparative analysis of results is presented for different cases of building stories. Table 1. shows the analyzed building specification referring to their stories.

Table 1. Number and percentage of analyzed buildings

Number of story	No analyzed buildings	Total no of selected Buildings	Percentage of analyzed Buildings
5	2	16	29.10
4	3	14	25.45
3	7	22	40.00
2	3	4	7.30

### a. Five storey/floor buildings

Displacements of separate structural elements at various levels are different and depend on the overall building stiffness for the respective directions. As building consists of five levels, displacements are not very different along orthogonal directions and are under the Ulcinj-Albatros earthquake impact at the collapse peak, displacements along the transversal direction y is 1.044cm and along the x direction is 1.732cm for PGA = 0.25g. This can be the reason of total building collapse for small PGA differences along orthogonal directions x and y.

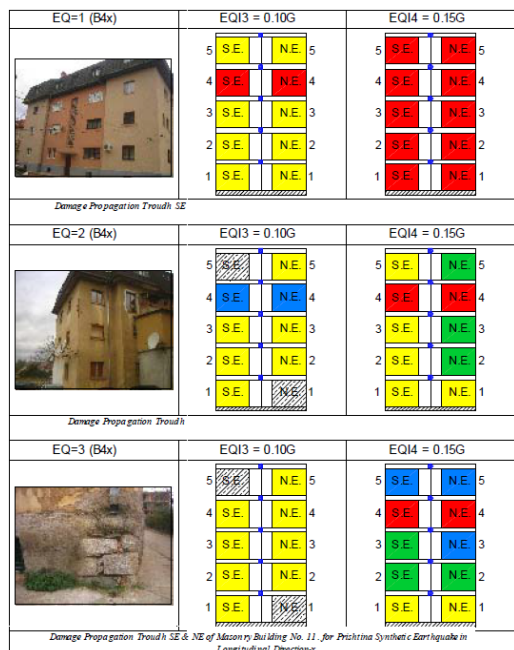


Figure 6. Damage propagation in five storey/floor buildings.

Total loss is 3.45% from the total building cost in the collapse moment in case of Ulcinj

Albatros earthquake acting in referent longitudinal direction-x, meanwhile structural elements take part in this loss with 2.25% and non-structural elements with 3.45%. Collapse takes place for low values of damage propagation. Figure 6 shows the damage propagation for different PGA values.

### b. Fourth story/floor buildings

Maximum building displacements correspond to PGA producing collapse for the corresponding direction. Table 2 shows that values of displacements the building collapse state are not high, having in mind height of buildings.

Table 2. Maximum computed relative displacement for PGA producing collapse.

No Build	Max displace (cm)		PGA (g)	Earth quake	Direct colla
	X	Y			
3	<b>4.149</b>	2.123	<b>0.20</b>	Synt.	X
7	2.073	<b>2.237</b>	<b>0.15</b>	U-A	Y
15	2.493	<b>2.345</b>	<b>0.30</b>	U-A	Y

In the stoke of buildings with four floors the horizontal displacements are bigger than five floor buildings, but collapse is happened for almost the same value of PGA.

### c. Three and two storey/floor buildings

Referring to actual storey capacity diagrams we can group three storey buildings to the ones with higher capacity (buildings No. 14, 4, 12, 9, 8, 2) and building No.10, which has a lower **storey** capacity respective direction, see table 3.

Table 3. Maximum computed relative displacement for PGA producing collapse.

No Build	Max displace (cm)		PGA (g)	Earth quake	Direct colla
	X	Y			
2	<b>2.161</b>	<b>2.082</b>	0.25	U-A	X & Y
4	1.239	<b>3.474</b>	0.20	U-A	Y
8	<b>1.945</b>	1.099	0.25	U-A	X
9	1.201	<b>2.064</b>	0.25	U-A	Y
10	<b>1.732</b>	1.044	0.25	U-A	X
12	<b>3.385</b>	0.825	0.30	U-A	X
14	<b>2.228</b>	0.715	0.15	U-A	X

Even though collapse takes place, the computed values of relative displacements are considerably low. The results prove that collapse takes place in the first and in the second storey, and always under the impact of considered Ulcin Albatros earthquake record.

For the class of two-storey buildings it is also evident that relative displacements in the collapse stage are relatively low.



## COMPOSITES MATERIALS WITH INDUSTRIAL BY-PRODUCTS

### AUTHORS

#### **Asoc.prof.dr. Merima Sahinagic-Isovic**

Dzemal Bijedic University of Mostar  
Faculty of Civil Engineering  
merima.sahinagic@unmo.ba

#### **Asoc.prof.dr. Azra Spago**

Dzemal Bijedic University of Mostar  
Faculty of Civil Engineering  
azra.spago@unmo.ba

Concrete is the most used material in construction industry, and thus major consumer of natural resources through production of cement and aggregate. In recent years, numerous studies have been conducted in order to find replacement for cement and aggregate in concrete. In this paper, locally available industry waste materials are presented, that can be added in concrete, or act as a substitute for cement and/or aggregate. These waste materials are not used further in the industry and are treated as waste and as such deposited in landfills.

**Keywords:** fly ash, silica fume, red mud, slag.

### 1. INTRODUCTION

Today, the demand for alternative materials that can substitute natural raw materials for obtaining cement composites is growing. Production of mortar and concrete, most widely used cement based materials (composites), has reached numerous records in recent years. Use natural raw materials when producing these composites has increased significantly. Negative environmental impact is also evident by the loss of natural resources, but also the pollution of the environment by emissions CO<sub>2</sub> emissions during production. This production is directly responsible for approximately 8 percent of total CO<sub>2</sub> emissions into the atmosphere [1], with cement production dominating.

The cement industry is one of the largest pollutants environment. According to the IMARC Group, the total world cement production in 2010 was approximately 3.3 billion tons, and in 2017, production exceeded the amount of 5 billion tons, an annual increase of approximately 7% [2]. An interesting fact is that, according to some predictions, cement production in such quantities was expected in 2050.

One idea was to use industrial by-products as raw materials for cement production or cement replacement in composites. Mostly it is waste materials that do not apply further in the industry. Justification of industrial applications by-products are found in their chemical composition and particle size [1]. In cement production materials like fly ash, silica dust and limestone are successfully applied. In this

paper some materials suitable for application in cement or composite production will be presented.

## 2. MATERIALS

### 2.1 SILICA FUME

Silica fume (amorphous electro filter  $\text{SiO}_2$  dust) is obtained as a secondary product in the production of ferrosilicate and similar materials. The silica fume is an industrial mineral additive by origin, and according to its characteristics it is a pozzolan. Silica fume added to concrete is expected to improve hydration and produce CSH gel (calcium silicate hydrate). Silica fume is most active pozzolan with the highest pozzolanic activity. It consists mainly of  $\text{SiO}_2$  with frequency ranges from 85 to 97%. The silica fume particle size ranges from 0.01 to 0.3  $\mu\text{m}$  (10–300 nm) (Figure 1). After being added to the concrete, the silica fume is initially inert. Only when the Portland cement and water begin to react, i.e. the beginning of hydration, silica fume is activated. The chemical reaction creates two chemical compounds: calcium silicate hydrate (CSH) and calcium hydroxide (CH), which is still called free lime, serves only as a coating of concrete pores as a filler or drains out of concrete [3]. Pozzolanic reaction is taking place between the CH and silica fume, producing additional CSH in pores around hydrated cement. This process leads to the creation of a much denser mixtures of concrete, at the expense of undesirable voids in the concrete.



Figure 1. Silica fume in solid state (left) and comparison between cement and silica fume particle size (right)

With the proper use of silica fume not only the mechanical properties can be improved, but also the durability of concrete. Numerous studies have been carried out on use of silica fume as an additive for concrete, which confirm the improved properties of the concrete, primarily an increase in compressive strength

and water resistance [4]. Also, small silica fume particles contribute to the fresh concrete behavior by improving the workability and increasing the cohesiveness and filling the inner structure because they are considerably smaller than the cement particles.

The company Timgrad from Jajce, Bosnia and Herzegovina, produces alloys which has as a byproduct microsilica. About 9,000-10,000 tonnes of microsilica are generated annually. Small part of this amount is used further, major rests in the landfills.

### 2.2 FLY ASH

Flying ashes is an industrial mineral additive, and according to the characteristics it belongs to pozzolan because it actively participates in the process of hydration of cement. It is obtained by combusting coal dust in coal-fired power plants and by separating the electrostatic filter equipment from waste gases. The chemical composition and characteristics of flying ash depend on a large number of factors, and hence its ability to use.  $\text{SiO}_2$  is in the range of 20 – 60%, and  $\text{CaO}$  1 – 12%. Actively used in the manufacture of some types of cement and can be used directly in the concrete mixture [5]. Particle size of fly ash is from 0.5  $\mu\text{m}$  to 300  $\mu\text{m}$ . In practice, it is known that fly ash improves the performance and quality of concrete. It has an impact on the improvement of plastic properties of concrete and workability, reduces the amount of water required, reduces segregation and bleeding and affects the reduction of the hydration heat. In addition, it increases the strength of concrete, reduces permeability, reduces corrosion of reinforcing steel, increases resistance, and reduces the alkaline-aggregate reaction [6]. Guidelines for the use of fly ash in construction have been included in the standards and can be found in EN 197-1, EN 450-1 and ASTM 618. It is actively used in the production of certain types of cement and can also be used directly in concrete mixtures.

TPP Kakanj in Bosnia and Herzegovina generates about 600,000 tonnes of fly ash annually from coal consumption, which is about 75% of the total amount of waste material. Kakanj Cement uses as a raw material in cement production about 20-25% of annual production of fly ash or 120,000-150,000 tons. CEM II / B-W 42,5N cement is produced which has 21-35% fly ash. The remaining amount of fly ash is deposited in landfills.



### 2.3 SLAG

There are three types of slag: slag in the production of iron and steel, slag in the production of copper and slag in the production of zinc. The targeted application of slag in the concrete industry is as a partial replacement of aggregates in concrete and as a substitute for cement. In construction industry it can also be used: as an aggregate in road construction, for embankment construction - river banks, as a fill for laying pipelines, as a fill for drainage, etc. [5].

For every ton of raw iron produced, it is produced between 150 and 347 kg of slag. According to 2008 figures, 46.9 million tonnes of slag are produced annually in Europe, 87% of which is reused in construction, which is incredibly high percentage.

The effect of the slag in concrete depends on the percentage of replacement with cement and can go up to 50%. Slag in concrete improves workability and pumpability of concrete, increases strength, reduces hydration heat and permeability, increases durability and has a beneficial effect on sustainability factors. As a substitute for the aggregate, slag can be used up to 50% of total aggregate mass [6].

In the city of Zenica, Bosnia and Herzegovina, company Arcelormittal is producing iron and steel, and as residue slag is generated. In 2011, about 185,000 tonnes were generated, and in the following years about 239,000 tonnes per year of slag. Most of this is deposited in landfill, and only a small amount is used further in the industry.

### 2.4 RED MUD

Red mud is a byproduct of industrial aluminum production. Aluminum is commercially produced from bauxite in two steps. In the first stage, aluminum is obtained by Bayer's procedure, and in the second stage, aluminum is electrolysed to obtain metal for use. In this process, insoluble residue is created. That residue is known as red mud. It is estimated that at 1 t of produced aluminum, it creates 0.3 to 1.7 t of red mud [7]. Red mud consists mainly of iron oxide, quartz, sodium aluminosilicate, calcium carbonate, titanium dioxide and sodium hydroxide. Iron oxide is giving it recognizable red color (Figure 2). It has an average pH value of 10 to 12.5 and a particle size of less than 10  $\mu\text{m}$ . Red mud can not be fully considered artificial pozzolana, because it does not meet all the requirements. However, its pozzolanic activity index is good. Main oxide in the

chemical composition of the red mud is  $\text{Fe}_2\text{O}_3$  12 – 56%, followed by  $\text{Al}_2\text{O}_3$  6 – 12% and  $\text{SiO}_2$  6 – 20% [6].



Figure 2. Dried red mud

The addition of red mud to concrete refers primarily to the partial substitution of this waste material with cement. Numerous studies have been done in this area and the general conclusion is that red mud can be used for these purposes, but only for non-load bearing concrete elements. A small percentage of cement substitution with red mud (up to 10%) even shows a certain increase in the compressive strength of concrete. However, with a percentage increase in the content of red mud in the mix, the physical and mechanical properties decline.

There are currently two red mud landfills in Bosnia and Herzegovina, in the village of Birač near Zvornik and near Mostar in Dobro Selo. It is estimated that about 10 million tonnes of red mud have been deposited in Dobro Selo.

Since 2017, an extensive exploration of the possibility of using red mud as a substitute for cement in mortar and concrete has begun at the Faculty of Civil Engineering of the "Džemal Bijedić" University in Mostar. Preliminary data have shown that it is possible to use this red mud in mortar and concrete mixtures. The results of physical and mechanical properties of mortars are satisfying for low percentage of red mud (10 and 15%). Testing of concrete is currently being implemented (Figure 3 and 4).



Figure 3. Mixture of mortar with high percentage of red mud (20%)



Figure 4. Mixture of concrete with high percentage of red mud (20%)

## REFERENCES

- [1] Mehta, P.K., Monteiro, P.J.(2006) Concrete: Microstructure, Properties, and Materials, Third edition, McGraw-Hill, New York.
- [2] IMARC Group Report: Cement Market: Global Industry Trends, Share, Size, Growth, Opportunity and Forecast 2018-2023
- [3] Jain A., Pawade P. Y. (2015), "Characteristics of Silica Fume Concrete". International Conference on Quality Up-gradation in Engineering, Science and Technology (ICQUEST2015). Maharashtra. India. pp. 22 – 26.
- [4] King D. (2012). "The effect of silica fume on the properties of concrete as defined in concrete society report 74", Cementitious materials. 37th Conference on Our World in Concrete & Structures: 29 - 31 August 2012, Singapore.
- [5] Bjegović D., Štirmer N., Banjad Pečur I. (2016), "By-products of the metallurgical industry as an alternative raw material in the construction industry", 6th International Scientific Conference "Construction - Science and Practice", GNP 2016, 07-11 March 2016, Zabljak, Montenegro, pp. 679 - 687.
- [6] Šahinagić – Isović, M., Čećez, M., Popovac, M., Logo, A.Š. (2017), "Industrial waste materials as admixtures for concrete", XXVII International Symposium on Research and Application of Contemporary Achievements in Construction in Materials and Structures, Vršac, Srbija, pp. 47 – 57, 2017.
- [7] Patel, S., Pal, B.K. (2015), "Current Status of an Industrial Waste: Red Mud an Overview", International Journal of Latest Technology in Engineering, Management & Applied Science Vol. 4 (2015) 8, pp. 1 – 16.

## OVERVIEW OF RESEARCH PROJECTS: PROJECT STREP AND PROJECT MPC

### AUTHORS

#### **Sergey Churilov**

PhD, Associate Professor  
Ss. Cyril and Methodius University,  
Faculty of Civil Engineering-Skopje  
blvd. Partizanski odredi 24, 1000 Skopje  
North Macedonia  
curilov@gf.ukim.edu.mk

#### **Elena Dumova-Jovanoska**

PhD, Full Professor  
University "Ss. Cyril and Methodius"  
Faculty of Civil Engineering-Skopje  
blvd. Partizanski odredi 24, 1000 Skopje  
North Macedonia  
dumova@gf.ukim.edu.mk

As a former scholarship holder of the SEEFORM PhD program, the first author would like to express his gratitude for participation in the program by publishing an overview of two ongoing research projects in the special issue of the Scientific Journal of Civil Engineering dedicated to the celebration of 15 years of SEEFORM. Both projects are reflecting the current research interest and show the progress after the graduation.

The project STREP targets experimental investigations of mechanical properties of two repointing mortars, polymer fibre-reinforced cement-based mortar, Reparatur Mortar FZ + polypropylene straps and lime mortar with crushed brick. The main target of the second project, MPC, is testing of a real-time digital structural health monitoring solution applied to a representative structure, reinforced concrete bell tower of a church.

**Keywords:** Masonry, strengthening, structural repointing, monitoring, vibration, ambient.

### 1. RESEARCH PROJECT STREP

The research project "Masonry strengthening by structural repointing-Project STREP" aims to experimentally investigate the mechanical properties of two repointing mortars, polymer fibre-reinforced cement-based mortar, Reparatur Mortar FZ + polypropylene straps and lime mortar with crushed brick. The experimental program is designed to assess the physical and mechanical properties of masonry components and strength characteristics of masonry exposed to compressive and diagonal compressive stresses, both on unstrengthened and strengthened test specimen. The main aim of the testing campaign is to compare the behavior of the masonry, its bearing capacity and to determine the effect from the structural repointing method in favor of recommendations and procedures of its application for seismic protections of existing masonry buildings.

The motivation of this research arises from the inherent seismic vulnerability of masonry structures and the aspiration for upgrading their seismic resistance by using affordable and

reliable strengthening techniques. Structural repointing is considered as a commonly used strengthening method, generally for brick and block masonry buildings. Although many papers dealing with experimental and analytical investigations of strengthening methods have been published [1-8], their practical application many times is based solely on engineering judgement and workman experience. Therefore, the motivation of this research was based on the need for detailed investigation of the seismic behavior of strengthened masonry with traditional methods.

The research project STREP targets on experimental research of structural repointing method, Fig. 1, by using 2 different mortars (1) traditional lime mortar with crushed brick powder and (2) contemporary polymer fibre-reinforced cement-based mortar, Reparatur Mortar FZ + polypropylene straps.

### 1.1 RESEARCH METHODOLOGY

The greatest part of the research is laid on experimental testing [9-14], to determine:

- Mechanical properties of solid clay bricks
- Mechanical properties of 2 mortar types: lime mortar with brick powder and Reparatur mortar
- Compressive strength of unstrengthened (W-AP) and repointed masonry by 2 mortars (WS-AP-RPP and WS-AP-LM)
- Diagonal tension strength of unstrengthened (W-DP) and repointed masonry by 2 mortars (WS-DP-RPP and WS-DP-LM)

A part of the investigation will address the mathematical modeling and simulation of experimental results.



Figure 1. Structural repointing and testing in STREP

### 1.2 PROJECT OUTCOMES

The main scientific contribution of the project shall be determination of:

- Strength and deformation properties of masonry components
- Strength and deformation properties of structural masonry for both unstrengthened and strengthened conditions
- The effect of the structural repointing method to the advantage of delivering provisions and guidelines for seismic protection of existing masonry structures
- The adaptability, construction method and financial effects of the strengthening method.

The investigated strengthening method is considered as traditional, cost-effective and effortless seismic upgrading method of masonry buildings. The used materials are available in the country and neighboring region and one mortar type is currently produced in the partner institution in this project.

### 1.3 PROJECT PARTNER INSTITUTIONS

The project STREP was established and funded by a mutual collaboration between academia and industry institutions. The consortium was created from Faculty of Civil Engineering-Skopje (FCE), Institute of Earthquake Engineering and Engineering Seismology (IZIIS) and an industry partner for production and sale of construction chemicals ADING. It was originally proposed by FCE as an extension of a master thesis of a student employed at ADING and mentored by the first author.

### 1.4 PROJECT STRUCTURE

The project work is structured in 3 work packages (WP) as shown in Fig. 2.



Figure 2. Structure of project STREP



The research activities in the work packages are divided between the project partner specialties and expertise. Testing of the compressive strength and initial shear strength of masonry wallets is responsibility of FCE, testing of diagonal tension strength of masonry walls will be performed at IZIS, while testing of masonry components, modelling and calibration of mortar batches by testing is performed in ADING.

Since the project is still on-going, no results can be published yet. At the moment, compressive strength tests of W-AP and WS-AP-RPP series, as well as diagonal tension strength tests of W-DP series were completed. Some photos from the building of the specimens and performed testing are shown in Fig. 3.



Figure 3. Activities in project STREP

## 2. PROJECT MPC

Structural Health Monitoring (SHM) is considered as a process of implementing a damage detection and characterization strategy for engineering structures in order to maintain their functionality, safety and stability during exploitation. The SHM process involves assessment of the performance of a structural system by monitoring selected set of typical properties over time, extracting characteristic and damage-sensitive features from those observations and performing statistical analysis of those features to determine the current state of the structural system health.

This second research project led by the first author is entitled “Long-term monitoring of the bell tower of church of St. Clement of Ohrid in Skopje – project MPC”. The main target of the project is testing of a real-time digital structural health monitoring solution applied to a representative structure, a reinforced concrete bell tower of a church. In the following paragraphs the project structure, research team, the expected results and outcomes of the project are clearly outlined. The performed activities within the project are briefly discussed.

The main motivation of the research project was based on an attempt to highlight two targets: (1) testing of new monitoring solution and (2) long-term monitoring of a representative structure.

Lately, structural health monitoring was intensively applied at relatively tall and slender structures, such as high-rise buildings, telecommunication towers, masts, bell- and clock-towers and etc. The range of benefits obtained from such monitoring applications includes damage detection, assessment of maintenance and operability conditions and structural assessment for regular and incidental loadings.

Many published papers in this field describe the monitoring solutions, used equipment, obtained results and provoked decisions of the monitored structures [15-20].

### 2.1 RESEARCH METHODOLOGY

The SHM is relatively new scientific area, but its progress is quite extensive in the last few years. The development of new techniques and analysis tools lead the development, but also give the overall motivation of this research project.

The investigations foreseen have two targets: (1) to examine, test and compare the new monitoring solution from Digitex Systems and (2) to study the structural behavior of a RC bell-tower by continuous monitoring of selected parameters: acceleration, temperature, wind speed and direction and air humidity.

The targets set have scientific, but also applicative contribution. The testing of the new real-time structural health monitoring solution xDAS [21] for its calibration, fine-tuning and further development is of primary interest, Fig. 4. The SHM system is the development of a network of sensors and gages throughout a structure to monitor its health. This system of sensors combined with computer software and data collection methods are used to develop the SHM system that can be used in any structure.

## 2.2 PROJECT OUTCOMES

The greatest part of the planned investigations is directed to:

- Defining the structural geometry and materials of the bell-tower
- Long-term monitoring of selected parameters
- Acquisition, initial processing and archiving of recorded signals
- Interpretation of recorded data by analysis tools and methods
- FEM simulation of the structural behavior in correlation with recorded data from ambient vibrations
- Development of an approach for identification of critical events, automatic event-based data processing and in-time alerting after exceeding threshold values.

## 2.3 PROJECT STRUCTURE

The project run time is determined within 2 years, starting from early 2019.

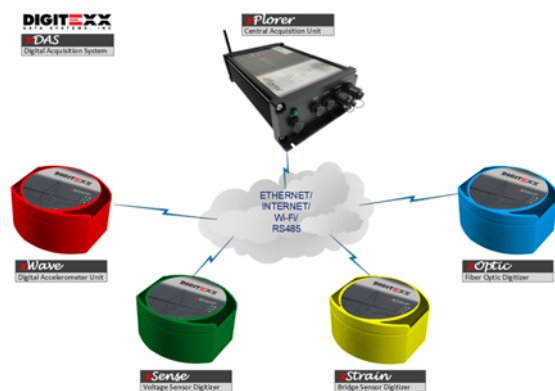


Figure 4. xDAS real-time SHM solution



Figure 5. Structure of project MPC

The project activities are divided in three work packages (WP), Fig. 5.

The WP1 was established to select a representative structure for the project goals set. The final selection was made among several different structural types, such as steel tower, cable-stayed bridge and RC bell-tower. These activities started in the end of 2016, while the final decision and start of the preparatory works were committed in the beginning of 2019. Within the WP1, the bell-tower was extensively measured for determination of its geometry by means of manual measuring methods, but also by drone photogrammetry and LiDAR technology.

WP2 aims to select the appropriate monitoring sensors, select the sensor locations and perform the necessary hardware and software installation. The initial tests were performed to compare the results with a well-known portable ambient vibration testing solution from the same company. The system set-up is schematically presented in Fig. 6.

The largest part of WP3 contains in structural identification of the bell-tower under influence of traffic, wind and bell action loads. FEM model was developed to calibrate the model and simulate the structural behavior. Also, an on-line monitoring, maintenance and management system of the SHM solution was developed.

## 2.4 PROJECT PARTNER INSTITUTIONS

As with the previous project, MPC aims to connect and enforce collaboration between academia and industry institutions. The consortium was created from Faculty of Civil Engineering-Skopje (FCE) and industry partner Digitex Systems and Makedonski Telekom AD that supported the project by providing broadband internet at the bell-tower location.



Figure 6. xDAS Bell-tower application

Digitex Systems are responsible for acquisition of the equipment, installation, maintenance of all system components, as well as for development on-line management tools and decision supported tools for the SHM system. FCE is responsible for geometry and material identification, data processing, FEM modeling, calibration of mathematical models and structural analysis.

## 2.5 CURRENT PROJECT RESULTS

Most of the activities in the WPs were successfully implemented. The structural geometry was fully determined and technical drawings were prepared. Drone photogrammetry and LiDAR scanning were applied and 3D models are expected to be delivered soon, Fig. 7.

SHM system is composed of 4 MEMS tri-axial accelerometers xWave attached along the height of the tower, 1 weather station for monitoring wind speed and direction, temperature and air relative humidity positioned at the top and data acquisition system xPlover.

FEM modelling, calibration and bell-induced vibration analysis were performed, Fig. 8.

Initial structural identification was performed and dynamic characteristics of the bell-tower were established. The on-line SHM management system was developed during summer 2019, Fig. 9.

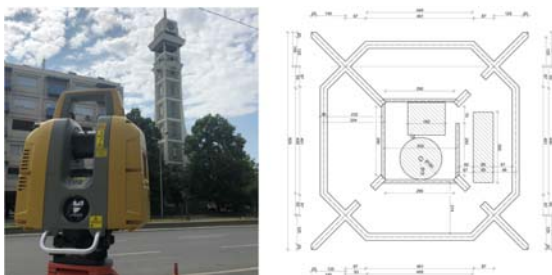


Figure 7. Geometry identification of the bell-tower



Figure 8. FEM modelling and modal analysis

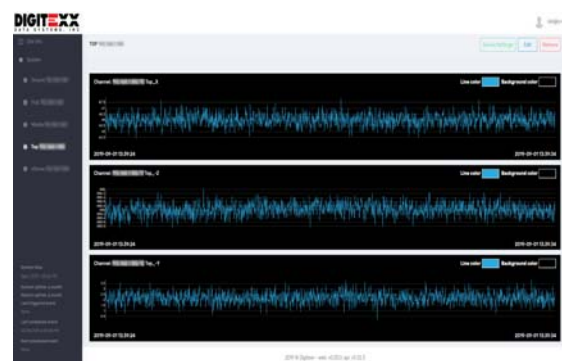


Figure 9. On-line monitoring management system

## Acknowledgements

The authors acknowledge all involved institutions in both research projects for their support and help during realization of the project's activities. The projects were supported by Ss. Cyril and Methodius University, Faculty of Civil Engineering-Skopje, Institute for Earthquake Engineering and Engineering Seismology, construction chemicals factory ADING-Skopje, Digitex Systems-Skopje and Makedonski Telekom AD Skopje.

The mutual understanding and grateful support from Macedonian Orthodox Church - Archdiocese of Ohrid is highly appreciated.

The authors would like to thank the participants of both projects without whom the projects would not be successful. Our deepest gratitude goes to Prof. Veronika Shendova (IZIIS), Prof. Lidija Krstevska (IZIIS), MSc. Bojan Damchevski (ADING), Dime Janchev (ADING), Sasho Atanasovski (Digitex), Tino Mihajlovic (Digitex), Assoc. prof. Gjorgji Gjorgjiev (FCE) and our MSc students Maja Gosheva and Stefan Stankovski.



## REFERENCES

- [1] Brunner, J. D. and P. B. Shing (1996). Shear strength of reinforced masonry walls. *TMS Journal of Composite Materials*, Vol. 14(1).
- [2] Da Porto, F. (2005). In Plane Cyclic Behaviour of Thin Layer Joint Masonry. PhD thesis, University of Trento, Italy.
- [3] Drysdale, R. G., A. A. Hamid and L. R. Baker (1993). *Masonry Structures, Behaviour and design*. Inglewood, Cliffs, NJ, Prentice Hall Inc.
- [4] Goel R.K. (2004). *Seismic Retrofit of Unreinforced Masonry Buildings*. Oral presentation, San Luis Obispo, CA, USA.
- [5] Haach V. G. (2009). Development of a design method for reinforced masonry subjected to in-plane loading based on experimental and numerical analysis. PhD thesis, Universidade do Minho, Escola de Engenharia, Minho, Portugal.
- [6] Haach, V. G., G. Vasconcelos and P. B. Lourenço (2011). Parametrical study of masonry walls subjected to in-plane loading through numerical modeling. *Engineering Structures*, Vol: 33, Issue: 4, pp. 1377-1389.
- [7] Hansen, K. F., E. Nykanen and F. R. Gottfredsen (1998). Shear Behaviour of Bed Joints at Different Levels of Precompression. *Masonry International*, Volume 12, Issue 2, pp. 70-78.
- [8] Luo, W.K., Zhu, X.C., Liao, C.S (1997). Correlation analysis of shear-compression correlation and the shear friction coefficient values. *Eng. Mech*, 2:135–141.
- [9] MKS B.D8.011. Testing methods of clay bricks, blocks and slabs. No. 07-4713/1 (25.11.1986), Official Gazette of (former) SFRY, No. 4, January 1987.
- [10] MKC EN 771-1:2011/A1:2016. Спецификација за сидарски единици - Дел 1: Сидарски единици од глина-Амандман 1, ИСПМ, [www.isrm.gov.mk](http://www.isrm.gov.mk).
- [11] MKC EN 12190:2009. Производи и системи за заштита и поправка (репарација) на бетонски конструкции - Методи на испитување - Определување на цврстина на притисок кај малтерот за поправки, ИСПМ, [www.isrm.gov.mk](http://www.isrm.gov.mk).
- [12] MKC EN 1052-1:2009. Методи за испитување за зидање - Дел 1: Одредување на јакост под притисок, ИСПМ, [www.isrm.gov.mk](http://www.isrm.gov.mk).
- [13] ASTM E519-02, Standard Test Method for Diagonal Tension (Shear) in Masonry Assemblages, ASTM International, West Conshohocken, PA, 2002, [www.astm.org](http://www.astm.org).
- [14] Damchevski B., Churilov S., Dumova-Jovanoska E. (2018). Mechanical characterisation of polymer fibre-reinforced cement-based mortar for masonry joint repointing. 16th European Conference on Earthquake Engineering, Thessaloniki 2018.
- [15] Ribeiro D., Leite J., Pinto N., Calçada R. (2019). Continuous monitoring of the dynamic behaviour of a high-rise telecommunications tower. *Struct Design Tall Spec Build*. 2019; 28:e1621. <https://doi.org/10.1002/tal.1621>.
- [16] Li Q., He Y., Zhou K., Han X., He Y., Shu Z. (2018). Structural health monitoring for a 600 m high skyscraper. *Struct Design Tall Spec Build*. 2018; 27:e1490. <https://doi.org/10.1002/tal.1490>.
- [17] Luzi G., Crosetto M., Cuevas-González M. (2014). A radar-based monitoring of the Collserola tower (Barcelona). *Mechanical Systems and Signal Processing*, Vol: 49, Issue: 1, pp. 234-248.
- [18] Gentile C., Ruccolo A., Saisi A. (2019). Continuous Dynamic Monitoring to Enhance the Knowledge of a Historic Bell-Tower. *International Journal of Architectural Heritage*. Taylor & Francis, pp. 1-13.
- [19] Azzara R.M., Girardi M., Iafolla V., Lucchesi D., Padovani C., Pellegrini D. (2019). Ambient vibrations of age-old masonry towers: results of long-term dynamic monitoring in the historic centre of Lucca. arXiv:1907.00765 [eess.SP].
- [20] Vincenzi L., Bassoli E., Ponsi F., Castagnetti C., Mancini F. (2019). Dynamic monitoring and evaluation of bell ringing effects for the structural assessment of a masonry bell tower. *Journal of Civil Structural Health Monitoring*. 10.1007/s13349-019-00344-9.
- [21] Digitex Systems. (2019). xDAS – Real-Time Digital Structural Health Monitoring Solution, Bell Tower in Skopje, North Macedonia.

## AUTHORS

### **Stanko Coric**

PhD, Assistant Professor  
Faculty of Civil Engineering  
University of Belgrade, Serbia  
cstanko@grf.bg.ac.rs

# **NUMERICAL PROCEDURE FOR STABILITY CALCULATION IN INELASTIC DOMAIN**

The problems of instability of steel frame structures have been of interest to many investigations for a long time. The fast development of computer technology has created the possibility of a complete solution to such a problem. This paper briefly presents one numerical procedure for the global stability analysis that is based on the FEM. The stiffness matrices are derived using the trigonometric shape functions. Also, when the buckling of the structure occurs in the inelastic domain, the tangent modulus theory is applied. Obtained results show justification for applying such a procedure for the stability calculation of the frame structures.

**Keywords:** inelastic buckling, tangent modulus, finite element method.

## **1. INTRODUCTION**

The study of the stability of linear structures begins with the first Euler's researches in the 18th century [7]. His and many other solutions were mainly based on determining the differential equation of buckling according to the second order theory. Later, for the analysis of more complex structures, the researchers had to make some simplifications [14]. So, the compressed elements of the frame were extracted from the whole structure. Corresponding boundary conditions introduce the presence of other structural beams and girders that are connected with the analyzed one. In this case, the results of the stability analysis are presented by the approximate formulas and diagrams, separately for the braced and unbraced frames [1]. These solutions then served to formulate procedures for multi-story frame calculation. The methods most commonly used for such analysis were slope deflection method and stiffness distribution method [1,12]. Such a theory of isolated member later becomes the basis of many recommendations and regulations for the stability analysis of the frame structures, for example [9,8]. The design of such structures is defined by the determination of the effective length factor  $k$ . However, despite the frequent use of such an approach, it has numerous limitations, as it was shown in [2]. First of all, such calculation does not consider the rigidity of the whole structure. Also, the influence of inelastic material behavior and

imperfections are not taken into account [3]. The development of the finite element method enabled the global stability analysis of frame structures [11]. In its usual procedure, it reduced to solving a well-established eigenvalue problem. This paper will outline the procedure where the shape functions are used in the trigonometric form, according to the exact solution of stability differential equation. Also, material nonlinear behavior will be considered using the tangent modulus concept [10].

## 2. APPLICATION OF THE TANGENT MODULUS THEORY

The main goal of this analysis is to formulate, conditionally speaking, the exact procedure for the stability calculation of steel frames. Therefore, as it is already emphasized, it is applied finite element method with interpolation functions in the trigonometric or hyperbolic form. So, the buckling problem will be reduced to the solution of the transcendental equation which depends, in a very complicated way, upon the axial forces in columns and beams [3].

Corresponding stiffness matrices also have to take into account nonlinear material behavior. The tangent modulus concept has been used for that purpose. The concept of the tangent modulus was introduced in [6], a later developed by many other authors, for example [10,13]. So, in the "classic" elastic analysis Young's modulus of elasticity (E) should be replaced with tangent modulus ( $E_t$ ), which is stress dependent function. This module is used to estimate the gradual yielding effect due to residual stresses along the length of members under axial loads [2]. The expression that is used in this analysis was firstly suggested in [5], and latter accepted in some relevant researches [13]:

$$E_t = 4 \cdot E \cdot \left[ \frac{\sigma}{\sigma_y} \cdot \left( 1 - \frac{\sigma}{\sigma_y} \right) \right] \quad (1)$$

where  $\sigma_y$  is yield stress. This is empirical an expression designed to represent the performance of structural steel columns in the inelastic domain [10]. This formula is valid for  $\sigma > 0.5 \cdot \sigma_y$ .

To solve this buckling problem it is important to formulate corresponding stiffness matrices. The

$$\mathbf{K} = \frac{E_t I}{l^3 \Delta_t} \begin{bmatrix} \omega_t^3 \sin \omega_t & \omega_t^2 l (1 - \cos \omega_t) & -\omega_t^3 \sin \omega_t & \omega_t^2 l (1 - \cos \omega_t) \\ \omega_t l^2 (\sin \omega_t - \omega_t \cos \omega_t) & -\omega_t^2 l (1 - \cos \omega_t) & \omega_t l^2 (\omega_t - \sin \omega_t) & \\ \omega_t^3 \sin \omega_t & -\omega_t^2 l (1 - \cos \omega_t) & & \\ \text{simetr.} & & \omega_t l^2 (\sin \omega_t - \omega_t \cos \omega_t) & \end{bmatrix} \quad (5)$$

procedure for deriving these matrices is presented in [4]. Here is given only the stiffness matrix of the member that is clamped at both ends and subjected to compression axial force, Eq.(5).

$$\omega_t = \sqrt{\frac{P_{cr,i}}{E_t \cdot I}} \cdot l \quad (2)$$

$$\Delta_t = 2 \cdot (1 - \cos \omega_t) - \omega_t \cdot \sin \omega_t \quad (3)$$

where with is  $P_{cr,i}$  is marked critical force in the observed member.

When the global stiffness matrix is defined, it is possible to calculate the critical load from the homogeneous matrix equation:

$$\mathbf{K} \mathbf{q} = 0 \quad (4)$$

where  $\mathbf{q}$  is the vector of generalized coordinates. This problem can be solved by an incremental process, i.e. finding the solution for  $\det(\mathbf{K}) = 0$ .

The real challenge in this research was to carry out an appropriate numerical analysis. Namely, as it was already emphasized, the buckling problem is reduced to the solution of the transcendental equation which depends, in a very complicated way, upon the normal forces in columns and beams [3]. Although in this case only one finite element is needed for each column or beam, the problem is more complicated to solve than the "usual" eigenvalue problem for which there are several established methods. So, for this purpose, an appropriate computer program was developed using the C++ programming language and it is presented in detail in [4]. The basic possibilities of this program are analysis according to the first and the second-order theory and stability analysis of linear frames. This paper briefly presents only part of an algorithm related to the calculation of the critical load in an elastic and inelastic domain.

The program firstly needs to calculate the critical load in the elastic domain. The first iteration is performed according to the first-order theory. Then obtained forces are used as initial values in the second-order theory calculation. Afterward, the program continues the iterative calculation until the displacement difference in two consecutive iterations

becomes smaller than some pre-set small value. At the end of this procedure, the stiffness matrix of the whole system is obtained, and only the active degrees of freedom are considered. That stiffness matrix must satisfy the condition for the existence of the nontrivial solution. The final result of this procedure gives the critical force for the constant modulus of elasticity (i.e. in the elastic domain).

After that, columns where the critical stress ( $\sigma_{cr}=P_{cr}/A$ ) greater than the proportionality limit ( $\sigma_p$ ) need to change their stiffness. Namely, tangent modulus ( $E_t$ ), according to Eq.(1), should be introduced for them. Columns with  $\sigma_{cr}$  which did not reach  $\sigma_p$  should keep "old characteristics". Then, the iterative calculation should be performed again in the same way as for the "elastic" analysis. As a result, this procedure gives the corresponding critical load factor and the value of tangent modulus for all elements buckling in the inelastic domain.

### 3. NUMERICAL EXAMPLES

Only some of the calculation possibilities of this program will be presented in this paper. In all examples is used steel with characteristic:  $E = 210,000,000 \text{ kN/m}^2$  and  $\sigma_y = 240,000 \text{ kN/m}^2$ . First results are obtained by variation of columns stiffness for the simplest one-story sway frame (Figure 1).

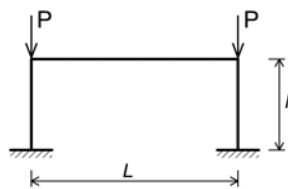


Figure 1. One-story sway frame.

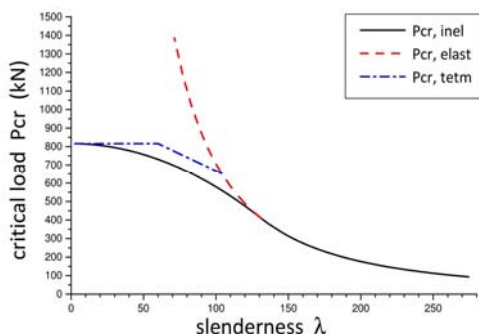


Figure 2.  $P_{cr} - \lambda$  diagram for the frame (Fig.1).

The critical column stress variation vs. slenderness ratio for the one-story sway frame is presented in Figure 2. The results of the presented elastoplastic analysis are shown by a solid line. Euler curve (results of elastic stability analysis) is marked with a dashed line. The

dash-dotted line represents Tetmajer's linear formula [13]. From these results, obtained by a self-developed program, it can be seen the usefulness of applying the analysis in the inelastic domain, particularly for the columns with low slenderness (or short columns).

The critical stress–strain curve for analyzed numerical example is given in Figure 3. As it was expected, below a proportionality limit, modulus of elasticity  $E$  is constant, and above this point, a nonlinear relationship between stress and strain is obtained.

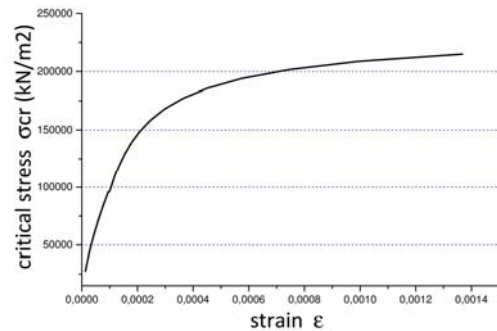


Figure 3.  $\sigma_{cr} - \epsilon$  curve for the frame (Fig.1).

It is clear that these results represent a good verification of the proposed program. Similar results for the two-story and six-story frames are given in [4].

In order to illustrate some other possibilities of the presented numerical procedure, a steel five-story three-bay sway is considered, Fig.4.

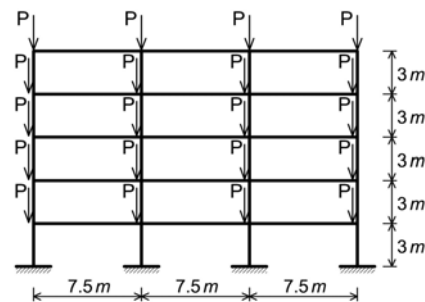


Figure 4. Five-story three-bay sway frame.

Rigid connections for columns ends including their supports at the base are assumed. Concentrated loads  $P$  are imposed on each column at each story level. Since the axial load in the columns increases from the stories above to the base level, presented elastoplastic stability analysis leads to the different behavior of the columns in the different levels. Six different IPB cross-sections of the columns are assumed for the parametric analysis, while floor beams are IPE300.

Table 1 gives the critical load values for the analyzed cross-sections for elastic and proposed elastoplastic stability analysis. It is

clear that the application of proposed stability analysis in the inelastic domain is justified for such a numerical example. Namely, this is a rather rigid frame and it can be exposed to significant axial load. In the case of similar frames [3] but with higher columns, this difference in result is smaller.

Table 1.  $P_{cr}$  for the frame (Fig.4).

	$P_{cr,el}$	$P_{cr,inel}$
IPB120	364.3	146.0
IPB160	851.9	245.2
IPB200	1383.2	360.6
IPB240	1875.5	495.3
IPB280	2315.5	616.9
IPB320	2825.9	751.1

The corresponding values of the tangent moduli (for only two floors) at the moment of buckling are presented in Table 2.

Table 2.  $E_t$  for the frame (Fig.4).

	tangent moduli	
	3 <sup>rd</sup> floor	1 <sup>st</sup> floor
IPB120	208,861,665	79,146,292
IPB160	206,514,563	46,863,965
IPB200	204,992,189	30,691,635
IPB240	204,063,803	21,716,697
IPB280	203,404,726	15,644,936
IPB320	202,790,302	12,550,149

From these results it can be observed the difference in the behavior of the upper and lower columns. Overall buckling of this type of structure is governed by the behavior of the columns that are subjected to the highest axial load. Those are the columns on the first floor. The columns in the upper are loaded with smaller axial forces, so their characteristics (ie. modulus of elasticity) have not changed too much.

It should be noted that the above procedure can give some other results of stability problems. For example, the determination of the effective buckling length and the calculation of the load-bearing capacity of the compressed members are presented in [3].

#### 4. CONCLUSIONS

The goal of this paper was to indicate some of the possibilities of a program that was developed according to the presented

theoretical procedure. This procedure is based on the global stability analysis of steel frame structures. The calculation was performed for the elastoplastic stability analysis when the geometrically non-linear process is followed by the development of the material nonlinearity as well. Stiffness matrices were derived using the tangent modulus that is a stress-dependent function. Analyzed numerical examples confirm that this procedure is a good alternative for the stability calculation of steel frames in the inelastic domain.

#### Acknowledgements

The part of this research was financial supported through the SEEFORM project financed by DAAD, during the years 2008-2012. This support is gratefully acknowledged.

#### REFERENCES

- [1] Allen, H.G., Bulson, P.S. (1980), "Background to buckling", McGraw Hill, U.K.
- [2] Chen W.F. (2000), "Structural stability: from theory to practice", Engineering Structures, Vol.22, Iss.2, pp.116-122.
- [3] Ćorić S., Brčić, S. (2016), "Nonlinear stability analysis of the frame structures", Building materials and structures, no.59-3, pp.27-44.
- [4] Ćorić S. (2013), "Nonlinear stability analysis of the frame structures", Doctoral dissertation, Faculty of civil engineering, University of Belgrade.
- [5] CRC Japan (1971), "Handbook of Structural Stability", Corona, Tokyo.
- [6] Engesser F. (1892), "Ueber die Knickfestigkeit Gerader Stäbe", Zeitschrift für Architektur und Ingenieurwesen, 35.
- [7] Euler, L. (1744). "Methodus Inveniendi Lineas Curvas Maximi Minimive Proprietate Gaudentes (Appendix, De Curvis Elasticis)".
- [8] European Committee for Standardization (2006), "Eurocode 3, Design of Steel Structures - ENV 1993-1-1: 2005"
- [9] European Convention for Constructional Steelwork (ECCS) (1978), "European recommendations for steel structures"
- [10] Galambos T. V. (editor). (1988). "Guide to Stability Design Criteria for Metal Structures", 5th edition, John Wiley and Sons, New York, USA.
- [11] Gallagher R.H. (1975), "Finite Element Analysis", Prentice-Hall, Inc. New Jersey.
- [12] Horne, M.R., Merchant, W. (1965), "The stability of frames", Pergamon, Oxford.
- [13] McGuire W., Gallagher R., Ziemain R. (2000), "Matrix Structural Analysis", 2nd edition, John Wiley and Sons, New York, USA.
- [14] Timoshenko, S.P., Gere, J.M. (1961), "Theory of Elastic Stability", McGraw-Hill, New York.



## LATERAL-TORSIONAL BUCKLING OF ALUMINUM MULLION IN CURTAIN WALL

### AUTHORS

#### **Danijela Djuric Mijovic**

PhD, Research and Teaching Assistant  
University of Nis  
Faculty of Civil Eng. and Architecture  
A.Medvedeva 14, 18000 Niš, Serbia  
danijela.djuric.mijovic@gaf.ni.ac.rs

#### **Aleksandra Cilic**

PhD, Research and Teaching Assistant  
University of Nis  
Faculty of Civil Eng. and Architecture  
A.Medvedeva 14, 18000 Niš, Serbia

#### **Dragan Kostic**

PhD, Associate Professor  
University of Nis  
Faculty of Civil Eng. and Architecture  
A.Medvedeva 14, 18000 Niš, Serbia

Curtain wall as contemporary facade structures are often preferred by designers on different types of structures. In this paper, they are viewed in a more contemporary, complex and comprehensive way. Wind load was analysed using CFD. The supporting elements of the curtain wall made of aluminium alloys AW 6063.T5 and AW 6082.T5 have been specifically tested for lateral torsional buckling. Recommendations have been made for the use of specific cross-sections, the implementation of which would result in significant savings in the material on the buildings facades.

**Keywords:** Facade, curtain wall, aluminium, steel, lateral torsional buckling.

### 1. INTRODUCTION

Contemporary structures in every respect tend to go beyond the set boundaries, so consequently the contemporary facades have never been so complex. The basic function to protect the users is somehow put aside while only the design striving to the most attractive and challenging facades comes to the fore. Due to their complex function, facade structures are subject to many criteria, which is why they are the subject of constant theoretical and experimental research. "Curtain walls have been around for over a century; however, they still present a challenge for building designers, curtain wall manufacturers and installers" [10]. Curtain walls can be defined as lightweight, skin structure composed of industrially produced elements, most often glass and metal, which assumes all the functions of an outer wall, except the supporting one. They represent a synthesis of aesthetic and technical-technological solutions with practically no limit in formal and structural design. The curtain wall structure, unlike the main load-bearing structure, which receives all the loads of the building, must absorb, transmit and withstand the loads acting on it through carefully designed vertical and horizontal load-bearing elements of the facade. In most cases, problems that occur on facades of this type are a direct consequence of inadequate design, construction and incompatibility with the supporting structure of the building.

Wind is the dominant load for the curtain wall facades and belongs to the stochastic and complex loads and it is a subject of numerous researches [4,11]. Understanding nature and wind behaviour is of key importance for adequate designing of lightweight curtain wall type facade structures and the wind load on the building must be analysed in the earliest stages of designing [8,10].

This type of structures were analyzed in previous research more complexly and comprehensively in particular regarding the effect of wind using computational fluid dynamics as a contemporary method. Based on these results, the sensitivity of the supporting elements of the curtain wall to lateral-torsional buckling has been specifically addressed, and recommendations for the selection of cross-section shapes have been made.

## 2. MATERIALS & METHODS

### 2.1 CURTAIN WALL STRUCTURE, MATERIALS AND LOADS

The curtain wall structure consists of vertical bearing elements, mullions and horizontal elements, transoms. Mullions and transoms, placed at proper spacing create frames used to install infill elements, which are prevalently glass, but can be stone, aluminium, copper, composite materials etc. Mullions and transoms can vary, but most often those are tubular, double or mono-symmetrical I sections, T sections etc. These elements can be full and hollow. Some of them are shown in Figure 1. Connections between the elements but also the connections to the bearing structure must be such to ensure displacement due to the effects of external forces, primarily of the wind, to ensure expansion due to temperature and gravity effects, for instance due to the foundation settling.

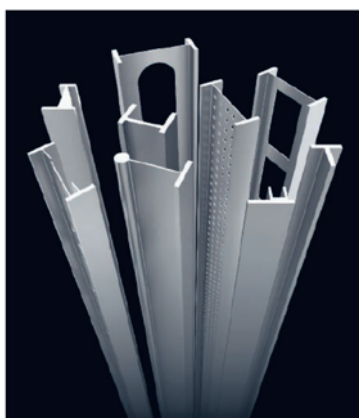


Figure 1

Characteristic loads for this type of structures, in addition to their own weight, are wind, snow, ice, temperature and earthquake. In some cases, depending on the static system and the shape of the facade, the load that would occur when maintaining the structure should be considered. Wind is the dominant load in light facade structures. What is important and what should be considered is the effect of wind on the corners of buildings and also on the parts of the facades near the roof. Here, due to the formation of the vortex, there is a strong suction effect of the wind and the pressure coefficients are many times higher than in the central parts of the surfaces loaded with wind. Particular attention should also be paid to the effect of temperature since the substructure is often made of aluminium and its thermal expansion coefficient is 3 times higher than that of steel and the dilations that occur in the elements are not small. This problem is usually solved by an adequate choice of the static system or using suitable sliding connections.

Since these are sections with a height much larger than the width of the flange, particular attention has been paid to the stability of the supporting elements of the curtain wall. The area of stability in steel and aluminium is a constant subject of research, and it should be noted that this problem is more complex regarding aluminium alloys than steel for many reasons. The first is that aluminium alloys make a much wider family of materials than is the case with structural steels, not only because of the different alloys and chemical composition, but also because of the considerable changes in mechanical characteristics due to the degree of processing.

Cross sections of the supports used for the load-bearing elements of the curtain wall, mullions and transoms belong to a group of narrow, but deep, cross sections. The reason why such sections are frequently a part of the curtain wall structures lies in several facts. Primarily, the infill elements with a load acting on them should be received from the outside, and on the inside the same elements should be connected to the supporting structure of the structure or to each other so as to allow displacements due to external effects and also the expansion of the elements themselves. What is characteristic of the open cross sections whose height is considerably higher than their width, is that the flexural stiffness about the stronger axis ( $I_y$ ) is considerably higher than the flexural stiffness about the weaker axis ( $I_z$ ), while the torsional stiffness ( $I_t$ ) of these cross-sections is also small. Support

elements of such characteristics are sensitive to lateral displacements and rotation about the shear centre. The situation is made additionally complex by the fact that the sections for the curtain wall elements are often symmetrical about one axis only. From all this, it can be concluded that the curtain wall elements need to be checked to lateral torsional buckling, especially those of open cross sections.

## 2.2 LATERAL TORSIONAL BUCKLING

Lateral torsional buckling of the support element comprises lateral displacement of the element with the simultaneous rotation about the vertical axis of the cross section resulting from the bending around the stronger axis of the cross section when the critical momentum value is reached (Figure 2). This type of element buckling is characteristic of both steel and aluminium supports. However, although there are similarities, the approach to this problem is not the same in the regulations regarding the two materials [5,6].

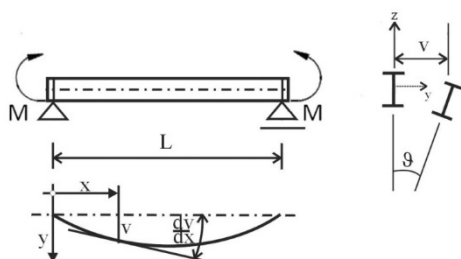


Figure 2. Lateral-torsional buckling

In order to provide a relative lateral torsional slenderness,  $\bar{\lambda}_{LT}$  it is necessary to compute the elastic critical momentum for lateral torsional buckling,  $M_{cr}$ . However, the standing versions of Eurocode 3 [5] does not provide any recommendations for computation of  $M_{cr}$  apart from the note that the computation of the elastic critical moment should be based on the gross cross sections, take into account the support or lateral bracing conditions and the type of load. The reason there is no clearly defined expression for  $M_{cr}$  and recommendations for its computation lies in the complexity of this problem, but also in the non-existing consensus of the EU members (Androić 2009). Contrary to the described situation for the calculation of the steel elements resistance to lateral torsional buckling, the regulations regarding the calculation of aluminium supports for lateral torsional bending approach to this problem and the calculation algorithm in Eurocode 9 [6] is clearly defined in Annex I. Stability problems and consequently the lateral torsional buckling problem are much more pronounced in

aluminium due to the lower value of the modulus of elasticity comparing to steel.

Equations (1) to (5) present the expression for the elastic critical moment, which when reached causes the loss of stability of the support due to the lateral torsional buckling:

$$M_{cr} = \mu_{cr} \frac{\pi \sqrt{EI_z GI_t}}{L} \quad (1)$$

$$\mu_{cr} = \frac{C_1}{k_z} \left[ \sqrt{1 + k_{wt}^2 + (C_2 \zeta_g - C_3 \zeta_j)^2} - (C_2 \zeta_g - C_3 \zeta_j) \right] \quad (2)$$

$$k_{wt} = \frac{\pi}{k_w L} \sqrt{\frac{EI_w}{GI_t}} \quad (3)$$

$$\zeta_g = \frac{\pi z_g}{k_z L} \sqrt{\frac{EI_z}{GI_t}} \quad (4)$$

$$\zeta_j = \frac{\pi z_j}{k_z L} \sqrt{\frac{EI_z}{GI_t}} \quad (5)$$

Where  $\mu_{cr}$  is a relative, dimensionless critical moment,  $G$  shear modulus,  $EI_z$  minor axis flexural rigidity,  $GI_t$  torsional rigidity,  $EI_w$  warping rigidity,  $L$  length between lateral bracings. Coefficients  $C_1$ ,  $C_2$ ,  $C_3$ ,  $k_z$  and  $k_w$  are defined in EN 1999-1-1:2007 [6].

Expressions (1) to (5) include different support conditions of the load-bearing element, effect of the position of the load application point, but also the cross sections symmetrical around one axis. In case of the cross sections symmetrical around both axes, the gravity and shear centre coincide, while in case of the cross sections symmetrical around one axis it is not true, so the computation equations are more complex. In Figure 3 is presented a mono-symmetrical cross section where  $G$  is gravity centre,  $S$  shear centre,  $z_s$  distance from the shear and gravity centre,  $z_g$  distance from  $S$  to load application point,  $z_a$  distance from  $G$  to load application point.

Parameter  $z_j$  is of extreme importance for determining the critical moment on the lateral torsional buckling. Equation (6) shows an exact formula for computation of parameter  $z_j$ , however, in literature there are numerous propositions for its approximation. When the cross section is symmetrical about the stronger axis ( $y$ - $y$  axis) then  $z_j=0$ . Equation (7) provides the approximation formula from Eurocode 9 [6]:

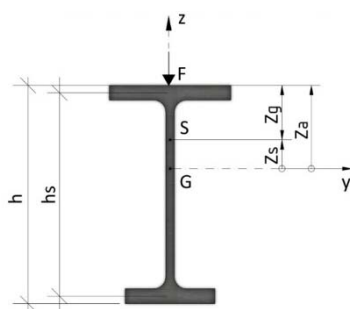


Figure 3

$$z_j = z_s - \frac{0,5}{I_y} \int_A (y^2 + z^2) z dA \quad (6)$$

where  $z_a$  is the coordinate of the load application point in relation to the gravity;  $z_s$  coordinate of shear centre in relation to the gravity;  $z_g$  coordinate of the load application point in relation to the shear centre (Figure 3).

$$z_j = 0,45\psi_f h_s \left(1 + \frac{c}{2h_f}\right) \quad (7)$$

$$\psi_f = \frac{I_{fc} - I_{ft}}{I_{fc} + I_{ft}} \quad (8)$$

In the previous equations  $h_f$  is the distance between the gravity centre of the top and bottom flange;  $c$  height of the flange reinforcing web (see Figure 3);  $\psi_f$  factor of cross section mono-symmetry;  $I_{fc}$  moment of inertia of the compressed flange about the weaker axis;  $I_{ft}$  moment of inertia of the tensioned flange about the weaker axis,  $h_s$  distance of the shear center of the top flange and shear center of the bottom flange.

For I cross section, with unequal flanges, without reinforcement, the following stands:

$$I_W = (1 - \psi_f^2) I_z (h_s/2)^2 \quad (9)$$

In case of the beams loaded the web plane, the position of the load application point has a considerable effect on the value of the critical moment of the lateral torsional buckling,  $M_{cr}$ . If the load application point is above or below the shear point S, this force causes additional torsional effects. These effects can be stabilizing in case the load is applied below the shear centre, and destabilizing when the load is applied above the shear centre.

In order to determine whether the beam is resistant to lateral torsional buckling, Equation (10) is used, where  $M_{Ed}$  labels the design bending moment, and with  $M_{b,rd}$  design

resistance to lateral torsional buckling, provided with Equation (11).

$$\frac{M_{Ed}}{M_{b,rd}} \leq 1,0 \quad (10)$$

$$M_{b,rd} = \kappa_{LT} \frac{\alpha W_{el} y f_o}{\gamma_{M1}} \quad (11)$$

$$\kappa_{LT} = \frac{1}{\phi_{LT} + \sqrt{\phi_{LT}^2 - \bar{\lambda}_{LT}^2}} \leq 1,0 \quad (12)$$

$$\phi_{LT} = \frac{1}{2} \left[ 1 + \alpha_{LT} (\bar{\lambda}_{LT} - \bar{\lambda}_{0,LT}) + \bar{\lambda}_{LT}^2 \right] \quad (13)$$

In the previous equations  $\kappa_{LT}$  is the reduction factor for lateral torsional buckling;  $\alpha_{LT}$  imperfection factor;  $\bar{\lambda}_{0,LT}$  horizontal plateau limit.

Relative slenderness of lateral torsional buckling is provided with equation (14):

$$\bar{\lambda}_{LT} = \sqrt{\frac{\alpha W_{el} f_o}{M_{cr}}} \quad (14)$$

where  $\alpha$  is the shape factor.

### 3. ANALYSIS & RESULTS

This research included the resistance analysis of the beams used for vertical load-bearing elements of curtain walls, mullions, to lateral torsional buckling [2]. Aluminium I beams and double as well as mono-symmetrical cross sections are considered. For this purpose, a program (application) was created which enables: input of the selected aluminium alloy, its characteristics and the corresponding buckling class; determining the class for each part of the cross-section (top flange, web, bottom flange) in the case of an evenly distributed load; adopting a cross-sectional class for whole cross-section; calculating the effective thicknesses of the cross-section elements in the case of a class 4 element; calculation of elastic, plastic and effective moments,  $W_{el}$ ,  $W_{pl}$ ,  $W_{eff}$ ; determining the cross section shape coefficient,  $\alpha$  depending on the cross section class.

Based on the obtained data, set beam length,  $L$  and design bending moment,  $M_{Ed}$  determination of the elastic critical moment to lateral torsional buckling,  $M_{cr}$ , is made possible for the given cross section and the given point of load application on the top flange, shear centre and bottom flange, and all the relevant coefficients and parameters necessary for its computation; determination of  $z_j$  according to the exact formula and its comparison with the



parameter  $r_z$ ; determination of the relative lateral torsional slenderness,  $\lambda_{LT}$  for all three positions of the point of load application; determining the reduction factor for the lateral torsion buckling,  $\chi_{LT}$  and parameters necessary for its determination; determination of design resistance to lateral torsional buckling,  $M_{b,Rd}$ ; determination whether the given beam is resistant to lateral torsional buckling.

It should be emphasized that the application is made for the case when the beams are loaded with evenly distributed load, and in addition to double symmetrical and mono-symmetrical I cross sections, T cross sections are included, too.

Previously described application is used for the analysis of the resistance of an arbitrary I cross section beam to a lateral torsional buckling. Two groups of cross sections are formed. The first group comprises the cross sections having the width of one flange  $b_{1,f}=50$  mm and the other group included the cross-sections with the flange width  $b_{2,f}=60$  mm. It should be emphasized that the analysis includes T cross-sections too, as special cases of I cross section. The heights of the cross sections of both groups are  $h= 100, 150, 200$  and  $250$  mm (Figure 4).

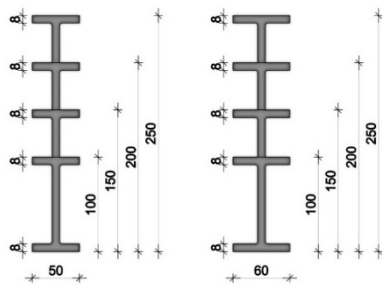


Figure 4. Groups of analysed mullions

Beams with different mono-symmetry factors,  $\psi_f$  (Figure 5) were compared using a relative dimensionless critical moment,  $\mu_{cr}$  [-] provided with equation (2).

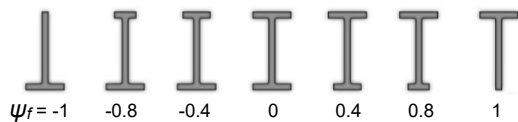


Figure 5. Analysed cross-sections

The load on mullions and transoms mostly acts on the so-called outer flange (flange closer to the exterior) since the infill elements are most often connected in such a way that the load-bearing elements are inside the building. This research, however, included the computation of the critical moment to lateral torsional buckling,

even when the load acts in the shear centre and inner flange.

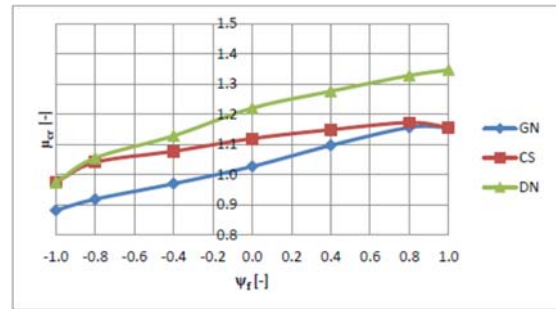
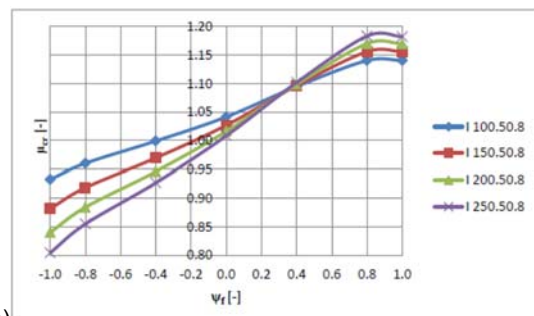
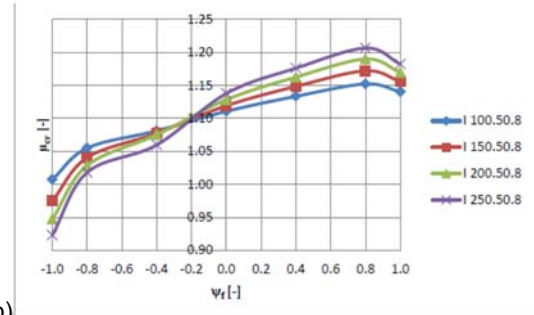


Figure 6. Dependence of  $\mu_{cr}$  on  $\psi_f$  for the cross-section height  $h= 150$  mm

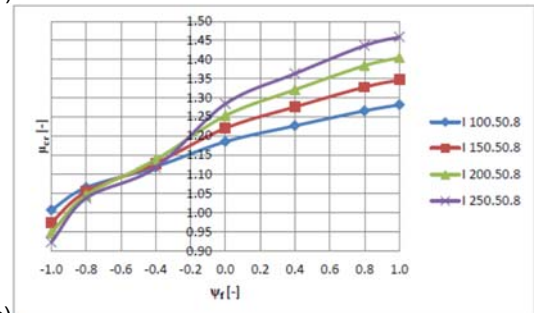
The results are also shown graphically in Figure 6. This diagram shows the resistance to lateral torsional buckling of the examined cross sections (Figure 4 and 5) when the point of load application is on the outer flange (GN), shear centre (CS) and bottom flange (DN) depending on the mono-symmetry parameter  $\psi_f$ , for all the examined cross section heights.



a)



b)



c)

Figure 7. Dependence of  $\mu_{cr}$  [-] on  $\psi_f$  for various cross section heights when the load is applied on GN (a), CS (b) and DN (c)

Figure 7 show dependence diagrams of the dimensionless critical moment  $\mu_{cr}$  [-] on the mono-symmetry factor  $\psi_f$  for the case when the load is applied on the top flange (GN), shear canter (CS) and bottom flange (DN), for the cases of various cross section heights.

#### 4. DISSCUSSION

By incorporating a dynamic analysis of the effect of wind on the facades of tall buildings, a more realistic picture of the loads and stresses generated in the supporting elements of the curtain wall, especially the elements at the corners of the building and at high altitudes, was obtained, given the change in wind speed with height.

A special attention is paid to the mono-symmetry parameter  $\psi_f$  and its effect on lateral torsional buckling. The increase of this parameter is followed by the increasing resistance of the tested cross sections to lateral torsional buckling. For the vertical support elements of curtain walls, regarding the lateral torsional buckling, it is convenient to use mono-symmetrical cross sections where the mono-symmetry parameters is  $\psi_f > 0$ . Cross sections with the values  $-1 \leq \psi_f \leq 1$  were examined, and a favourable behaviour was demonstrated by cross sections where  $0.2 \leq \psi_f \leq 0.8$ . By comparing the resistance of the examined cross sections to lateral torsional buckling, it was determined that the cross sections with the mono-symmetry parameter  $\psi_f = 0.8$  are most favourable when the load is applied on the top flange and shear canter (Figure 7 and 8). This research confirmed the fact that, as the position of the point of load application moves from the top flange towards the bottom flange, the resistance of the cross section to lateral torsional buckling increases. Another conclusion is that by increasing the height of the cross section this phenomenon becomes more prominent. Based on the previous facts, it is concluded that the vertical curtain wall elements would be more cost-effective if the infill panels were connected to the mullion shear canter or its lower flange.

#### CONCLUSION

The aim of this scientific research was to do a more complex analysis of the curtain wall as light facade structures. It is obvious that the cross-sectional shape, expressed via the mono-symmetry parameter, has a significant effect on its resistance to lateral-torsional buckling. Since the cross sections of the

supporting elements are often curtain wall only symmetrical about one axis, the advantages shown by these cross sections in relation to the resistance to lateral torsional buckling should be exploited. Proper selection of the appropriate cross-sectional shape and the position of the point of load application can increase the resistance to lateral-torsional buckling of the supporting elements of curtain walls. In this way, adopting mono-symmetrical I cross sections would result in significant material savings. This should not be neglected knowing the fact that the cost of the facade makes a considerable share of the total cost of the building.

#### REFERENCES

- [1] Androić, B., Dujmović, D., Džeba, I., 2009. Čelične konstrukcije 1, IA Projektiranje, Zagreb.
- [2] Đurić Mijović, D., 2016. Arhitektonsko-konstrukcijski dizajn fasadnih sistema od čelika i aluminijuma, Doktorska disertacija, Građevinsko-arhitektonski fakultet, Univerzitet u Nišu, Srbija.
- [3] EN 13116, 2001. Curtain walling. Resistant to wind load – Performance requirements, European committee for standardization, Brussels, Belgija.
- [4] EN 1991-1-4:2005. 2009. Dejstva na konstrukcije. Deo 1-4: Dejstva vetra. Građevinski fakultet Univerziteta u Beogradu, Beograd
- [5] EN 1993-1-3 (2006) (English): Eurocode 3: Design of steel structures - Part 1-3: General rules - Supplementary rules for cold-formed members and sheeting
- [6] EN 1999-1-1:2007 Desing of Aluminium Structures (Annex I).
- [7] Ferziger J.H., Peric M., 2002. Computational Methods for Fluid Dynamics, 3rd ed., Springer, Berlin.
- [8] Franke J., 2007. Introduction to the Prediction of Wind Loads on Buildings by CWE, editors: Stathopoulos T., Baniotopoulos C.C., Wind Effects on Buildings and Design of Wind-Sensitive Structures, p.67-103, Springer.
- [9] Holmes J. D., 2001. Wind Loading of Structures, Spon Press (Taylor & Francis Group), London.
- [10] Kazmierczak, K., 2008. Movements & Tolerances. Considerations for curtain wall and cladding design, The Construction Specifier, October 2008.
- [11] Simiu E., Scanlan R., 1996. Wind effects on structures, John Wiley & Sons, New York.

#### AUTHORS

##### **Marija Vitanova**

PhD, Assistant Professor  
Ss. Cyril and Methodius University  
Institute of Earthquake Engineering and  
Engineering Seismology (IZIIS), Skopje  
marijaj@iziis.ukim.edu.mk

##### **Kemal Edip**

PhD, Associate Professor  
Ss. Cyril and Methodius University  
Institute of Earthquake Engineering and  
Engineering Seismology (IZIIS), Skopje  
kemal@iziis.ukim.edu.mk

##### **Viktor Hristovski**

PhD, Full Professor  
Ss. Cyril and Methodius University  
Institute of Earthquake Engineering and  
Engineering Seismology (IZIIS), Skopje  
viktor@iziis.ukim.edu.mk

##### **Radmila Salic**

PhD, Assistant Professor  
Ss. Cyril and Methodius University  
Institute of Earthquake Engineering and  
Engineering Seismology (IZIIS), Skopje  
r\_salic@iziis.ukim.edu.mk

## **SEISMIC RESPONSE OF ISOLATED BRIDGES INCLUDING SOIL- STRUCTURE INTERACTION (SSI) EFFECTS**

Current practice usually neglects the effects of soil-structure interaction (SSI) in the seismic analysis and design of bridges. This work attempts to assess the significance of SSI on the seismic response of isolated multi span bridges.

The soil medium has been analyzed by applying different soil densities in order to consider the soil stiffness. The accent of the study has been given to the soil structure interaction effects and the results are analyzed accordingly. The soil medium has been taken into consideration as a four layered infill as dense and loose medium. The bridge structure is taken to be an RC structure. The boundaries in the soil medium are considered as infinite elements in order to absorb the radiating waves.

The formulation of infinite elements is the same as for the finite elements in addition to the mapping of the domain. Based on the iso-parametric concept, the infinite element in global coordinate is mapped onto an element in local coordinate system. In the formulation of the infinite element, only the positive direction extends to infinity thus allowing the waves to propagate outside of the soil medium.

Related comparisons are done with references and experimental results in which considerably acceptable results are obtained. The newly proposed methodology efficiently models both the interaction of soil and bridge structures and simultaneously the far field of soil model in which the wave reflections are softened. The case study chosen in this work considers different strength of soil models on which the bridge structural response is analyzed in detail.

**Keywords:** bridge structure, infinite elements, numerical analysis, SSI.

## 1. INTRODUCTION

Bridges are very important elements of the infrastructure in modern societies. Due to their importance, loss of functionality after a seismic event is not an acceptable performance criterion for most of those structures. In the past few decades, extensive research has been conducted regarding the effects of soil–structure interaction (SSI) on the seismic response of civil engineering structures. Until recently, the general concession between engineers and researchers was that SSI effects are beneficial to the response of civil engineering structures.

The response of a structure under earthquake loading could be conservatively evaluated without taking the SSI effects into consideration (NEHRP specifications, 1997, [1]). That is because SSI provides additional flexibility and damping to the structural systems, or said differently, naturally isolates them from the shaking ground. These two effects, the period lengthening and the increase of damping, are also the fundamental premises behind the seismic isolation concept.

This paper investigates the effects of SSI on the seismic response of three span girder seismically isolated bridge, representing a typical stiff freeway overcrossing, which are founded on soft and medium dense soil. Using a nonlinear hysteretic model, which could account for the behavior of the isolation system, and assuming the upper structure will behave linearly, the inertial interaction between the foundation–soil system and the superstructure is studied for real seismic excitation with two intensities 0.2g and 0.4g.

## 2. SOIL-STRUCTURE INTERACTION

The seismic SSI problem involves two major components: the response of the soil as seismic waves travel through the soil deposit and the coupled foundation–superstructure response, which is usually assumed to be a superposition of the response of the pile foundation itself to the excitation in the absence of the superstructure (kinematic response) and the effect of the additional flexibility caused by the foundation to the response of the superstructure (inertial response) [2].

The soil response analysis is one of the most important aspects of earthquake engineering, as it will determine the ground motion that will be experienced at the top of soil without the

presence of a structure or the so-called free field response. The analysis involves estimation of the seismologic characteristics of the region, and determination and modeling of the soil profile and its dynamic characteristics. Further, it accounts for the multiple reflections and refractions that will occur at the soil layer interfaces as the seismic waves propagate through the soil deposits. Although special purpose computer programs exist for this purpose, the validity of the results depend greatly on how accurate dynamic soil properties are estimated, which in spite the improvements in the in-situ testing, is still a challenging task. In the present study, no soil amplification analysis was performed, rather, the considered accelerograms were used directly to excite the structure and the springs, which were used to model the foundation.

The soil medium has been analyzed by applying different soil densities in order to consider the soil stiffness. The accent of the study has been given to the soil structure interaction effects and the results are analyzed accordingly. The soil medium has been taken into consideration as a four layered infill as dense and loose medium. The bridge structure is taken to be an RC structure. The boundaries in the soil medium are considered as infinite elements in order to absorb the radiating waves.

## 3. GOVERNING EQUATIONS OF MOTION

The equations of motion of the isolated bridge model with SSI effects (Fig. 1) under two horizontal components of earthquake ground motion is expressed in the following matrix form:

$$[M]\{\ddot{z}\} + [C]\{\dot{z}\} + [K]\{z\} = -[M][r]\{\ddot{z}_g\} \quad (1)$$

$$\{z\} = \{x_1, x_2, x_3, \dots, x_n, y_1, y_2, y_3, \dots, y_n\}^T \quad (2)$$

$$\{\ddot{z}_g\} = \begin{Bmatrix} \ddot{x}_g \\ \ddot{y}_g \end{Bmatrix} \quad (3)$$

where [M], [K] and [C] represents the mass, stiffness and damping matrix, respectively, of the foundation–bridge structure system;  $\{\ddot{z}\}$ ;  $\{\dot{z}\}$  and  $\{z\}$  represent structural acceleration, structural velocity and structural displacement vectors; [r] is the influence coefficient matrix;  $\{\ddot{z}_g\}$  is the earthquake ground acceleration vector;  $\ddot{x}_g$  and  $\ddot{y}_g$  represents the earthquake ground acceleration in longitudinal and transverse directions, respectively; and xi and



$y_i$  are the displacements of the  $i$ -th node of the bridge in longitudinal and transverse directions, respectively.

#### 4. DESCRIPTION OF THE BRIDGE

Three-span reinforced concrete (RC) bridge structure typical for Republic of N. Macedonian region [9] is selected. The bridge models under consideration consist of two piers supporting the superstructure. The central piers in this type of bridges most frequently had been designed as reinforced-concrete walls.

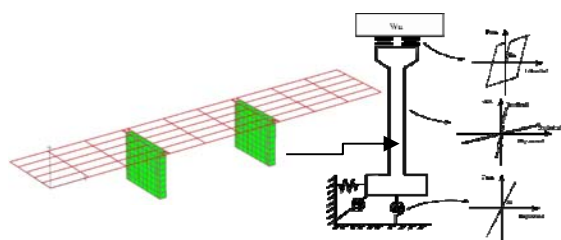


Figure 1. Three-dimensional mathematical FELISA/3M model composed of 3D finite girder and solid elements [3].

They are founded on strip foundation. The superstructure consists of 6 T shaped concrete girders resting on the substructure through elastomeric bearings and supporting the continuous reinforced-concrete slab. For the representative bridge, 3D finite element analytical model has been defined and analyzed by use of the verified FELISA/3M computer program [4]. A detailed description of the analytical model is given in Vitanova, 2015 [3]. Fig. 1 presents a typical isolated bridge structure and its corresponding model used in this study. The main and transverse girders have been defined as frame elements. The central piers have been modeled with solid elements. The support of the main girders at the ends has been modeled by link elements that represent the bearings. As for the surrounding soil, four layered infill as dense and loose medium assumption is adopted. The boundaries in the soil medium are considered as infinite elements in order to absorb the radiating waves. The effect of foundation flexibility is incorporated into the mechanical model via lateral, rocking, and cross-lateral-rocking springs.

Table 1. Geometric and mechanical properties of the models.

System properties	Loose medium	Medium dense soil
Pier height [m]	5.0	

Width of the superstructure [m]	8.0	
Middle pier cross sections [m]	0.8/7.2	
Bearing stiffness-vertical/horizontal [kN/m]	1000000.0/ 3380.0	
SSI stiffness - vertical/horizontal [kN/m]	17606.4/ 14499.8	95963.8/ 79029.7
Damping – vertical/horizontal [kN/m]	528.0/ 429.4	2722.8/ 2229.5

The seismic isolation system is considered to behave as a bilinear hysteretic spring with smooth elastic to post yielding behavior. Although this behavior is typical to lead rubber bearings, the results presented in this study could be applicable for isolation systems consisting of sliding bearings with metallic yielding devices, or sliding bearings with restoring force capabilities, such as the friction pendulum system isolators.

The geometric and mechanical properties of the models are listed in Table 1.

The bridge is subjected to a real ground motion records scaled to two intensity levels. One set of ground motion time histories is used in this study. It consists of pair of horizontal acceleration time histories from El Centro earthquake. The excitation is scaled to two levels of intensity 0.2g and 0.4g. The ground motion is used to analyze the bridge founded to loose medium and medium dense soil.

#### 5. ANALYSES RESULTS

Three span isolated girder bridge system with the soil structure interaction is analyzed using seismic excitation scaled to two levels of intensity. Nonlinear time-history analyses are performed, and the system response variables considered are the displacement of the isolation system (isolation drift) and the shear force the pier. These two response variables are critical for the design of the bridge superstructure and the design of the bridge substructure accordingly.

Fig. 2 represents the compared stress-strain curves for the middle pier bearing for loose medium and medium dense soil subjected to El Centro earthquake with 0.2g intensity. Fig. 3 show the behavior of the same bearing, but the bridge structure subjected to 0.4g intensity. All these diagrams show that the behavior of

the bearing in both horizontal directions does not change concerning the soil type.

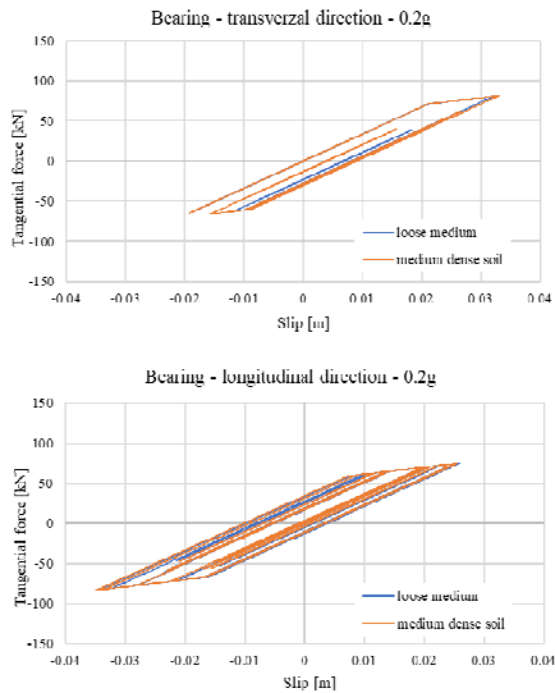


Figure 2. Stress-strain curves for bearing in horizontal directions, El Centro earthquake, 0.2g.

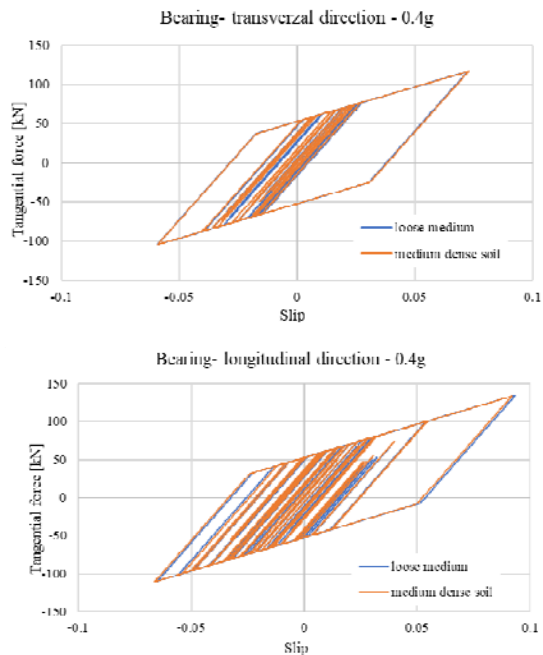


Figure 3. Stress-strain curves for bearing in horizontal directions, El Centro 1940, 0.4g.

The behavior of the upper part of structure is almost the same for both soil types. The acceleration and displacement time histories for both types of soil conditions are shown on Fig.4. The little difference can be noticed in the displacement in longitudinal direction for 0.2g. The same results are obtained for the

analyses of bridges exposed to earthquake intensity 0.4g but there are not presented in this paper. Regarding the displacement of the top point of the pier, i.e. bottom point of the bearing, the results are different. In this part of the structure, the difference is significant in both directions for the both earthquake intensity (Fig. 5). The difference is more distinct for the transversal direction.

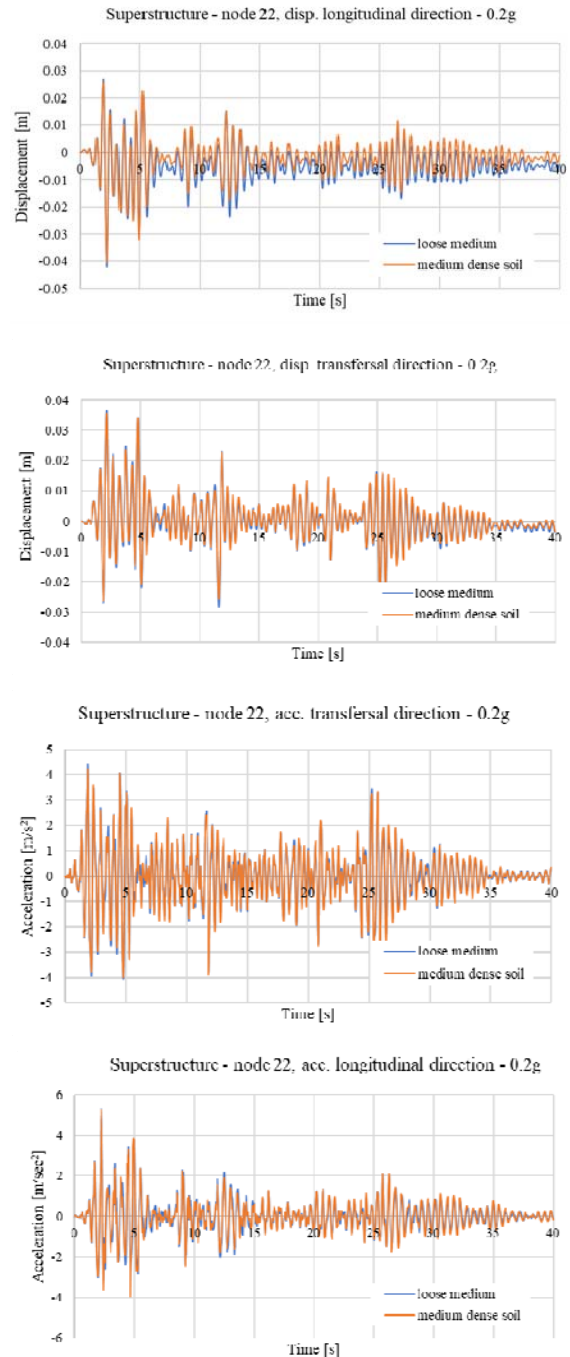


Figure 4. Time history of displacement (up) and acceleration (down) for superstructure in horizontal directions, El Centro, 1940, 0.2g.

These results show that the behavior of the upper part of the bridge structure is not adjective to the soil type of the foundation. The behavior of the substructure is directly subjected from the soil conditions. For both directions and for both intensities the displacements are larger when the structure is founded to the loose medium unlike medium dense soil.

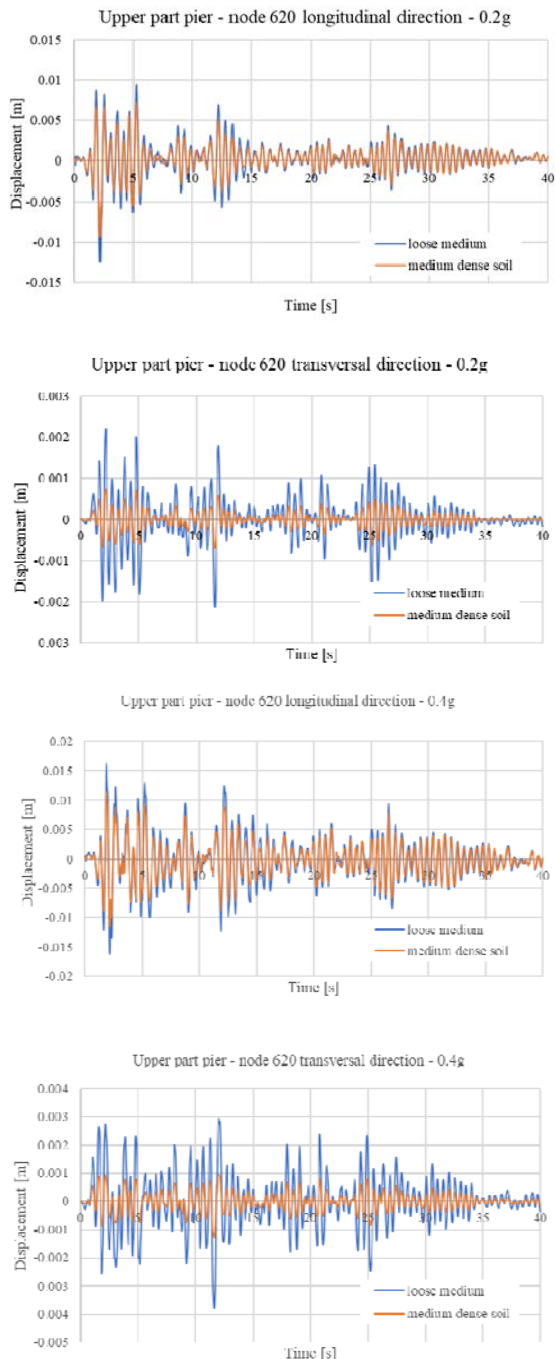


Figure 5. Time history of displacement (up) and acceleration (down) for superstructure in horizontal directions, El Centro, 1940, 0.2g, 0.4g.

Fig. 6 shows the P-Δ analyses for the bearing for both soil types and earthquake intensities. The difference between loose and medium dense soil is not so obvious.

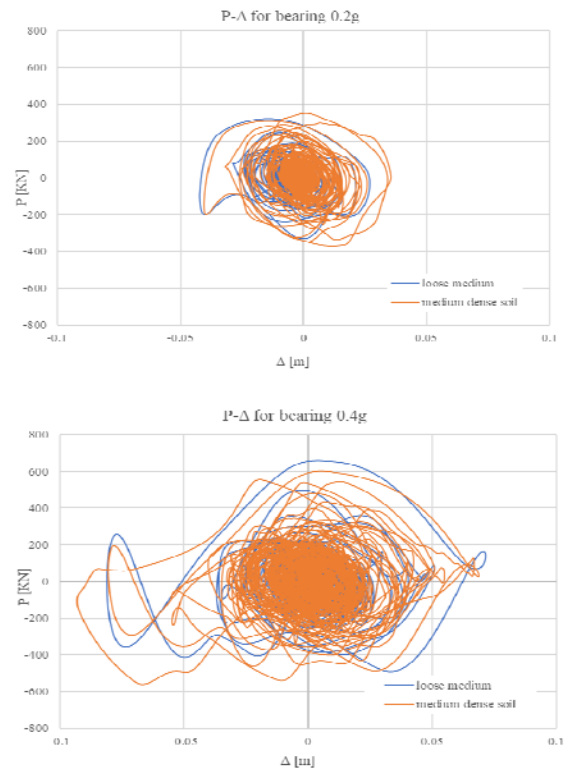


Figure 6. P-Δ diagram for the bearing, El Centro, 1940, 0.2g and 0.4g.

## 6. CONCLUSIONS

The isolated bridge system with two soil structure interaction conditions is analyzed. The soil mediums are modelled by frequency independent coefficients of soil stiffness and damping. Loose medium and medium dense soil are used for the analyses. Non-linear time history analyses are performed using real time history earthquake motion scaled to two intensities 0.2g and 0.4g. This analysis is used to account for the nonlinear hysteretic nature of the seismic isolation system on the bridge structure. The system response variables considered are displacement of the substructure and superstructure of the bridge and the shear force in the pier. These two response variables are critical for the design of the bridge superstructure and the design of the bridge substructure accordingly. From all the analyses results, the following concluding remarks can be made:

- The type of foundation soil does not have influence on the behavior of the superstructure of the bridge. The difference

of the displacement and acceleration in upper structure node due to earthquake with the same intensity and same is negligible.

- There is no significant difference between nonlinear behavior of the bearing elements when the bridge is analyzed on the loose medium and medium dense soil.
- The variation in the damping in the bearings does not have noticeable effects on the response of isolated bridges with SSI effects.

## REFERENCES

- [1] NEHRP. (1997). NEHRP recommended provisions for seismic regulations for new buildings and other structures, Parts 1 and 2, Building Seismic Safety Council, Washington, D.C.
- [2] Ucak, A., & Tsopelas, P. (2008). Effect of Soil–Structure Interaction on Seismic Isolated Bridges. *Journal of Structural Engineering*, 134(7), 1154–1164. doi:10.1061/(asce)0733-9445(2008)134:7(1154)
- [3] Vitanova, M. (2015). Seismic Fragility Assessment of Multi Span Concrete Bridge Structures Typical for Republic of Macedonia. PhD Thesis, Institute of Earthquake Engineering and Engineering Seismology, “Ss. Cyril and Methodius University”, Skopje, Republic of N. Macedonia
- [4] FELISA/3M (2007). Verification Manual for 3D Analyses. Institute of Earthquake Engineering and Engineering Seismology, “Ss. Cyril and Methodius University”, Skopje, Republic of Macedonia



## SEISMIC DESIGN CODES FOR TUNNELS AND UNDERGROUND STRUCTURES

### AUTHORS

#### **Elefterija Zlatanovic**

PhD, Assistant Professor  
University of Nis  
Faculty of Civil Engineering and Architecture – Niš  
Aleksandra Medvedeva 14, 18000 Niš, Serbia  
elefterija.zlatanovic@gaf.ni.ac.rs

#### **Vlatko Sesov**

PhD, Full Professor  
University “Ss. Cyril and Methodius” of Skopje  
Institute of Earthquake Engineering and  
Engineering Seismology (IZIIS) – Skopje  
Todor Aleksandrov 165, 1000 Skopje, North  
Macedonia  
vlatko@iziis.ukim.edu.mk

#### **Dragan Lukic**

PhD, Full Professor  
University of Novi Sad  
Faculty of Civil Engineering – Subotica  
Kozaračka 2a, 24000 Subotica, Serbia  
drlukic.lukic@gmail.com

#### **Zoran Bonic**

PhD, Associate Professor  
University of Nis  
Faculty of Civil Engineering and Architecture – Niš  
Aleksandra Medvedeva 14, 18000 Niš, Serbia  
zoran.bonic@gaf.ni.ac.rs

#### **Nebojsa Davidovic**

PhD, Assistant Professor  
University of Nis  
Faculty of Civil Engineering and Architecture – Niš  
Aleksandra Medvedeva 14, 18000 Niš, Serbia  
nebojsa.davidovic@gaf.ni.ac.rs

Transportation networks, with tunnels as their integral parts, are considered to be of paramount importance when the risk under strong earthquakes is considered. Namely, accessibility of roads affects the speed and the scope of the emergency measures to be provided in the very immediate post-earthquake emergency and relief operations. In addition, the seismically induced damage to the infrastructure could severely affect the economy of a region due to the time required to restore the functionality of the network. Moreover, underground structures are quite often located under densely populated urban areas. Considering all the former facts, these structures require very high standards in terms of their stability and safety.

In this respect, the paper is dealing with an overview of the current state of achievements in the area of seismic design codes for underground facilities, with an aim to point out to that nowadays, in spite of a significant step forward in the scientific–research work concerning seismic analysis of tunnels over the past decade or two, yet, even in the most developed countries, there still exists a lack of systematic and precisely established seismic design rules for tunnels and underground structures, which are of huge importance.

**Keywords:** tunnel structures, seismic performance, seismic design, codes.

### 1. INTRODUCTION

Contemporary streams of everyday life point out to the fact that the today necessity for using space under the ground is the greatest than ever. The steady rise of population in large cities, density of transportation, and need for storage capacity have led, inevitably, to an increased use of underground structures in modern civilisation. These facilities are a vital part of the infrastructure of the modern society and are used for a wide range of applications (Figure 1), including highways, railways, subways, material storage, water transport and sewage, as well as scientific purposes as the CERN in Switzerland.



Figure 1. Contemporary tunnel structures and underground facilities

Thus, for the reasons of the overpopulation and the lack of space, tunnels and underground structures have a significant role in the development of urban areas. Some of these areas are prone to frequent earthquakes. More than fifty percent of the world population live in urban areas, whereas over seventy percent of that population live in earthquake prone areas. The Balkan region is in the seismic active area.

Historically, underground facilities have experienced a lower rate of damage in comparison with surface structures, and initially, tunnel structures were designed with no regard to seismic effects. Namely, being confined by the surrounding medium (soil/rock), these structures have long been assumed to have good seismic performance, unless they are located within active faults or within liquefied soil zones. Therefore, in a quite long time, earthquake-induced tunnel damage did not take enough attention as it was the case with surface structures. Nevertheless, some underground structures have experienced significant damage in recent large earthquakes, including the 1995 Kobe earthquake in Japan, the 1999 Chi-Chi earthquake in Taiwan, as well as the 1999 Kocaeli earthquake and the Duzce earthquake in Turkey. As the tunnel number and its seismically induced damage and failure increased, the widely accepted idea that tunnels and underground structures are invulnerable to earthquakes has appeared to be illusive, and this problem has attracted the attention of experts and scientists around the

world, reviving the interest in the associated design and analysis methods.

The seismic response of tunnels, and in general of underground structures, is significantly different from that of above-ground facilities. Therefore, the design of underground facilities, in order to withstand earthquake-induced loading, has aspects that are quite different from the seismic design of surface structures and is unique from several viewpoints. Namely, the features of tunnels make their seismic behaviour distinct from most surface structures, among which the most notable are their complete enclosure in soil or rock as well as their significant length.

Since the overall mass of a tunnel structure is usually small in comparison with the mass of the surrounding medium (soil or rock), consequently, the inertia of the surrounding ground is large relative to the inertia of the structure, and the stress confinement provides high values of radiation damping. Therefore, the seismic response of tunnel structures is mainly controlled by the imposed strain field and its interaction with the structure, and not by the inertial characteristics of the structure itself [14]. Because of the restriction of the surrounding medium, it is unlikely that they could move to any significant extent independently of the medium or be subjected to vibration amplification. In comparison with surface structures, which are generally unsupported above their foundations, the underground structures can be considered to display appreciably greater degrees of redundancy due to the support from the ground. These are the main factors contributing to the better earthquake performance data for underground structures than their aboveground counterparts [16].

As a consequence of the constraint by the surrounding medium (soil or rock), the deformation shapes of underground structures and super-structures are different. The deformation of the underground structure under horizontal seismic loads appears a shear shape mainly, whereas the super-structure bears a combined action of moments, shear forces, and torques. Between the medium and underground structure the soil–structure interaction exists, which is under seismic impact to a great extent more complex in comparison with that one considering surface structures. Accordingly, the restriction of the surrounding ground cannot be neglected, which is different from super-structures, in which case only foundations are exposed to soil–structure interaction and vibrations of soil particles

imposed to foundations are being transmitted to a structure above the ground. On the contrary, when it comes to tunnel structures, soil–structure interaction effects are induced along an overall contour of the structure, and a shape of interaction depends mainly on a type of a construction procedure, i.e., on a methodology of excavation and installing of a tunnel support system.

For long structures such as tunnels, different ground motions may be encountered by different parts of the structure (the motion could vary significantly in amplitude and phase along tunnel's length), and travelling wave effects must be considered. This spatial incoherence may have a significant impact on the response of the structure, since it tends to increase the strains and stresses in the longitudinal direction. There are four major factors that may cause spatial incoherence: wave-passage effects, extended source effects, ray-path effects caused by inhomogenities along the travel path, and local soil site effects [6].

Earthquake damage to tunnel structures is also proved to be better correlated with ground particle velocity and displacements than acceleration.

A number of studies [6,12,15,16] have indicated that the damage of tunnels is influenced by numerous factors, which could be grouped in three major aspects. The first one is the earthquake motion in terms of the earthquake intensity, the spectrum characteristics, etc. The second aspect is the structure condition of the tunnel, such as (non)existence of lining, its integrity, and the construction quality. The third aspect is related to the tunnel environment conditions in terms of the properties of the surrounding medium, overburden depth, running across the fault zone, and so on.

Tunnels are crucial facilities in transportation network, and occurrence of a seismic event can cause a loss of human lives and damage to the infrastructure. It could severely influence the rescue operations and repair work after earthquake directly due to intermission of the transportation network and affect the economy of a region considering the time required to restore the functionality of the network.

## 2. SEISMIC DESIGN CODES FOR TUNNEL STRUCTURES

Considering that quite often tunnels are located under densely populated urban areas, these structures require very high standards

concerning their stability and safety. Nevertheless, even in the most developed industrial countries there is a perceptible discrepancy between presently relevant regulations for underground structures, particularly with respect to earthquake activity, and the requirements for design and construction of safe and cost-efficient underground facilities.

### 2.1 SEISMIC DESIGN CODES IN JAPAN

During the Hyogoken Nanbu (Kobe) earthquake in Japan in 1995 urban facilities in Kobe city were seriously destroyed. In this large earthquake, some subway stations and tunnels suffered extensive damage (Figures 2 and 3), which was the first case of severe earthquake-induced damage to modern underground facilities [11,12,18].

Although it was believed that underground structures are not at great seismic risk unless they are located within active faults or within liquefied soil zones, the experience in the Kobe earthquake showed this conviction to be incorrect.

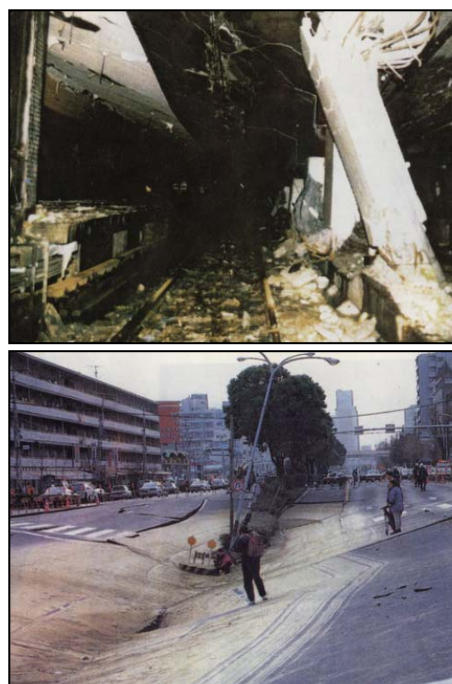


Figure 2. The seismic damage of the Daikai subway station (above) and the road subsidence above the station (below) [13]

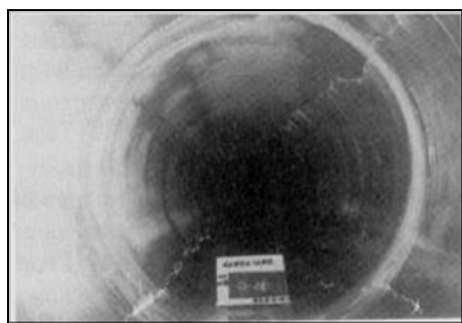


Figure 3. Damage to metro tunnel segments during the 1995 Kobe earthquake [12]

The Kobe earthquake has stirred the sharp rise in demand for rational seismic design regulations for urban underground structures.

Earthquake-resistant codes in Japan, in particular after the Kobe earthquake in 1995, have been revised by adopting two design levels representing low-to-moderate and strong earthquakes.

There are “Standard Specifications for Tunnelling” [9], published by the Japanese Society of Civil Engineers, considering mountain tunnels, shield tunnels, as well as cut-and-cover tunnels. As to the seismic analysis of shield tunnels, on the basis of the seismic deformation method, calculation approaches based on the bedded-beam model with corresponding ground-springs and structural joint-springs have been proposed. The earthquake-resistant calculation of shield tunnels employs elastic analysis.

According to the “Standard Specifications for Concrete Structures – Design” [10], in order to maintain the required seismic performance of underground structures, it is recommended to consider the use of structures and materials designed for enhancing flexibility.

## 2.2 SEISMIC DESIGN CODES IN USA

Although seismic design regulations are highly developed in the United States of America, there is an absence of proper codes in the area of seismic design of tunnel structures. The ASCE/SEI 7-10 Standard “Minimum Design Loads for Buildings and Other Structures” [1], published by the American Society of Civil Engineers, is not dealing with underground structures. As it is highlighted in Chapter 15 “Seismic design requirements for non-building structures”, buried utility lines and their appurtenances are excluded from the scope of the non-building structure requirements.

For tunnel structures, Chapter 13 of the “Technical Manual for Design and Construction

of Road Tunnels” [5], proposed by the Federal Highway Administration, is giving good practice. It provides general procedure for seismic design and analysis of tunnel structures, which are based primarily on the ground deformation approach, as opposed to the inertial force approach typical for above-ground structures. In other words, the structures should be designed to accommodate the deformations imposed by the ground. Nevertheless, the recommended procedure is not standard or regulation.

## 2.3 SEISMIC DESIGN CODES IN RUSSIA

The latest edition of the seismic standards in the Russian Federation is named SP14.13330.2014 [4] and represents the latest version of the seismic design code SniP II-7-81. In contrast to the European norms, it is a single document that covers everything needed from foundations to fire safety. In Section 7.9, which is dedicated to tunnel structures, general recommendations in terms of the application of the appropriate type of lining depending on the level of seismicity and the use of antiseismic expansion joints are given. When it comes to the calculation procedure, in Section 8.4 the impact of an earthquake is to some extent defined through the corresponding dynamic coefficients.

## 2.4 SEISMIC DESIGN CODES IN THE EUROPEAN UNION

In the countries of the European Union, standards for the seismic design of structures are implemented in Eurocode 8.

In particular, the European Standard EN 1998-4 “Eurocode 8: Design of structures for earthquake resistance – Part 4: Silos, tanks, and pipelines” [3] specifies principles and application rules for the seismic design of above-ground and buried pipeline systems, as well as storage tanks and silos of different types and uses.

In addition, the European Standard EN 1998-5 “Eurocode 8: Design of structures for earthquake resistance: Foundations, retaining structures, and geotechnical aspects” [2], as Part 5 of the European seismic regulations, has established requirements, criteria, and rules for earthquake-resistant design of different foundation systems and retaining structures, as well as for soil–structure interaction under seismic action. Yet, provisions related to the seismic design of tunnel structures are not provided within the scope of these Standards.



## 2.5 SEISMIC DESIGN STANDARDS IN SERBIA

Standards in the Republic of Serbia are being prepared in accordance with the European standards and related documents.

In the area of seismic design, there are SRPS EN 1998-4 [7] and SRPS EN 1998-5 [8], which are related to the corresponding European Standards. Accordingly, as in the case of Eurocode 8, SRPS standard prescriptions and guidelines do not specifically address the issue of seismic design of underground structures.

Previously, the “Collection of Yugoslav regulations and standards for engineering structures” [17] was published, in which within the part “Actions on structures”, a draft version of “Regulations on technical rules for the design and calculation of engineering structures in seismic areas” has been proposed. This version of the regulations envisaged the methodology of determining the seismic ground pressure on underground and buried facilities. It was the beginning of raising awareness about the importance of aseismic design when it comes to underground structures, as well as the beginning of putting this issue in the framework of standards. In spite of this concept, which at that time represented a big improvement in practice of standardisation, however, this draft is kept at the level of ideas and proposals, and never entered into force.

## 3. CONCLUDING REMARKS

By reviewing the existing standards and codes for aseismic design of structures, the conclusion that could be drawn is that there is a lack of systematic and precisely defined seismic design rules for tunnels and underground structures that are of paramount significance. The worst scenarios related to severe damage and failure of tunnels, experienced particularly during recent earthquakes, impose a necessity for a deeper consideration in terms of aseismic design and construction of these types of structures.

In addition, when it comes to twin-tunnel structures, it should be noted that investigations of the mutual effect of closely spaced tunnels are still staying in the preliminary stage. For that reason, particularly the case of closely running tunnel structures should be turned into an important direction of further development of seismic design codes, where the aspect of their minimum seismically safe distance should be an issue of all concerns [19].

Taking all into account, it should be said that a serious task lies ahead. By this work, an improvement of this situation has been attempted, as it demonstrates the call for consideration of the effects of seismic events in the design codes as the key parameters in aspects involving aseismic design and construction of tunnels and underground structures.

## Acknowledgements

The authors gratefully acknowledge the support of the “SEEFORM PhD Programme (South Eastern European Centre for PhD Formation in Engineering)”, financed by the German Academic Exchange Service (DAAD).

The support of the Ministry of Education, Science, and Technological Development of the Republic of Serbia in the frame of the scientific–research project “Development and improvement of methods for analysis of the soil–structure interaction based on theoretical and experimental research” TR36028 (2011–2019) is also greatly appreciated.

## REFERENCES

- [1] ASCE (2010), “ASCE/SEI 7-10 Standard: Minimum Design Loads for Buildings and Other Structures”, American Society of Civil Engineers, Los Angeles, USA.
- [2] CEN (2004), “EN 1998-5 Eurocode 8: Design of Structures for Earthquake Resistance – Part 5: Foundations, retaining structures, and geotechnical aspects”, European Committee for Standardisation, Bruxelles, Belgium.
- [3] CEN (2006), “EN 1998-4 Eurocode 8: Design of Structures for Earthquake Resistance – Part 4: Silos, tanks, and pipelines”, European Committee for Standardisation, Bruxelles, Belgium.
- [4] FAUFCC (2014), “SP14.13330.2014 Construction in Seismic Regions”, Federal Centre for Regulation, Standardisation, and Conformity Assessment of Technical Construction, Moskva, Russia.
- [5] FHWA (2009), “Technical Manual for Design and Construction of Road Tunnels – Civil Elements”, Publication No. FHWA-NHI-10-034, U.S. Department of Transportation, Federal Highway Administration, Washington, DC, USA.
- [6] Hashash, Y. M. A., Hook, J. J., Schmidt, B., Yao, J. I.-C. (2001), “Seismic design and analysis of underground structures”, *Tunnelling and Underground Space Technology*, Vol. 16, pp. 247–293.
- [7] ISS (2012), “SRPS EN 1998-4 Eurocode 8: Design of Structures for Earthquake Resistance – Part 4: Silos, tanks, and pipelines”, Institute for standardisation of Serbia, Belgrade, Serbia.



- [8] ISS (2012), “SRPS EN 1998-5 Eurocode 8: Design of Structures for Earthquake Resistance – Part 5: Foundations, retaining structures, and geotechnical aspects”, Institute for standardisation of Serbia, Belgrade, Serbia.
- [9] JSCE (2006), “Standard Specifications for Tunnelling”, Japanese Society of Civil Engineers, Tokyo, Japan.
- [10] JSCE (2007), “Standard Specifications for Concrete Structures: Design”, Japanese Society of Civil Engineers, Tokyo, Japan.
- [11] Konagai, K. (2005), “Data archives of seismic fault-induced damage”, *Soil Dynamics and Earthquake Engineering*, Vol. 25, pp. 559–570.
- [12] Lanzano, G., Bilotta, E., Russo, G. (2008), “Tunnels under seismic loading: a review of damage case histories and protection methods”, In G. Fabbrocino and F. Santucci de Magistris (Eds.), *Strategies for Reduction of the Seismic Risk*, pp. 65–74.
- [13] Liu, J., Liu, X. (2008), “Pushover analysis of Daikai subway station during the Osaka-Kobe earthquake in 1995”, *Proceedings of the 14th World Conference on Earthquake Engineering*, Beijing, China.
- [14] Ornthammarath, T., Corigliano, M., Lai, C. G. (2008), “Artificial neural networks applied to the seismic design of deep tunnels”, *Proceedings of the 14th World Conference on Earthquake Engineering*, Beijing, China.
- [15] Pakbaz, M. C., Yareevand, A. (2005), “2-D analysis of circular tunnel against earthquake loading”, *Tunnelling and Underground Space Technology*, Vol. 20, pp. 411–417.
- [16] Wang, J.-N. (1993), “Seismic Design of Tunnels: A State-of-the-art Approach”, Parsons, Brinckerhoff, Quade and Douglas, Inc., New York.
- [17] YASE (1995), “Collection of Yugoslav regulations and standards for engineering structures”, Yugoslav Association of Structural Engineers, Belgrade, Serbia.
- [18] Yoshida, N. (1999), “Underground and buried structure”, In Seco e Pinto (Ed.), *Earthquake Geotechnical Engineering*, Balkema, Rotterdam.
- [19] Zlatanović, E. (2016), “Contribution to the Methods of Seismic Analysis of Twin-Tunnel Structures”, Doctoral dissertation, Institute of Earthquake Engineering and Engineering Seismology (IZIIS) of Skopje, University “Ss. Cyril and Methodius” of Skopje, Republic of Macedonia, Skopje, July 2016, 223 pages.

## AUTHORS

### **Vlatko Sheshov**

PhD, Full Professor

Institute of Earthquake Engineering and Engineering Seismology - Skopje

vlatko@iziis.ukim.edu.mk

### **Marija Vitanova**

PhD, Assistant Professor

Ss "Cyril and Methodius" University  
Institute of Earthquake Engineering and Engineering Seismology - Skopje

marijaj@iziis.ukim.edu.mk

### **Radmila Salic**

PhD, Assistant Professor

Ss "Cyril and Methodius" University  
Institute of Earthquake Engineering and Engineering Seismology - Skopje

r\_salic@iziis.ukim.edu.mk

### **Kemal Edip**

PhD, Associate Professor

Ss "Cyril and Methodius" University  
Institute of Earthquake Engineering and Engineering Seismology - Skopje

kemal@iziis.ukim.edu.mk

### **Slobodan Micajkov**

BSc

Ss "Cyril and Methodius" University  
Institute of Earthquake Engineering and Engineering Seismology - Skopje

micajkov@iziis.ukim.edu.mk

### **Borjan Petreski**

MSc, Assistant

Ss "Cyril and Methodius" University  
Institute of Earthquake Engineering and Engineering Seismology - Skopje

borjan@iziis.ukim.edu.mk

# **SAFETY ASSESSMENT OF BRIDGE STRUCTURES EXPOSED TO EARTHQUAKE HAZARD**

Assessment of the stability of existing bridges is very significant in the process of defining the optimal structural measures for their maintenance and strengthening. To define the optimal structural measures for repair and strengthening, it is necessary to establish a complete database on existing bridge structures containing their identification data as well as monitor their conditions. This paper describes a study on the bridge infrastructure network in Republic of N. Macedonia realized as part of the INFRA-NAT project ([www.infranat.eu](http://www.infranat.eu)). The bridge database was developed based on the data collection form and allows to establish the detailed exposure model of the entire bridge network.

By considering the general characteristics of all the structures, to develop fragility functions for bridges exposed to seismic hazard, representative samples of bridges are considered. The connectivity of the network is modelled and the entire bridge network vulnerability is considered in a more comprehensive and global manner for seismic hazard. The scope of this work is to provide practical web-based tools and databases for each country with which more informed decisions can be made related to the most vulnerable parts of the country and where resources should be invested for increased resilience.

**Keywords:** bridge structures, seismic hazard, data base, fragility functions, NLTHA.

## **1. INTRODUCTION**

A functioning infrastructure network during emergencies is an important aspect for every country. Bridges represent critical elements as they provide reliable modes of transportation throughout a region. The growth of traffic loads, the variability of wind, seismic and hydraulic forces, and the natural deterioration of constitutive materials of bridges tend to increase their vulnerability. Since their collapse imposes high costs for their users and the local economies, they require proper and timely maintenance. Without adequate maintenance, the risk of collapse and the

costs for their repair are increasingly higher over time, especially at the end of their serviceability period. Adding that much of the bridge infrastructure in N. Macedonia was constructed prior to the 1990s, when new legislation became effective [1], it is of crucial importance to monitor and assess the existing bridge infrastructure. Due to the fact that the collapse of bridges and the risk pertaining to fatalities are undesirable for the society, bridge engineering has developed tools for achieving acceptable conditions regarding bridge safety and functionality. These tools allow integration of assessments of bridge conditions, making decisions about maintenance and planning maintenance budget allocation over time for the road network or a single bridge.

A major component in determining the vulnerability of bridge infrastructure is associated with seismic events. Ensuring bridges do not collapse and are usable during the aftermath of an earthquake is crucial for relief efforts (e.g. access to hospitals, aid to be dispatched).

## 2. SELECTION OF BRIDGES

For the needs of the project aim, extensive activities have been carried out to collect and harmonise the bridge inventory data, with focus on the bridge structures placed on the main transportation routes. Depending on the level of available data, categorisation of the bridges was performed. Systematisation of the bridge inventory results in proper definition of characteristic bridge typologies for which physical vulnerability is assessed.

According to data completeness, the bridges are divided into 3 levels, starting from the Level 0 (most basic data involving location and total length) up to detailed data referring to type of superstructure, dimensions of structural elements, type of abutments and central piers, materials used for construction of the super- and sub-structure, type of traffic for which a bridge is intended as well as conditions of bridge structures (Level 1 and Level 2).

Out of the total number of collected bridges, there is data for material and structural system (Level 1) for 398 bridges, accounting for 59% of the total number of bridges, while more detailed information including data about damages (Level 2) exists for 196 bridges, or 29% of the total number of bridges, presented in Figure 1.

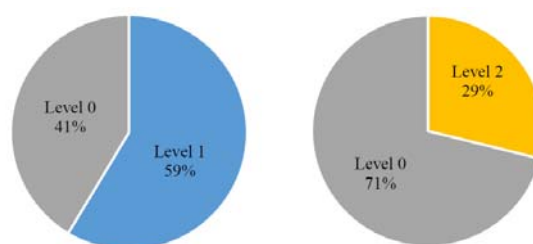


Figure 1. Percentage of bridges belonging to each information level.

Additionally, several classes of bridges were identified according to the building material. The statistics show that the most numerous are the reinforced concrete bridge structures, accounting for 92% of the total number of bridges. Considerably smaller number of bridges accounting for 4% of the total are composite reinforced concrete and stone, while the remaining bridges account for 4% of the total number of bridges. Therefore, it is straightforward to state that the reinforced concrete bridges dominate the bridge stock in N. Macedonia and that their importance weighs mostly in the selection of the bridge typologies.

Regarding the deck structural system, out of the total number of bridge structures located along the main routes in N. Macedonia, the most numerous are simply supported beam bridges (57%) and continuous beam bridges (32%) shown in Figure 2. From the total number of bridge structures, 9% represent frame systems, while negligible are the arch bridges with 2% and the remaining 1% with other structural systems.

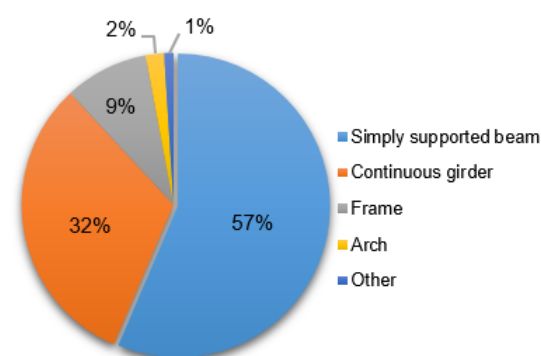


Figure 2. Percentage of bridges according to the structural system.

Considering the need for classifying the bridge stock into several categories, several other characteristics of the bridges were taken into account. Namely, the number of spans, deck width, span length and pier height were the key parameters for developing the most representative bridge taxonomies and subjecting them to nonlinear time history analyses.

Thus, it was obtained that most of the bridge structures have a total deck width of around 10m. As to the number of spans, the most common are single span bridges (37%) and three-span bridges (33%). Bridges with two spans account for 11% of the total number of bridges, whereas bridges with four and more than four spans individually account for less than 10%. The mean value of the maximum span of the considered bridges amounts to 16m, i.e., most of the bridges (90%) are with a maximum span ranging between 7 to 25m.

In the end, according to the relevance of each taxonomy, 4 types of representative bridges were selected for analysis. The selection was based on the number of bridges from each typology in the total bridge stock of N. Macedonia. Figure 3 describes the selection process of the bridges and presents the most relevant bridge typologies.

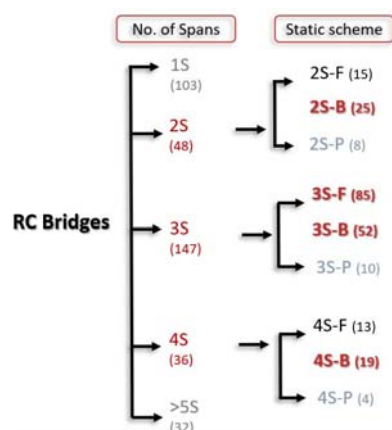


Figure 3. Bridge taxonomy definition.

It is noticed from Figure 3, that even though there are many single span (1S) bridges in the bridge stock of N. Macedonia, they are not critical for the seismic resilience of the infrastructure since they behave rather well during seismic events. Therefore, 1S bridges are not included in the fragility analysis. In contrast, the bridges with 5 or more spans (>5S) were not considered in the fragility analysis due to the low number of representative specimens. Under the static scheme column, F, B and P stand for frame, beam and plate systems accordingly.

### 3. BRIDGE MODELING

The modelling of the bridges was performed in OpenSees software following the need for fast and reliable nonlinear time history analysis [8]. Basically, the bridges are composed of a single roadway supported on sub-structural components. Being the most critical parts for

the seismic response of a bridge structure, the elements of the sub-structure are modelled in a more detailed way. For the deck and pier segments, frame elements were used. *Elastic* and *BeamWithHinges* elements were employed for the modelling of the deck and the piers, respectively following the assumption that plastic hinges might occur in the piers exclusively. The other comprising elements were mostly *zeroLength* and *twoNodeLink* elements applied for the deck connections and the bearings. Inelasticity was applied through the *BeamWithHinges* and the *zeroLength* elements using cross-sectional discretization with fibers. The mathematical model of a characteristic bridge is presented below in Figure 4.

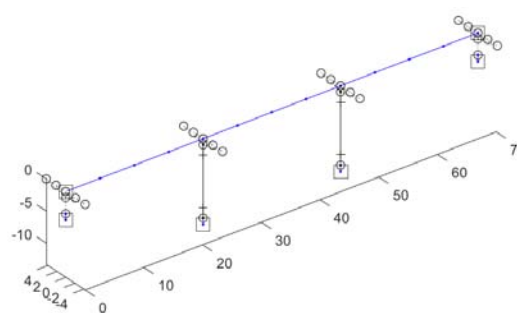


Figure 4. FE model of a characteristic 3 span simply supported beam bridge.

Regarding the materials, *Concrete01* and *Steel01* materials from the OpenSees database were applied for the fiber section of inelastic elements.

The analyses were performed in a semi-automated manner. To be precise, the geometry was defined manually but the other processes were generated by an application developed specifically for the need of computing the fragility curves for bridges - BRI.T.N.E.Y (BRidge auTomatic Nonlinear analysis based Earthquake fragilitY). BRI.T.N.E.Y performs tasks to read the bridge geometry data and creates its FE models for carrying out analysis with OpenSees [3]. The post-processing of the results is also performed by the same automatic application.

### 4. SEISMIC HAZARD DEFINITION

One of the basic project objectives was to select a reliable and up-to-date seismic hazard model that will provide a realistic estimate on the expected ground motion intensity, leading to achieve best vulnerability estimate on the bridge infrastructure. Reliable estimation of seismic hazard is one of the key components in selection

of appropriate ground motion accelerograms that will be further used for the dynamic analysis of the specific bridge typologies.

For the purpose of the project, the most updated research, namely the EC8 National Model [9], was chosen to be used as reference seismic hazard to be implemented for further calculations in the OpenQuake engine [6].

Six sites (Figure 5, 6) were selected for further analyses. They were selected according to three main criteria: bridge locations, different hazard values considering the peak ground acceleration (PGA) for the 475 year-return period, Figure 5, and different soil categories according to the  $V_{S30}$  values of Figure 6.

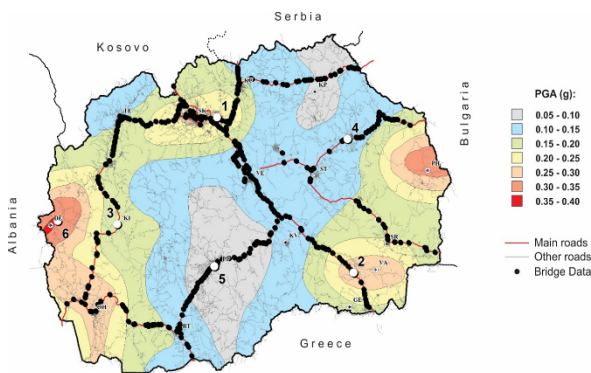


Figure 5. Selected sites with different hazard levels, superimposed on the PGA map for rigid soil conditions and the 475 year-return period.

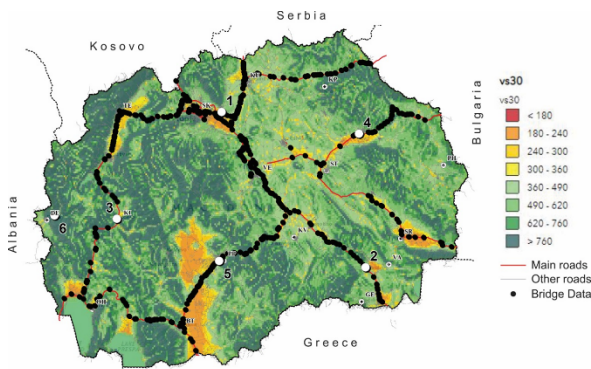


Figure 6. Selected sites with different site conditions, superimposed on the USGS VS30 map.

In particular, sites numbered 3, 5 and 6 are representative of bridges located in regions characterized by stiff soil conditions, corresponding to EC8 soil class B, while sites numbered 1, 2 and 4 are representative of bridges located on soft soil conditions, corresponding to EC8 class C. Site-specific hazard analyses were performed for the 6 sites for 7 return periods (98, 224, 475, 975, 2475, 4975 and 9975 years, corresponding to probabilities of exceedance in 50 years of 40%, 20%, 10%, 5%, 2%, 1% and 0.5%)

assuming a representative value of  $V_{S30}=600\text{m/s}$  for EC8 soil class B and  $V_{S30}=300\text{m/s}$  for EC8 soil class C.

The disaggregation analyses were performed both in terms of PGA and average spectral acceleration (AvgSA) [7] for the six selected sites for the most representative branch of the adopted logic tree, which was associated with the gridded source model (M1) and the GMM by Chiou and Youngs (2014) [4]. The AvgSA was computed over the range of periods 0.2s-1.0s, which was considered sufficiently wide to capture the first mode responses of most bridge structures, in addition to their associated higher mode response.

In this study, the Conditional Spectrum (CS) was used as an alternative to the more common and widely adopted Uniform Hazard Spectrum (UHS). The CS represents the expected response spectrum conditioned on the exceedance of a target spectral acceleration value at the period of interest [2].

Accelerogram selection for this study was performed by recasting of conditional spectrum record selection based on AvgSA [7]. An example of the records selection for Site 2, referred to the return period of 475 years, is shown in Figure 7 (the 30 green lines are the RotD50 response spectra of selected ground motions, while their average is represented by the blue line). The red lines represent the target conditional spectrum (average and average  $\pm 2$  standard deviations).

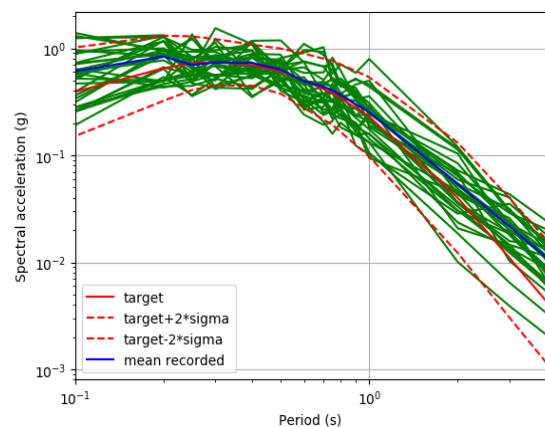


Figure 7. Conditional spectrum AvgSa-based record selection performed for Site 2, considering the 475-year return period.

## 5. FRAGILITY CURVES

Bridge fragility curves are essential for the estimation of the road system's resilience,



recovery planning, as well as pre- and post-earthquake retrofit prioritization [10]. However, it is impossible to compile a database encompassing all usual types of bridges within a single study [11]. Thus, the database presented herein may be used for a large number of bridges, with special focus on typologies commonly found in the main roads in N. Macedonia.

Methodologies for obtaining the fragility curves can be categorized based on several parameters, such as: analysis methods, seismic hazard, choice of critical components, engineering demand parameters, limit states etc.

The adopted methodology for the fragility assessment of the bridges in this study is based on inelastic response history analysis. As previously mentioned, the fragility curve is obtained point by point for 7 increasing hazard levels.

Regarding the critical components for the fragility analysis of bridges, previous research studies have been addressed in order to choose the most suitable methodology. Having in mind the extensiveness of the study and the bridge stock, the most appropriate approach was to limit the choice of critical components to the piers and bearings [5,12,13] in order to concentrate only on the structural elements that suffer greatly during seismic events.

Then, the failure mechanisms are defined for the chosen critical elements. The failure of the piers is reached either due to shear failure  $V$  or because the chord rotation  $\theta$  is exceeded. Bearings, on the other hand, can fail because of exceedance of their displacement capacity. It is termed as 'unseating' and can either be manifested as a simple fall of the deck from the bearing or a full loss of support from the pier head.

In the end, two performance levels or limit states (LS) are considered in this study, both adequate for the purpose of connectivity analysis over the damaged road network and consistent with current resolution of damage predictions via numerical analysis: damage (SLD) and collapse (SLC). The methodology previously described for computing fragility curves is therefore applied twice, with different response threshold (capacity) values. Figure 8 shows the characteristic fragility curves for the pier deformation capacity and unseating of the bearings for a single bridge analysis.

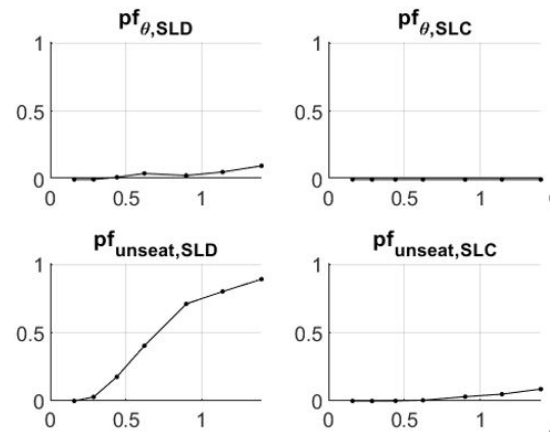


Figure 8. Characteristic fragility curves for a single bridge regarding deformation capacity  $\theta$  and unseating.

The fragility curves for each typology are defined as pairs of mean ( $\mu_{lnY}$ ) and standard deviation ( $\sigma_{lnY}$ ) that define a lognormal distribution, Equation 1, which describes the probability of exceedance of a specific damage state (i.e. damage or collapse,  $LS$ ) based on the intensity of ground motion shaking,  $IM$ . After the thorough application of the previously defined methodology, the results obtained for the taxonomies considering the beam bridges are presented in Figure 9.

$$p_f(LS | IM : x) = \Phi \left( \frac{\ln\left(\frac{x}{\mu_{lnY}}\right)}{\sigma_{lnY}} \right) \quad (1)$$

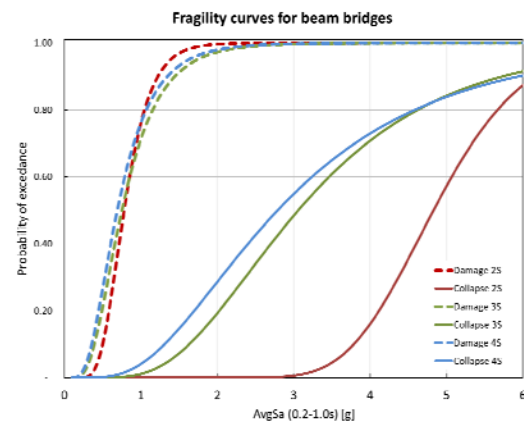


Figure 9. Fragility curves for beam bridges.

## 6. CONCLUSIONS

The study presents the developed and implemented methodology in order to obtain taxonomy level fragility curves for

representative bridge types within the context of INFRA-NAT project. Once the inventories were categorized, a numerical modelling framework was executed to produce sets of synthetic numerical models that are characteristic of a group to the taxonomies they represent, based on the necessary assumption that the behavior of the synthetic group will be equivalent to the one of the real bridges that are a part of that same taxonomy. The performance of each taxonomy was evaluated by performing an extensive number of non-linear time-history analysis of the synthetic bridge models to sets of earthquakes, consisting of 30 bi-directional ground motion records for each of the seven intensity measure levels (total of 210 records per set). The performance of each bridge-record combination was then associated to the probability of exceedance of two limit states (damage and collapse) and later processed to obtain continuous fragility functions for each. Finally, results were combined to produce taxonomy level fragility curves that will be applied to the real bridges in the inventory of N. Macedonia by implementing them in a specifically built web-based platform that will carry out risk calculations, developed as a part of the scope of INFRA-NAT.

### Acknowledgements

This research has been carried out under the INFRA-NAT project ([www.infra-nat.eu](http://www.infra-nat.eu)) co-funded by European Commission ECHO – Humanitarian Aid and Civil Protection. Project reference: 783298 – INFRA-NAT – UCPM-2017-PP-AG.

### REFERENCES

- [1] Austroads. (2002), "Bridge Management Systems: The State of the Art." Rep. No. AP-R198, Australian and New Zealand Road Transport and Traffic Authorities, Australia.
- [2] Baker J. W. (2011), "Conditional Mean Spectrum: Tool for ground motion selection". *Journal of Structural Engineering*, 137(3), pp. 322-331.
- [3] Borzi, B., Ceresa, P., Franchin, P., Noto, F., Calvi, G. M., Pinto, P. E. (2015), "Seismic vulnerability of the Italian roadway bridge stock", *Earthquake Spectra*, 31(4), pp. 2137-2161.
- [4] Chiou B. S-J., Youngs R. R. (2014), "Update of the Chiou and Youngs NGA model for the average horizontal component of peak ground motion and response spectra". *Earthquake Spectra*, 30(3), pp. 1117–1153.
- [5] Choi E., DesRoches R., Nielson B. (2004), "Seismic fragility of typical bridges in moderate seismic zones". *Engineering Structures* 26(2), pp. 187–199.
- [6] GEM. (2019), "The OpenQuake-engine User Manual", *Global Earthquake Model (GEM) OpenQuake Manual for Engine version 3.6.0*.
- [7] Kohrangi M., Bazzurro P., Vamvatsikos D., Spillatura A. (2017), "Conditional spectrum-based ground motion record selection using average spectral acceleration". *Earthquake Engineering and Structural Dynamics*, 46, pp. 1667–1685.
- [8] McKenna F., Scott M. H., and Fenves G. L.; (2010), "Nonlinear finite-element analysis software architecture using object composition", *Journal of Computing in Civil Engineering*; 24; pp. 97–105.
- [9] Milutinovic Z., Salic R., Dumurdzanov N., Cejkovska V., Pekevski L., Tomic D. (2016), "Seismic Zoning Maps for Republic of Macedonia according the Requirements of MKS-EN 1998-1:2004 - Eurocode 8", IZIS Report, 2016-26 (MKC EN 1998-1:2012/HA:2018). 8
- [10] Stefanidou S., Kappos A. (2019), "Bridge-specific fragility analysis: when is it really necessary?". *Bulletin of Earthquake Engineering*, 17(4), pp. 2245-2280.
- [11] Stefanidou S., Kappos A. (2017), "Methodology for the development of bridge-specific fragility curves". *Earthquake Engineering and Structural Dynamics*, 46(1), pp. 73-93.
- [12] Tsionis G., Fardis M. (2012), "Seismic fragility of concrete bridges with deck monolithically connected to the piers or supported on elastomeric bearings". In: 15th World conference of earthquake engineering, Lisbon, Portugal.
- [13] Yi J., Kim S., Koshiyama S. (2007), "PDF interpolation technique for seismic fragility analysis of bridges". *Engineering Structures* 29(7), pp. 1312–1322.

## AUTHORS

### **Koce Todorov**

PhD, Associate Professor  
University "Ss. Cyril and Methodius"  
Faculty of Civil Engineering – Skopje  
todorov@gf.ukim.edu.mk

### **Ljupco Lazarov**

PhD, Full Professor  
University "Ss. Cyril and Methodius"  
Faculty of Civil Engineering – Skopje  
lazarov@gf.ukim.edu.mk

# **DISPLACEMENT DISTRIBUTION INDEX AS A TOOL FOR IDENTIFICATION OF VERTICAL IRREGULARITY OF STRUCTURES**

Vertical regularity plays an important role in the behavior of structures exposed to seismic action. The structure can be classified as regular if it meets certain prescribed requirements, which are usually explicitly defined in the seismic design codes. In this paper, the vertical irregularity of structures has been identified through the ratio between the maximum inter-story drift and maximum roof drift. In order to quantify this relationship, regardless of the number of stories, the parameter named as index for distribution of displacement at height (DDH) has been defined. Evaluation of the proposed index has been done through an extensive incremental dynamic analysis of six masonry infilled reinforced concrete frames with open first story. Obtained results shows that this index can be used as an indicator for the detection of structural potential to go into the unfavorable failure mechanism.

**Keywords:** vertical irregularity, displacement distribution index, masonry infill.

## **1. INTRODUCTION**

Building structures with irregular distribution of mass, stiffness, strength and geometry along building height may be classified in the group of structures with vertical irregularities. Vertical irregularity is manifested by the appearance of two effects: weak story and soft story. The term weak story is used when lateral strength of one story is less than lateral strength of the story above, while the term soft story is defined to exist where there is a story in which the lateral stiffness is less than the stiffness in the story above. During the strong earthquakes, such an irregular stiffness and strength configuration may result with the concentration of lateral deformations at the level of a single story, which may lead to an undesirable soft story failure mechanism, Figure 1. Many building structures having soft story, suffered major structural damage and collapsed in the recent earthquakes. Large

open areas with less infill and exterior walls in ground floor compared to upper floors are the cause of damages. In such buildings, the stiffness of the lateral load resisting systems at those stories is quite less than the stories above or below [5,6,7].



Figure 1. Soft-story mechanism in the ground floor.

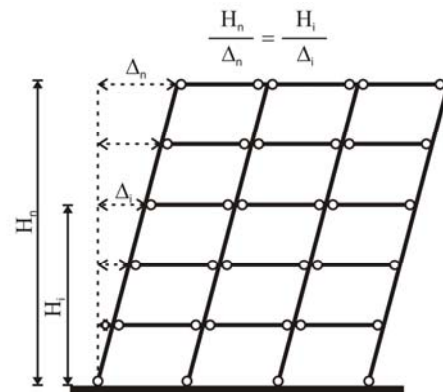
There are many variable parameters and constructional features that affect regularity and therefore it is quite difficult to characterize whether a structure is regular or irregular [2,8]. An additional impact on the degree of irregularity amplification may also be caused by non-structural elements such as infill walls, whose impact is often neglected in the process of analysis and design.

Taking into account the above facts, the codes for design of seismic resistant structures define different levels of design seismic forces, depending on whether the prescribed vertical regularity criteria are met. According to the applicable Rulebook in our country, Rulebook on technical norms for construction of buildings in seismic areas [4], structures with flexible story, i.e. with a sharp change of stiffness in height, are designed for double greater seismic lateral force compared to regular structures. Although such a provision exists, the Rulebook does not have an objective criterion for classification of structures as a flexible story structure. According to EN1998-1 [1,3] structures that do not meet the vertical regularity criteria are designed with a 20% reduced behavior factor value, resulting in a 1.25 times greater design seismic forces compared to regular structures. Although there are criteria for vertical irregularity in EN1998-1, some of them are subjective in nature.

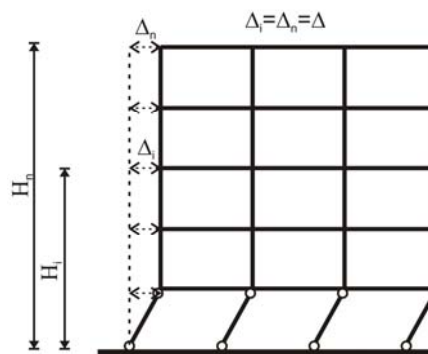
## 2. INDEX FOR DISTRIBUTION OF DISPLACEMENT AT HEIGHT

The displacements at the top of the structure represent a global measure of the degree of deformation which can be close related with the degree of structural damage. The limit

values of the total displacements which correspond to a certain degree of damage, depends on the distribution of the displacements by height. For a multi-story structure, peak top displacement in the range of 0.2% from the total height may represent an insignificant degree of damage, if the inter-story drifts are uniformly distributed along the height, Figure 2a) or they can be an indicator of serious damage, if the inter-story drifts are concentrated at one story level, Figure 2b).



a) beam sway mechanism of failure



b) soft story mechanism of failure

Figure 2. Soft-story mechanism in the ground floor.

The ratio between maximal inter-story drift  $\max ISD = (\Delta_i - \Delta_{i-1})_{\max} / h_i$  and maximal top drift  $\max TD = d_n / H_n$  can be a good indicator of damage distribution along the building height. In order to quantify this relationship, regardless of the number of storeys ( $n$ ), the parameter named as index for distribution of displacement at height (DDH) with the boundary values from 0 to 1 was defined, Equation 1.

$$DDH = \frac{\frac{\max ISD}{\max TD} - 1}{n - 1} \quad (1)$$

For the same values of  $\max ISD$  and  $\max TD$ , which implies a triangular distribution of displacement, or formation on beam sway

mechanism, the value of this index is close to 0. Higher values of this index (close to 1) indicate a concentration of inter-story drift on one story level, which is characteristic for the formation of soft story mechanism.

### 3. EVALUATION OF PROPOSED INDEX FOR MASONRY INFILLED FRAMES WITH OPEN FIRST STORY

The proposed index for distribution of displacement at height was evaluated through an extensive nonlinear dynamic analysis. Six reinforced concrete frames with different number of story ( $n=2, 3, 5, 7, 10$  and  $13$ ) in the following text marked as frames R1, R2, R3, R4, R5 and R6 were analyzed. All analyzed structures are designed as three bay plane frames with a span of 5m and a constant story height of 3m. In the phase of assessment, all frames were additionally upgraded with the presence of masonry infill panels in all spans and stores, except for the first one. Masonry infill was defined with two different strength

and stiffness characteristics, namely weak infill (WI) and strong infill (SI). All frames were exposed to twenty-one different earthquake ground motions, grouped into three groups of 7 records. All selected records were scaled to ten different amplitudes, based on scaling of pick ground acceleration [6,7].

#### 3.1 TOP DISPLACEMENT V.S. INTERSTORY DRIFT RATIO

The relationship between the maximal inter-story drifts (maxISD) and the maximal top drifts (maxTD) for the sixth analyzed frames obtained with the individual records from the three groups of earthquakes scaled to ten levels of peak ground acceleration are presented at Figure 3. From the presented diagrams a nearly linear tendency of this relationship can be noticed. The largest deviations are observed at the bare frames (BF) and usually are result of earthquakes records from the first group, which contains registrations of earthquakes with a dominant frequency range of low periods.

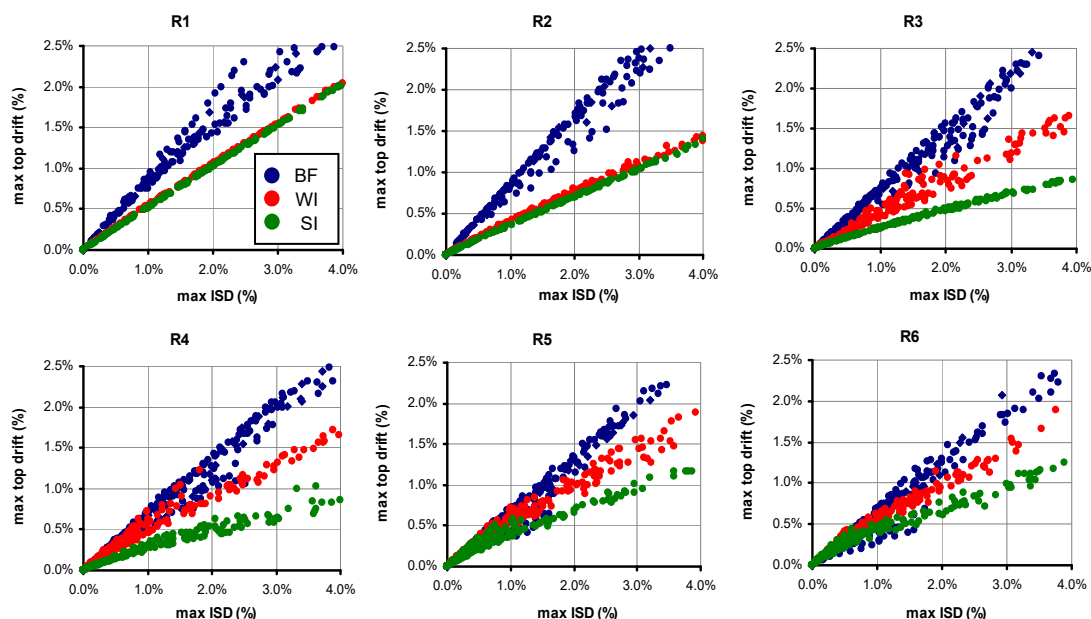


Figure 3. Ratio between the maximal inter-story drifts (maxISD) and the maximal top drifts (maxTD) of the analyzed frames.

In infilled frames R1 and R2, as well as the frame R3 with strong infill, there are almost no deviations from the linear relationship, which is due to the concentration of displacements at the level of the first story. In the higher infilled frames, the ratio between the maximal top drift and maximal inter-story drift is greater, indicating a more uniform distribution of the displacements in height. With increasing of the displacements, this ratio decreases, indicating a concentration of damages on separate

floors. For frames R1 and R2 with weak and strong infill the ratio  $\text{maxTD} - \text{maxISD}$  is almost identical, indicating a slight influence on the characteristics of the infill on the distribution of displacements. In the higher frames with a strong infill this ratio is lower, indicating the concentration of displacements at the level of one (in the case of frames R1, R2 and R3) or at the level of several floors (in frames R4, R5 and R5) of the considered structures.



The change of the DDH index, in the function of the peak ground acceleration, for the analyzed frames, exposed on the individual

records from the second and third group of earthquakes is presented at Figure 4.

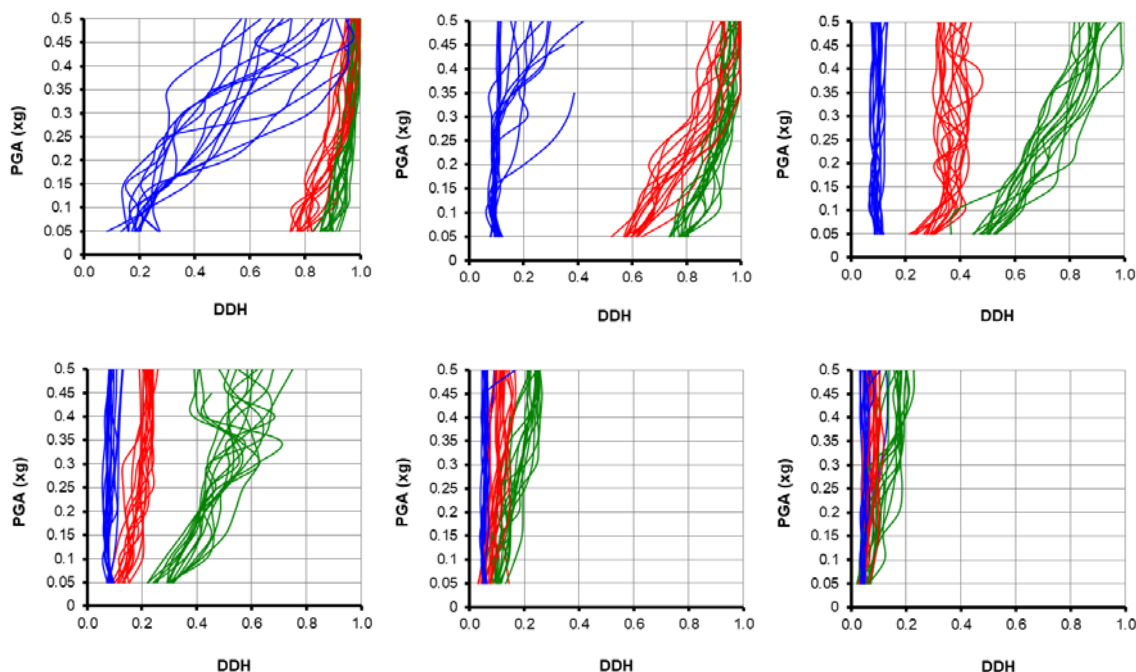


Figure 4. DDH index in function of PGA for analyzed frames.

#### 4. CONCLUSIONS

The ratio between maximal inter-story drift and maximal top drift can be a good indicator for the distribution of damages by height of the building. For the quantification of this ratio, regardless to the number of stories, an Index for Distribution of Displacement at Height (DDH) was defined. When this index, for low levels of earthquake intensity, is greater than 0.2 to 0.3 a concentration of the relative displacement at the level of one or more stories can be expected. This concentration of displacement can lead to occurrence of a soft story mechanism of failure at higher levels of peak ground acceleration. Although the failure mechanism that can lead to structural collapse is difficult to predict from the results obtained from the linear analysis, this index can be used as a marker-indicator for the detection of structural potential to go into the unfavorable plastic mechanism.

#### REFERENCES

[1] CEN – European Committee for Standardization (2004), Eurocode 8: Design of structures for earthquake resistance – Part 1. European standard EN 1998–1.

[2] De Stefano M., Pintucchi B. (2008), „A review of research on seismic behavior of irregular building structures since 2002“, *Bulletin of Earthquake Engineering*, Vol.6, No.2, 2008, pp. 282-308.

[3] Fardis M.N., Carvalho E.C., Fajfar P., Pecker A. (2015), „Seismic design of concrete buildings to Eurocode 8“ CRC Press, Taylor & Francis Group, 6000 Broken Sound Parkway NW.

[4] Federal Institute for Standardization (1981), *Rulebook on Technical Norms for Construction of Buildings in Seismic Areas*, Official gazette of SFRJ, N31, pp. 841-855.

[5] Halde V.V., Deshmukh A.H. (2015), „Review on behavior of soft storey in building“, *International Research Journal of Engineering and Technology*, Vol.2, Issue:08, November 2015, p.p. 327-329.

[6] Todorov K. (2014), „Seismic Performance of Masonry Infilled Reinforced Concrete Frames with Open First Story“, PhD thesis, Faculty of Civil Engineering, University Ss. Cyril and Methodius, Skopje, R. Macedonia.

[7] Todorov K., Lazarov Lj. (2018), "Nonlinear Static vs. Incremental Dynamic Analysis of Infilled Frames with Open First Floor", *Building Materials and Structures* 61 (2018) 4, p.p. 3-22.

[8] Varadharajan S., Sehgal V.K., Saini B. (2013), „Review of different structural irregularities in buildings“, *Journal of Structural Engineering*, Vol. 39, No. 5, December 2012 - January 2013 pp. 393-418 No. 39-51.

## AUTHORS

### **Simona Bogoevska**

MSc, Assistant  
Ss. Cyril and Methodius University  
Faculty of Civil Engineering – Skopje  
Partizanski Odredi 24, 1000 Skopje  
simona.bogoevska@gf.ukim.edu.mk

### **Eleni Chatzi**

PhD, Full Professor  
ETH, Zurich, Switzerland  
Department of Civil, Environmental and  
Geomatic Engineering  
chatzi@ibk.baug.ethz.ch

### **Elena Dumova-Jovanoska**

PhD, Full Professor  
University “Ss. Cyril and Methodius”  
Faculty of Civil Engineering – Skopje  
dumova@gf.ukim.edu.mk

### **Ruediger Hoeffler**

PhD, Full Professor  
Ruhr University Bochum, Bochum, Germany  
Faculty of Civil and Environmental Engineering  
ruediger.hoeffler@rub.de

## **DATA-DRIVEN TOOL FOR STRUCTURAL HEALTH MONITORING OF OPERATING WIND TURBINES**

The growing number of existing infrastructure with decreased or indeterminate reliability, and on the other hand, constant design of lighter, albeit more productive structures facilitate the adoption of automated Structural Health Monitoring (SHM) identification tools capable of unprejudiced diagnosis of in-service structures. In comparison with customarily exploited simulation-based approaches, data-based schemes or hybrid analysis (data/finite element model) can often introduce a more objective perspective on the behavior of operating structures, and as a result can enable long-term, automated and even online assessment.

Recent trends for energy conservation have placed the focus on Wind Turbine (WT) structures, which represent systems characterized with complex dynamics and alternating operating nature. We propose a diagnostic framework able to describe the variability of such monitored systems. The novel approach combines the Smoothness Priors Time Varying Autoregressive Moving Average (SP-TARMA) method for modeling the non-stationary structural response, and a Polynomial Chaos Expansion (PCE) probabilistic model for modeling the propagation of response uncertainty.

The computational tool is applied on long-term data, collected from an active sensing system installed for four years on a real operating WT structure located in Dortmund, Germany. The long-term tracking of the obtained PCE-SPTARMA Diagnostic Indicator (DI) is further assessed by means of a statistical analysis. The results demonstrate that the proposed treatment yields a DI sensitive to unfamiliar fluctuations in measured Environmental and Operational Parameters (EOP).

**Keywords:** Data-driven SHM, Operating wind turbine, Structural variability, Environmental variability.

## 1. INTRODUCTION AND CONCEPT

Data-driven SHM tools hold the potential to reduce the multiple sources of uncertainty and variability typical for real systems, and thus become particularly valuable for infrastructures that bear critical importance in society. In this context, as result of today's rising trends of energy management, wind turbines reached the forefront of significant infrastructures that demand instantaneous implementation.

However, EOP-born variations in measured structural responses, known to mimic real damage states of the structure, underline the necessity of utilization of SHM strategies which rely on elimination or integration of environmental factors from/with obtained structural performance indicators [1-4, 6]. On the other hand, structures characterized with time-varying dynamics are resilient to traditionally applied Operational Modal Analysis (OMA)-based methods limited to implementation with time invariant systems [7].

The proposed diagnostic tool represents a multicomponent algorithm with a "binocular" visualization of the problem since it is adept in providing a link between output-only vibration response data and measured EOPs, Figure 1.

More precisely, the fluctuations that are typical for the inherent (short-term) system dynamics are modeled by means of a parametric SP-TARMA method (Step 1). In a second step identified structural performance indicators, corresponding to short-term modeled responses, are integrated into a PCE tool. The PCE probabilistic modeling approach connects the variability of the structural response to the randomness of measured EOPs.

Finally, the statistical model (Step 3) enables the long-term tracking of a selected PCE-SPTARMA descriptive indicator and facilitates timely reaction to any identified changes in patterns or distributions of the selected output indicator.

## 2. THEORY AND APPLICATION

The described SHM strategy is applied on a 0.5MW WT erected in 1997, located in the vicinity of Dortmund, Germany. The continuous measurement of acceleration data is recorded by triaxial accelerometers installed at five different height positions of the WT structure. The vibration data is supported with SCADA data records, both sampled with the frequency of 100 Hz, Figure 2.

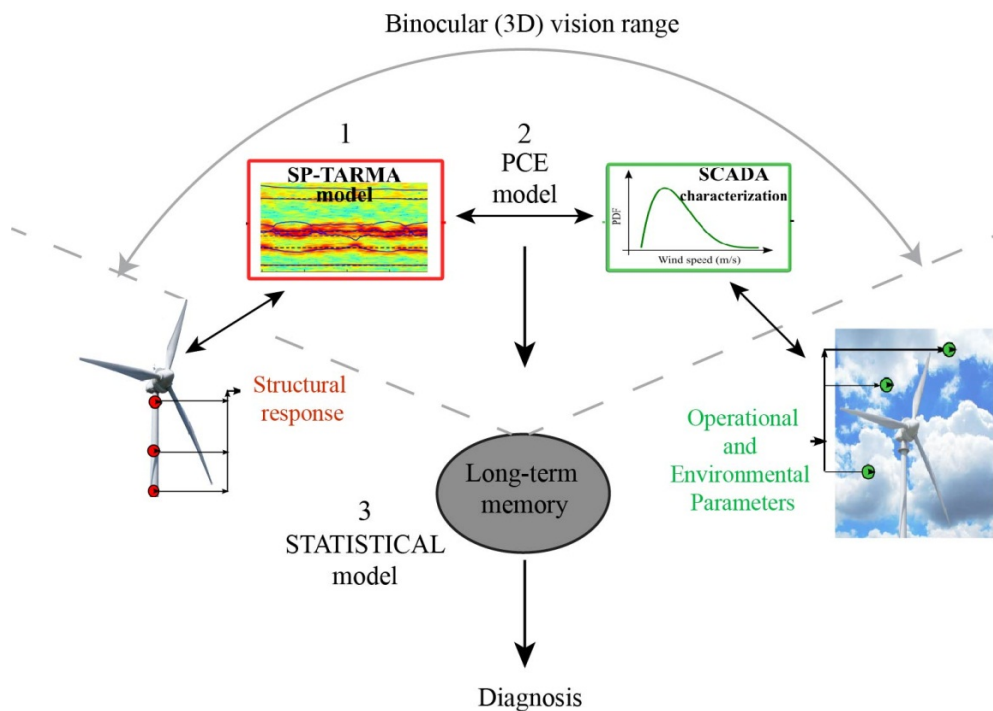


Figure 1. Conceptual model of the SHM strategy and applied methods.

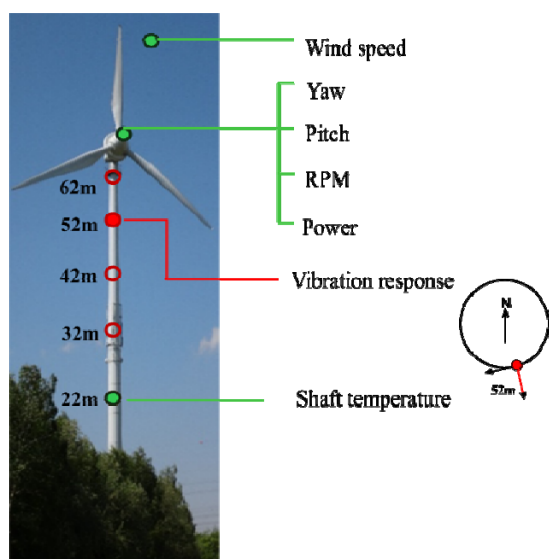


Figure 2. Photo of the actual structure and schematic overview of utilized data.

The nonstationary dynamics typical for an operating WT structure can be successfully tracked via the compact parametric formulation provided by the SP-TARMA models [2]. A full SP-TARMA model is described by an assemblage of three equations, one representing the modeled signal (system response), and two stochastic difference equations governing the time evolution of the unknown AR and MA parameters of the model. Thus, an adequate modelling of a measured nonstationary signal is ensured by proper selection of three user-defined parameters, i.e. the AR/MA order  $n$ , the ratio of the residual variances  $\nu$ , and the order of the stochastic difference equations  $\kappa$ , Figure 3.

The PCE tool is an uncertainty quantification method, which enables the relationship between outputs (structural response performance indicators) and inputs (environmental and operational loads) to the system. A PCE model can be described by a mathematical expansion of a random system output variable on multivariate polynomial chaos basis functions [2]. Spectral representations, such as the PCE method, rely on several regularity requirements, namely finite variance of the outputs, orthonormality of the polynomial basis, and statistical independence of the input variables [5].

The statistical modelling is based on Control chart analysis on the obtained PCE-SPTARMA residual (DI), Figure 4. The results from a univariate outlier analysis of SCADA records verify the sensitivity of the obtained PCE-SPTARMA model to novel fluctuations in

measured EOPs. For a two-month training period, the validation set of the estimated DI illustrates that index values exceeding the  $\pm 3$ std thresholds (99.7% confidence intervals calculated for the fitted Gaussian distribution of the estimation set) can be linked to novel data ranges of the measured influencing agents, more precisely temperature and RPM values between months March and November 2012, as well as April and September in year 2013.

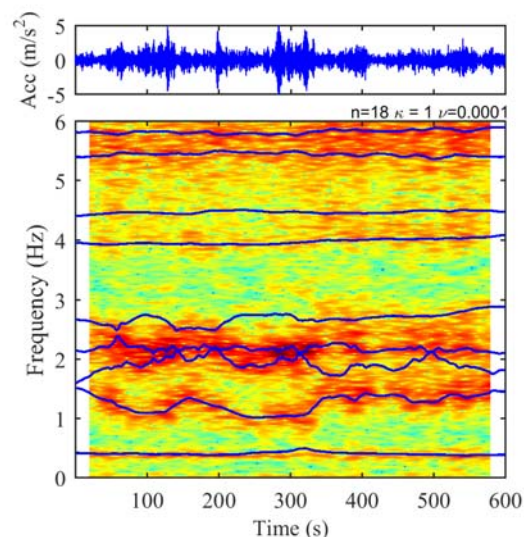


Figure 3. SP-TARMA frequency estimates for fitted model  $M(n=18, \nu=0.0001, \kappa=1)$  (spectrogram in the background).

### 3. CONCLUSIONS

The proposed data-based strategy delivered a sensitive PCE-SPTARMA diagnostic indicator able to capture the non-stationary response and the long-term response variability of the actual operating WT structure for a monitoring period of twenty one months. The obtained data-driven model verifies the future prospective of the strategy for development of an automated SHM diagnostic tool capable of separating benign EOP fluctuations from pattern alterations due to actual structural damage. The sensitivity of the diagnostic indicator to scheduled changes in operating regimes and system fluctuations of the WT structure will be sought in a following step.

#### Acknowledgements

The first author would like to acknowledge the funding support provided from SEEFORM, RUB Research School and Cost Action TU1402 which made this research a possible undertaking.



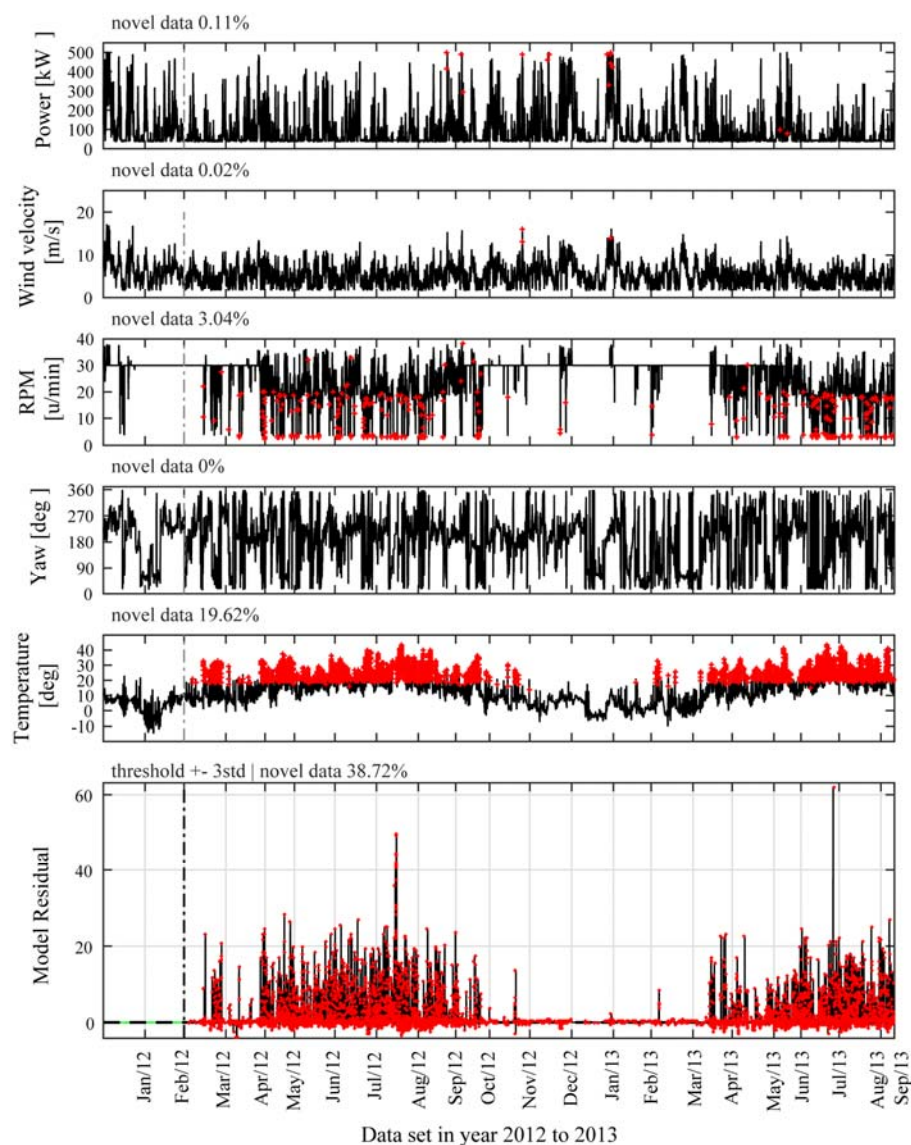


Figure 4. Two-month training set: Identified novel data (red points) within time history of 10-min mean values of measured SCADA and Control chart of the PCE-SPTARMA residual.

## REFERENCES

- [1] Avendaño-Valencia L.D., and Chatzi, E.; (2017); Sensitivity driven robust vibration-based damage diagnosis under uncertainty through hierarchical Bayes time-series representations; *Procedia Engineering*; 199/ 1852-1857.
- [2] Bogoevska S., Spiridonakos M., Chatzi E.; Dumova-Jovanoska E., and Höffer R.; (2017); A Data-Driven Diagnostic Framework for Wind Turbine Structures: A Holistic Approach; *Sensors* 17, 720.
- [3] Dervilis N., Worden K. and Cross E. J.; (2015); On robust regression analysis as a means of exploring environmental and operational conditions for SHM data; *Journal of Sound and Vibration*; 347/ 279–296.
- [4] Hu W. H., Thöns S., Rohrmann R. G., Said, S. and Rücker, W.; (2015); Vibration-based structural health monitoring of a wind turbine system Part II: Environmental/operational effects on dynamic properties; *Engineering Structures*; 89/ 273–290.
- [5] Le Maître O. P., and Knio O. M.; (2010); *Spectral Methods for Uncertainty Quantification*; Springer; Netherlands.
- [6] Spiridonakos M. and Chatzi E.; (2014); Polynomial chaos expansion models for SHM under environmental variability; *Proceedings of 9th International Conference on Structural Dynamics*; Porto; Portugal.
- [7] Tcherniak D., Chauhan S. and Hansen M. H.; (2010); Applicability limits of operational modal analysis to operational wind turbines; *Proceedings of 28th International Modal Analysis Conference*; Jacksonville; Florida USA.



## AUTHORS

### **Miroslav Marjanovic**

PhD, Assistant Professor  
University of Belgrade  
Faculty of Civil Engineering  
Bulevar kralja Aleksandra 73  
11000 Belgrade, Serbia  
mmarjanovic@grf.bg.ac.rs

### **Marija Nefovska-Danilovic**

PhD, Associate Professor  
University of Belgrade  
Faculty of Civil Engineering  
Bulevar kralja Aleksandra 73  
11000 Belgrade, Serbia  
marija@grf.bg.ac.rs

### **Mira Petronijevic**

PhD, Professor (retired)  
University of Belgrade  
Faculty of Civil Engineering  
Bulevar kralja Aleksandra 73  
11000 Belgrade, Serbia  
pmira@grf.bg.ac.rs

## **DEVELOPMENT OF DYNAMIC STIFFNESS METHOD FOR FREE VIBRATION ANALYSIS OF PLATE STRUCTURES**

In the paper, an overview of the development of the dynamic-stiffness-method-based computational model for the free vibration analysis of plates has been presented. Starting from several formulations of the so-called dynamic stiffness elements, formulated at the Institute for Numerical Analysis and Design of Structures (INP) at the Faculty of Civil Engineering, University of Belgrade in the last decade, a novel software framework FREEVIB has been developed and validated. FREEVIB is object-oriented software in Python environment, designed to predict free vibration characteristics in a wide range of possible structural problems (stepped, stiffened and folded plate structures, implying isotropic or orthotropic material formulations). The presented methodology still serves as a strong basis for further improvements through the extensive research efforts of authors, their collaborators and students.

**Keywords:** free vibration, dynamic stiffness method, software development, Python.

## **1. INTRODUCTION**

Dynamic stiffness method (DSM), also known in the literature as spectral element method (SEM), is nowadays used as an alternative to the finite element method (FEM) in the free vibration analysis of different engineering structures [1, 2]. It is highly competitive against the FEM in terms of computational time and cost in mid and high frequency ranges where very fine mesh of finite elements is required for the computation of the free vibration response.

Main component of the DSM is the strong form solution of the governing equations of motion of the corresponding elastodynamic problem formulated in the frequency domain, based on which frequency dependent dynamic stiffness matrix is formulated. As a consequence, structural discretization is frequency independent and affected only by the geometrical and/or material discontinuities of the structure, implying that only one dynamic stiffness element can exactly represent structural behavior at any frequency.

First dynamic stiffness matrices have been formulated for one-dimensional elements (beams and bars) for which closed-form solution of the governing equations of motion can be found. Kolousek [3] was the first who developed dynamic stiffness matrix for beam element, based on Bernoulli-Euler theory. Later on, dynamic stiffness matrices for wide range of one-dimensional dynamic stiffness elements have been developed [4-7].

In a series of contributions [8-11], dynamic stiffness matrices of two-dimensional elements have been derived and applied in the free vibration and buckling analysis of both isotropic and anisotropic long plate assemblies based on classical or first order shear deformation plate theory. In the works of Boscolo and Banerjee [12-17], dynamic stiffness elements of Levy-type plates have been developed enabling free vibration study of isotropic and composite plates and stiffened plate assemblies.

All afore mentioned studies were limited to plates and plate assemblies having special boundary conditions (i.e. two opposite edges simply supported), for which closed-form solutions of the governing equations can be found. This issue has been overcome by Casimir et al. [18], who derived dynamic stiffness matrix for a completely free isotropic rectangular plate element for transverse vibration based on classical plate theory (CPT), using the projection and superposition methods.

The research in the field of dynamic stiffness method at the Faculty of Civil Engineering, University of Belgrade, started in a frame of the research project TR-36046: "Towards development of sustainable cities: Influence of traffic induced vibrations on buildings and humans". Within the framework of the project, numerical model for dynamic analysis of soil-structure system has been formulated using the substructure approach, where the structure has been modeled using dynamic stiffness elements, while for soil modeling, integral transform method has been applied [19]. In a series of further studies, authors formulated dynamic stiffness matrices for a completely free rectangular isotropic plate element based on the first order (FSDT) [20] and higher order shear deformation theory (HSDT) [21], as well as for the plate element ongoing in-plane vibration [22]. Recently, the above formulations have been extended to the free vibration analysis of sandwich [23], symmetric cross-ply laminated composite plates [24, 25], and composite stiffened plate assemblies [26]. Moreover, starting from the developed dynamic stiffness elements, object-oriented

software in Python environment – FREEVIB [27] has been developed, enabling free vibration analysis of a wide range of possible structural problems. Finally, recent efforts in this field are related to the development of the dynamic stiffness element of an open cylindrical shell [28, 29] and its implementation in FREEVIB.

Main objective of the paper is to give an overview of the dynamic-stiffness-method-based computational model for vibration analysis of plates incorporated in the FREEVIB software, developed by the authors.

## 2. FUNDAMENTALS OF THE DYNAMIC STIFFNESS FORMULATION

The dynamic stiffness matrix of a corresponding plate element is obtained through several steps. The first one is derivation of Euler-Lagrange equations of motion for the considered plate theory, by using the Hamilton's principle in terms of the displacements. The next steps are explained as follows.

**Transformation of the governing equations of motion to frequency domain.** The equations of motion are transformed into the frequency domain by assuming a harmonic representation of the displacement/rotation field:

$$u(x, y, t) = \hat{u}(x, y, \omega)e^{i\omega t} \quad (1)$$

In Eq. (1),  $\hat{u}(x, y, \omega)$  are the amplitudes of the displacement/rotation  $\hat{u}(x, y, t)$  in the frequency domain. Having in mind that Eq. (1) is valid for all angular frequencies  $\omega$  in the considered frequency range, the argument  $\omega$  will be omitted in further representations. After the substitution of the above transformation into the governing equations of motion, the equations of motion are transformed into the following set of partial differential equations:

$$\mathbf{L}\hat{u}(x, y) = 0 \quad (2)$$

where  $\mathbf{L}$  is the matrix of the differential operators [20-24] defined in terms of the plate stiffness coefficients, the mass moments of inertia and the angular frequency  $\omega$ .

**Superposition of symmetry contributions.** Displacement or rotation amplitudes of a rectangular plate element  $\hat{u}(x, y)$  can be presented as a superposition of four symmetry contributions: both symmetric (SS), symmetric - anti-symmetric (SA), anti-symmetric - symmetric (AS) and both anti-symmetric (AA), [20-

24]. By the superposition of 4 symmetry contributions, it is possible to analyze only one quarter of a rectangular plate, which significantly reduces the size of the corresponding dynamic stiffness matrices. By using the method of separation of variables, the general solution for each symmetry contribution can be represented in the Fourier series form as:

$$\tilde{u}^{ij}(x, y) = \sum_m^{\infty} {}^1U_m^{ij}(x) {}^1f_m^{ij}(y) + \sum_m^{\infty} {}^2U_m^{ij}(y) {}^2f_m^{ij}(x) \quad (3)$$

In Eq. (3),  $\tilde{u}^{ij}(x, y)$  is the corresponding displacement/rotation function,  ${}^1U_m^{ij}(x)$  and  ${}^2U_m^{ij}(y)$  ( $ij = SS, SA, AS$  or  $AA$ ) are the unknown displacement/ rotation functions, while  ${}^1f_m^{ij}(y)$  and  ${}^2f_m^{ij}(x)$  are the base trigonometric functions, depending on the symmetry case. In practical calculations, the infinite Fourier series must be truncated. Thus, the accuracy of solution depends on the number of terms in the general solution.

The solutions for all symmetry contributions are given in [20-24].

**Projection method.** The vector of displacement components  $\hat{u}^{ij}$  along plate boundaries is denoted as displacement vector  $\hat{\mathbf{q}}^{ij}$ . The corresponding force vector  $\hat{\mathbf{Q}}^{ij}$  consists of force components along plate boundaries. Both vectors are functions of spatial variables  $x$  and  $y$ , so they cannot be related explicitly, as in the case of one – dimensional elements. The issue can be overcome with the aid of the projection method [18]. Therefore, instead of using the vectors  $\hat{\mathbf{q}}^{ij}$  and  $\hat{\mathbf{Q}}^{ij}$ , new projection vectors  $\tilde{\mathbf{q}}^{ij}$  and  $\tilde{\mathbf{Q}}^{ij}$  are introduced, which components are the Fourier coefficients in the series expansion (see [20-26] for details).

The relation between the projection vectors  $\tilde{\mathbf{q}}^{ij}$  and  $\tilde{\mathbf{Q}}^{ij}$  and the vector of integration constants  $\mathbf{C}^{ij}$  is obtained as [20-22]:

$$\tilde{\mathbf{q}}^{ij} = \tilde{\mathbf{D}}_D^{ij} \mathbf{C}^{ij}, \quad \tilde{\mathbf{Q}}^{ij} = \tilde{\mathbf{F}}_D^{ij} \mathbf{C}^{ij} \quad (4)$$

Finally, by eliminating the vector  $\mathbf{C}^{ij}$  from Eq. (4) the following relation between the projection vectors  $\tilde{\mathbf{Q}}^{ij}$  and  $\tilde{\mathbf{q}}^{ij}$  is obtained:

$$\tilde{\mathbf{Q}}^{ij} = \tilde{\mathbf{F}}_D^{ij} \left( \tilde{\mathbf{D}}_D^{ij} \right)^{-1} \tilde{\mathbf{q}}^{ij} = \tilde{\mathbf{K}}_D^{ij} \tilde{\mathbf{q}}^{ij} \quad (5)$$

where  $\tilde{\mathbf{K}}_D^{ij}$  is the dynamic stiffness matrix for the  $ij$  symmetry contribution.

The dynamic stiffness matrix for a completely free dynamic stiffness element, which relates the projections of the forces and displacements along the four plate boundaries, is obtained by using the transformation matrix  $\mathbf{T}$  (for details see [20-26]). The size of the dynamic stiffness matrix  $\tilde{\mathbf{K}}_D$  depends on the number of terms in the general solution  $M$ , the type of the vibration problem (in plane or transverse) and applied plate theory (CPT, FSDT, HSDT).

Finally, considering that transverse and in-plane vibrations of a single plate represent two independent states, the dynamic stiffness matrix of the single plate can be written as:

$$\tilde{\mathbf{K}}_D = \begin{bmatrix} \tilde{\mathbf{K}}_{Dt} & 0 \\ 0 & \tilde{\mathbf{K}}_{Di} \end{bmatrix} \quad (7)$$

In Eq. (7),  $\tilde{\mathbf{K}}_{Dt}$  denotes the dynamic stiffness matrix of plate element for transverse vibrations, while  $\tilde{\mathbf{K}}_{Di}$  is the dynamic stiffness matrix of plate element undergoing in-plane vibrations which can be determined in the same way as  $\tilde{\mathbf{K}}_{Dt}$ .

**Rotation of dynamic stiffness matrices to global coordinates.** For two stiffened plate assemblies where plate 1 and plate 2 are connected to each other with an arbitrary angle between them, vibrations of plate 1 causes vibrations of the corresponding plate 2, and vice versa. Consequently, it is necessary to transform the displacement and force projection vectors  $\tilde{\mathbf{q}}$  and  $\tilde{\mathbf{Q}}$  defined in the local coordinate system of the single plate to the corresponding projection vectors  $\tilde{\mathbf{q}}^*$  and  $\tilde{\mathbf{Q}}^*$  in the global coordinate system of the plate assembly. This is accomplished by using the rotation matrix  $\mathbf{T}_R$ , which depends on the number of terms in the general solution, angle between the local and global coordinate system and the selected dynamic stiffness element. After that, the dynamic stiffness matrix of the single plate in global coordinate system is derived in the same way as in the conventional FEM. The assembly procedure is then performed as in the conventional FEM.

**Computation of natural frequencies and mode shapes.**

In the analysis, arbitrary boundary conditions can be applied by removing the rows and columns of the global dynamic stiffness matrix that correspond to the components of the constrained displacement projections. After that, the natural frequencies can be computed from the following equation:

$$\det \left| \tilde{\mathbf{K}}_{D,nn}^G(\omega) \right| = 0 \tag{8}$$

where  $\tilde{\mathbf{K}}_{D,nn}^G$  is the global dynamic stiffness sub-matrix of the plate assembly related to the unknown generalized displacement projections  $\tilde{\mathbf{q}}_n^G$  of the plate assembly. Since the elements of the dynamic stiffness matrix  $\tilde{\mathbf{K}}_{D,nn}^G$  contain transcendental functions, the solutions can be obtained using some of the search methods. To avoid numerical difficulties when calculating the zeroes of Eq. (8), the natural frequencies can be determined as maxima of the following expression [1]:

$$g(\omega) = \log \frac{1}{\det \left| \tilde{\mathbf{K}}_{D,nn}^G(\omega) \right|} \tag{9}$$

The expression (9) is computed for all frequencies in the frequency range of interest with a frequency increment  $\Delta\omega$ . Consequently, the accuracy of the computed natural frequencies is affected only by the frequency increment. After the natural frequencies have been computed, the  $i^{\text{th}}$  mode shape corresponding to the natural frequency  $\omega_i$  is obtained in the usual manner.

**3. DEVELOPMENT OF COMPUTER CODE FREEVIB**

Formulated dynamic stiffness elements served as basis for the development of computational framework for free vibration analysis of plate-like structures. The object-oriented software FREEVIB has been developed at the Institute for Numerical Analysis and Design of Structures (INP) at the Faculty of Civil Engineering, University of Belgrade.

FREEVIB is written in Python [30], which comes with a large standard library that covers areas such as string processing, software engineering and operating system interfaces. Object-oriented design is introduced to enable code encapsulation, class inheritance and further code reusability.

For input parameters related to the geometry, material and number of terms in trigonometric series ( $M$ ), simple text file may be created in the prescribed format, or generated using the existing graphical pre-processors. Using the procedure described in the previous sections, a variety of plate-like structural problems, illustrated in Fig. 1, can be analyzed: (a) individual plates, (b) plate assembly of arbitrary shape, (c) stepped plates, (d) stiffened plates, (e) cracked plates. In addition, different material properties of single- and multi-layer plates can be considered: (f) single layer isotropic or orthotropic plates, (g) sandwich panels, or (h) laminated composite plates.

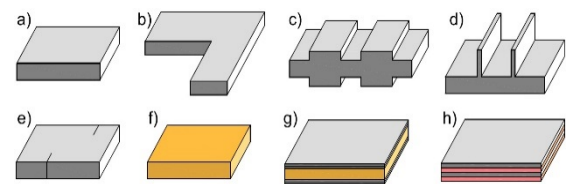


Figure 1. Structural problems which can be analyzed using the proposed computational framework

In Fig. 2, general FREEVIB class structure is illustrated. Note that `DynStiffElement` class is the super class which implements almost all methods related to the creation of the dynamic stiffness matrix. Detailed class structure can be found in [27].

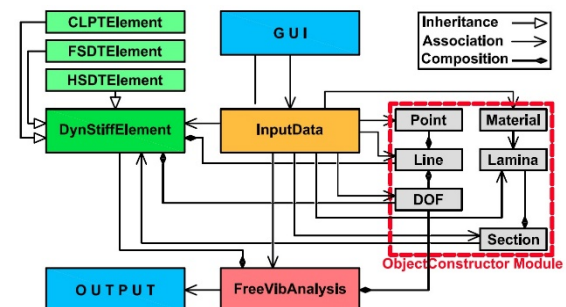


Figure 2. FREEVIB class structure

The so-far developed code could be extended by adding new dynamic stiffness element formulations. The example is the open cylindrical shell element [28, 29]. The family of implemented algorithms could be extended by adding new analysis types, such as response or buckling analysis. With the rapid development of multicore CPU technique, using the multiprocessing module in Python's Standard Library would enable the parallel execution of the code and speed up program execution. Namely, the solving of the equation (9) is time consuming, since it should be performed for every frequency in the considered range. This process is mutually independent for each frequency, thus the parallelization of the code by using the



parallel FOR-loops would drastically increase the speed of the sequential execution.

#### 4. ILLUSTRATIVE EXAMPLE

To illustrate the reliability of the presented methodology, free vibration properties of the 5-layer rectangular cross-laminated timber (CLT) panels have been derived using FREEVIB. FSDT-based dynamic stiffness elements ( $M=5$ ) have been used that give accurate results for considered panels [31]. The panels are 2.5m wide ( $b$ ), with different spans ( $a$ ): 2.5m, 5.0m, 10m and 15m. Considered panel thicknesses are 16cm and 20cm. The panels are simply supported along all edges (S-S-S-S) and composed from timber of class C24 ( $E_1 = 11000$  MPa,  $E_2 = 370$  MPa,  $\nu_{12} = 0.44$ ,  $G_{12} = G_{13} = 690$  MPa,  $G_{23} = 50$  MPa and  $\rho = 420$  kg/m<sup>3</sup>).

The results from FREEVIB are compared against the predictions from commonly used handbooks for CLT design [32, 33] and illustrated in Figure 3.

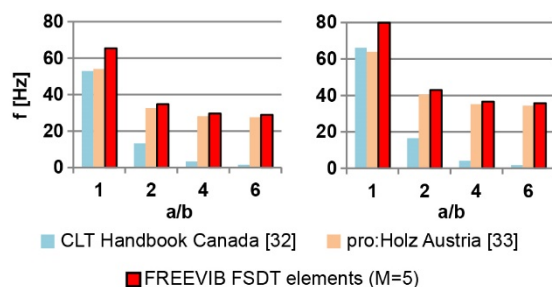


Figure 3. Fundamental frequencies of 5-layer C24 SSSS CLT panel considering different computational models:  $h=0.16$ m (left) and  $h=0.20$ m (right)

Fundamental frequencies calculated using [32-33] obviously are not matching the exact solution obtained using FREEVIB. Such high discrepancies are due to the simplified (beam) models used in [32-33], which are unable to predict the free vibration characteristics for plates with all edges simply supported. Better agreement is achieved for plates with higher  $a/b$  ratio. Finally, as shown in [31], better agreement would be achieved for plates with two opposite edges simply supported (SFSF).

#### 5. CONCLUSIONS

An overview of the dynamic stiffness method and a family of novel dynamic stiffness elements developed at the Institute for Numerical Analysis and Design of Structures (INP) at the Faculty of Civil Engineering, University of Belgrade, has been presented in the paper. The

dynamic stiffness elements have been implemented in the object-oriented software FREEVIB enabling free vibration analysis of a wide range of plate-like structures, considering different plate theories, isotropic or orthotropic behavior and multi-layer plates.

Free vibration study of the 5-layer rectangular CLT panel undergoing transverse vibration has demonstrated high accuracy and efficiency of the developed methodology, as well as its practical application.

#### Acknowledgements

The financial support of the Ministry of Education, Science and Technological Development, Republic of Serbia under the Projects TR-36046 and TR-36048, is acknowledged. The authors are also grateful for the through-years financial support provided within the SEEFORM project.

#### REFERENCES

- [1] Doyle, J. F. (1997), "Wave propagation in structures", Springer-Verlag, New York.
- [2] Lee, U. (2009), "Spectral element method in structural dynamics", John Wiley & Sons (Asia) Pte Ltd.
- [3] Kolousek, V. (1943), "Berechnung der schwingenden Stock-werkrahmen nach der Deformationmethode", Der Stahlbau Vol. 16 No. 5-6, pp. 11-13.
- [4] Wang, T. M., Kinsman, T. A. (1971), "Vibration of frame structures according to the Timoshenko theory", Journal of Sound and Vibration Vol. 14, pp. 215-227.
- [5] Banerjee, J. R., Williams, F. W. (1992), "Coupled bending-torsional dynamic stiffness matrix for Timoshenko beam elements, Computers and Structures, Vol. 42 No. 3, pp. 301-310.
- [6] Hawson, W. P., Zare, A. (2005), "Exact dynamic stiffness matrix for flexural vibration of three-layered sandwich beams", Journal of Sound and Vibration, Vol. 282, pp. 753-767.
- [7] Banerjee, J. R., Ananthapuvirajah, A. (2019), "Coupled axial-bending dynamic stiffness matrix for beam elements", Computers and Structures, Vol. 215, pp. 1-9.
- [8] Wittrick, W. H. (1968), "General sinusoidal stiffness matrices for buckling and vibration analyses of thin flat-walled structures", International Journal of Mechanical Sciences, Vol. 10 No. 12, pp. 949-966.
- [9] Wittrick, W. H., Williams, F. W. (1974), "Buckling and vibration of anisotropic or isotropic plate assemblies under combined loadings," International Journal of Mechanical Sciences, Vol. 16 No. 4, pp. 209-239.

- [10] Anderson, M. S., Williams, F. W., Wright, C. J. (1983), "Buckling and vibration of any prismatic assembly of shear and compression loaded anisotropic plates with an arbitrary supporting structure", *International Journal of Mechanical Sciences*, Vol. 25 No. 8, pp. 585–596.
- [11] McGowan D. M., Anderson, M. S. (1999), "Development of curved-plate elements for the exact buckling analysis of composite plate assemblies including transverse shear effects", Technical Report, American Institute of Aeronautics and Astronautics, Plymouth, NH, USA.
- [12] Boscolo M., Banerjee, J. R. (2011), "Dynamic stiffness elements and their applications for plates using first order shear deformation theory", *Computers and Structures*, Vol. 89, pp. 395–410.
- [13] Boscolo M., Banerjee, J. R. (2011), "Dynamic stiffness method for exact inplane free vibration analysis of plates and plate assemblies", *Journal of Sound and Vibration*, Vol. 330 No. 12, pp. 2928–2936.
- [14] Fazzolari, F. A., Boscolo, M., Banerjee, J. R. (2013), "An exact dynamic stiffness element using a higher order shear deformation theory for free vibration analysis of composite plate assemblies", *Composite Structures*, Vol. 96, pp. 262–278.
- [15] Boscolo, M., Banerjee, J. R. (2014), "Layer-wise dynamic stiffness solution for free vibration analysis of laminated composite plates", *Journal of Sound and Vibration*, Vol. 333 No. 1, pp. 200–227.
- [16] Boscolo, M., Banerjee, J. R. (2012), "Dynamic stiffness formulation for composite Mindlin plates for exact modal analysis of structures. Part I: Theory", *Computers and Structures*, Vol. 96-97, pp. 61–73.
- [17] Boscolo, M., Banerjee, J.R.B (2012), "Dynamic stiffness formulation for composite Mindlin plates for exact modal analysis of structures. Part II: results and applications", *Computers and Structures*, Vol. 96-97, pp. 74–83.
- [18] Casimir, J. B., Kevorkian, S., Vinh, T. (2005), "The dynamic stiffness matrix of two-dimensional elements: application to Kirchhoff's plate continuous elements", *Journal of Sound and Vibration*, Vol. 287 No. 3, pp. 571–589.
- [19] Nefovska-Danilović, M. (2013), "Dynamic analysis of soil-structure system using spectral element method", Doctoral dissertation, University of Belgrade, Faculty of Civil Engineering.
- [20] Kolarević, N., Nefovska-Danilović, M., Petronijević, M. (2015), "Dynamic stiffness elements for free vibration analysis of rectangular Mindlin plate assemblies", *Journal of Sound and Vibration*, Vol. 359, pp.84-106.
- [21] Kolarević, N., Marjanović, M., Nefovska-Danilović, M., Petronijević, M. (2016), "Free vibration analysis of plate assemblies using the dynamic stiffness method based on the higher order shear deformation theory", *Journal of Sound and Vibration*, Vol. 364, pp. 110-132.
- [22] Nefovska-Danilović, M., Petronijević, M. (2015), "In-plane free vibration and response analysis of isotropic rectangular plates using the dynamic stiffness method", *Computers & Structures*, Vol. 152, pp. 82-95.
- [23] Marjanović, M., Kolarević, H., Nefovska-Danilović, M., Petronijević, M. (2016), "Free vibration study of sandwich plates using a family of novel shear deformable dynamic stiffness elements: limitations and comparison with the finite element solutions", *Thin-Walled Structures*, Vol. 107, pp. 678-694.
- [24] Nefovska-Danilović, M., Kolarević, N., Marjanović, M., Petronijević, M. (2017), "Shear deformable dynamic stiffness elements for a free vibration analysis of composite plate assemblies – Part I: Theory", *Composite Structures*, Vol. 159, pp. 728-744.
- [25] Marjanović, M., Kolarević, N., Nefovska-Danilović, M., Petronijević, M. (2017), "Shear deformable dynamic stiffness elements for a free vibration analysis of composite plate assemblies – Part II: Numerical examples", *Composite Structures*, Vol. 159, pp. 183-196.
- [26] Damjanović, E., Marjanović, M., Nefovska-Danilović, M. (2017), "Free vibration analysis of stiffened and cracked laminated composite plate assemblies using shear-deformable dynamic stiffness elements", *Composite Structures*, Vol. 180, pp. 723-740.
- [27] Marjanović, M., Nefovska-Danilović, M., Damjanović, E. (2019), "Framework for dynamic-stiffness-based free vibration analysis of plate-like structures", *Shock and Vibration*, 1369235.
- [28] Kolarević, N. (2016), "Vibracije i izbočavanje ploča i ljuski primenom metode dinamičke krutosti", Doctoral dissertation, Univerzitet u Beogradu, Građevinski fakultet.
- [29] Kolarević, N., Nefovska-Danilović M., Petronijević, M. (2016), "Dynamic stiffness method in the vibration analysis of circular cylindrical shell", *Building Materials and Structures*, Vol. 59 No. 3, pp. 45-61.
- [30] Python Software Foundation. Python Language Reference, version 2.7. Available at <http://www.python.org>.
- [31] Jugović, V. (2019), "Slobodne vibracije ploča od unakrsno lameliranog drveta", Diplomski rad, Univerzitet u Beogradu, Građevinski fakultet.
- [32] Sylvain, G., Ciprian, P. (2011), CLT Handbook - Canadian Edition. FPInnovations, Special publications SP-528E, Quebec.
- [33] Markus, N., Koppelhuber, J., Pock, K. (2014), CLT Structural design: Basic design and engineering principles according to Eurocode. pro-Holz Austria.

## NUMERICAL MODELING OF PIEZOELECTRIC SMART AGGREGATES

### AUTHORS

#### **Nemanja Markovic**

Assistant, Dipl.–Ing.

Faculty of Civil Engineering and Architecture  
University of Nis, Serbia

nemanja.markovic@gaf.ni.ac.rs

#### **Dragoslav Stojic**

Dr.-Ing., Full Professor

Faculty of Civil Engineering and Architecture  
University of Nis, Serbia

dragoslav.stojic@gmail.com

#### **Tamara Nestorovic**

Dr.-Ing., Full Professor

Faculty of Civil and Environmental Engineering  
Ruhr University Bochum, Germany

tamara.nestorovic@rub.de

The article deals with numerical modeling of piezoelectric smart aggregates based on finite element method. Finite element modeling of piezoelectric patch is based on constitutive equations for coupled electro-mechanical behavior, while for surrounding concrete linear elastic material model is assumed. Different intensities of electric voltage were analyzed and displacements at control points were measured. Obtained results indicate that there is a complete linear relationship between the deformation and the electrical voltage at the control points, and nonlinear development of deformation by cross-sectional thickness of piezoelectric smart aggregate.

**Keywords:** Piezoelectricity, Smart Aggregates, ABAQUS, Finite Element Method, Structural Health Monitoring.

### 1. INTRODUCTION

Structural health monitoring and damage detection of reinforced concrete structures using piezoelectric actuators/sensors has become possible and practicable after piezoelectric smart aggregates (PZT SA) were developed. Multifunctional smart sensors, called PZT SA were developed at the University of Houston, USA. Since then, numerous researches have been conducted, aimed at the potential implementation of PZT SA for damage detection and monitoring in RC structures in real-time or near real-time. The goal of the developed methods and procedures for detection, localization and quantification of damage is acquisition of a sufficient number of reliable data on whose basis a decision of further interventions could be made. Further interventions (assuming the detection found damage in the structure) comprise making decisions on the visual inspection, potential detailed structural examination to serve as a basis for making a definitive decision on the rehabilitation, reconstruction or demolition of the structure. The paper is organized as follows: after the introduction, the description and application of PZT SA are presented in Section 2. Numerical simulation of PZT SA based on FEM is presented in Section 3, while the results and discussions are presented in Section 4.

Finally, conclusions and recommendations for further investigations are given in Section 5.

## 2. PIEZOELECTRIC SMART AGGREGATES

A lead zirconate titanate (PZT) patch, protected by a waterproof layer and embedded in a very small concrete block, marble or rock represents PZT SA. *Piezoelectric Smart Aggregate* got its name because: **Piezoelectric** – because it contains a patch with piezoelectric properties (effects), **Smart** – because it has smart characteristics and a multifunctional character, **Aggregate** – because it is embedded in a small concrete blocks of ordinary size which is within the boundaries of the real aggregate size of  $16 \div 31,5 \text{ mm}$ . The fabricating process PZT SA mainly consists of the following steps: a) selection of the size and shape of a PZT patch, b) soldering of an electric cable to the PZT patch, c) connecting of the electric cable to BNC connector, d) waterproofing of PZT patch, e) mixing of cement paste, f) making of formwork, g) lubrication of formwork for easy demolding, h) fixing of the PZT patch in the formwork, i) pouring of fresh cement paste, j) curing for 48h and k) demolding of PZT SA from the formwork. In addition to embedding the PZT patches into cement paste, patches can be embedded in small marble blocks (Fig. 1) or blocks of other types of rocks.

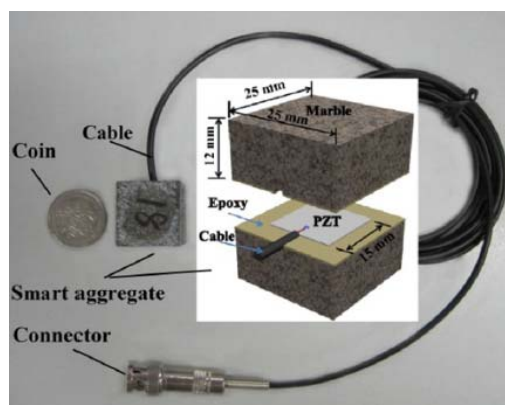


Figure 1. Marble PZT SA [1]

PZT patches are characterized by high brittleness and lack of resistance to moisture because of which they were unsuitable for usage in construction engineering. PZT SA protects the PZT patch from moisture and mechanical shocks during pouring of fresh concrete and during the building service. PZT SA is installed into a real structure by fixing it to the reinforcement bars (Fig. 2b, Fig. 2c) or formwork (Fig. 2a) at a predefined point. While

installing it very important to ensure that position and orientation of PZT SA does not change during pouring of fresh concrete mass.

After installing PZT SA in RC structures, damage detection is usually performed by the signal generator device for generation of sweep sinusoidal/harmonic/pulse voltage signals. This voltage signal is further amplified using power amplifier to drive the PZT SA actuator embedded in an RC structure. Spatial elastic waves propagate through an RC structure as a consequence of activation of the PZT SA actuator, using an inverse piezoelectric effect. On the other hand, the other PZT SA is used as sensor to receive of the incoming wave and for converting it into a voltage signal based on the direct piezoelectric effect. Finally, this output sensor signal is transferred to the storage device. This is a brief description of the procedure and equipment used for damage detection of RC structures using PZT SA.



Figure 2. Fixing PZT SA inside structural elements: a) installation of PZT SA inside the wooden formwork of RC beam [2], b-c) A PZT SA fixed on the rebar cage of column [3]

Usage of PZT SA for damage detection has been analyzed for different cases of damage, different structural elements, loading cases, etc. In the laboratory conditions, damage detection based on the energy approach and one-dimensional damage index was performed for beam elements [4]. Beam loading was performed using hydraulic press and onset of cracks their propagation was monitored [5]. It was concluded that the implemented damage detection procedure can detect damage, but in-detail information on the cracks, such as their location, dimensions (width, length), orientation, cannot be established using this procedure [6]. Also, monitoring of RC walls under pseudo-static load, up to the gradual onset of first cracks,



and further to failure was performed using PZT SA [7]. Similar to the previous research, the experimental measurements on the RC columns due to the seismic load were performed, and the obtained response in PZT SA was monitored. It was concluded that PZT SA can detect the severity of the damage to the RC columns due to the seismic load, but in addition, PZT SA can be used to detect the dynamic seismic response at the distributed locations of the concrete columns, and this amplitude of the sensor response can be used to evaluate the seismic excitation level [8].

All the examples of experimental laboratory research presented so far indicate that PZT SA have a future in monitoring of real civil engineering structures. It was demonstrated in situ on the Niu-Dou Bridge in the Yi-Lan region in Taiwan in 2010 [9]. The National Center for Research on Earthquake Engineering (NCREE) conducted a seismic research of the onset of damage on the bridge piers and detection using PZT SA. As in the previous research, PZT SA were successfully used in detection of large-scale real engineering structures.

PZT SA are multifunctional sensors characterized by the following properties: structural simplicity, low cost, quick response, high reliability, solid-state actuation, quick response, low weight, wide frequency range and multifunctionality. Multifunctionality characterizes them, because apart from the damage detection, they are used for: a) impact detection, b) early-age concrete strength monitoring, c) monitoring of water seepage in concrete structures, d) monitoring of P-wave velocity in early-age concrete, e) detection of interface debonding of concrete and reinforcement, f) monitoring of compressive and shear seismic stresses.

### 3. NUMERICAL SIMULATION

Numerical modeling of PZT SA based on FEM approach was analyzed in dozens research papers of which we select few [10-13]. In this paper modeling of the PZT SA actuator is done in the software package ABAQUS/STANDARD. The numerical simulation of PZT SA is done on a 3D model using the standard finite elements method. The smart aggregate model consists of two parts, a piezoelectric patch (12.7x12.7x0.25mm) and a small concrete block (30x30x10mm), as shown in Fig. 3. The FEM procedure used for modeling of PZT SA using software ABAQUS/

STANDARD treats the coupled piezoelectric problems with the following characteristics:

- coupled piezoelectric problems are solved using an eigenfrequency extraction, modal dynamic, static, dynamic, or steady-state dynamic procedure;
- require the use of piezoelectric elements;
- electric potential gradient causes straining, while stress causes an electric potential gradient in the material;
- can be performed for continuum problems in one, two and three dimensions;
- require the use of piezoelectric material properties;
- can be used in both linear and nonlinear analysis (in nonlinear analysis the piezoelectric part of the constitutive behavior is assumed to be linear).

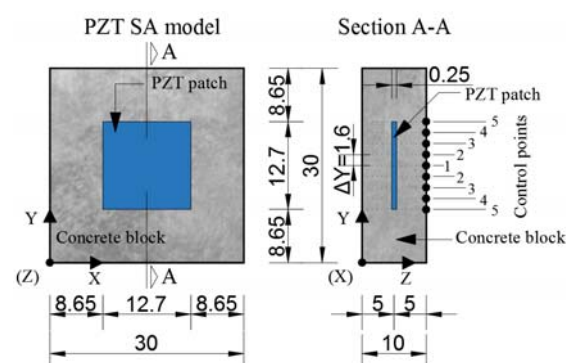


Figure 3. Geometry characteristics of PZT SA model (dimensions are in mm)

The applied FEM model for PZT patch is treated with next material characteristics:

- provides linear relations between mechanical and electric potential gradient;
- PZT is used in piezoelectric elements, which have both displacement and electric potential as model variables;
- PZT material is one in which an electrical field causes the material to strain, while stress causes an electric potential gradient.

FEM simulation of piezoelectric materials is based on constitutive equations for coupled electro-mechanical behavior. Defining of mechanical and electrical properties using

constitutive equations can be performed in three forms: (a) stress-charge form (Equations 1 and 2), (b) strain –charge form (Equations 3 and 4) and (c) strain-voltage (non-standard form):

$$\sigma_{ij} = D_{ijkl}^E \varepsilon_{kl} - e_{mij}^\varphi E_m \quad (1)$$

$$q_i = e_{ijk}^\varphi \varepsilon_{jk} + D_{ij}^{\varphi(\varepsilon)} E_j \quad (2)$$

$$\varepsilon_{ij} = S_{ijkl}^E \sigma_{kl} - d_{mij}^\varphi E_m \quad (3)$$

$$q_i = d_{ijk}^\varphi \sigma_{jk} + D_{ij}^{\varphi(\varepsilon)} E_j \quad (4)$$

with the following notation:  $\sigma_{ij}$ ,  $\varepsilon_{kl}$  - mechanical stress and strain tensor;  $q_i$  - electric “displacement” vector;  $D_{ijkl}^E$  - materials’ elastic stiffness matrix defined at zero electrical potential gradient;  $e_{mij}^\varphi$  - material’s piezoelectric stress coefficient matrix,  $d_{mij}^\varphi$  - material’s piezoelectric strain coefficient matrix;  $\varphi$  – electrical potential;  $D_{ij}^{\varphi(\sigma)}$  - material’s dielectric property;  $E_j$  - electric potential gradient vector.

A PZT patch responds to an electric potential gradient by mechanical straining (actuation effect), while the mechanical stress causes an electric potential gradient in the material (sensor effect). This coupling between the electric potential gradient and the strain is the material’s piezoelectric properties. When modeling PZT SA only the first piezoelectric effect was used – actuation effect (equation 3 and 4). Based on equation (3 and 4), it is obvious that electrical and electro-mechanical coupling behaviors are defined by the dielectric property  $D_{ij}^{\varphi(\sigma)}$  and the piezoelectric strain coefficient matrix  $d_{mij}^\varphi$ . PZT patch in this analysis is mechanically treated as linear-elastic model.

The mechanical equilibrium equation and electrical flux conservation equation for piezoelectric FEM analysis are:

$$\int_V \sigma : \delta \varepsilon \cdot dV = \int_S t \cdot \delta u \cdot dS + \int_V f \cdot \delta u \cdot dV \quad (5)$$

$$\int_V q \cdot \delta E \cdot dV = \int_S q_s \cdot \delta \varphi \cdot dS + \int_V q_v \cdot \delta \varphi \cdot dV \quad (6)$$

where  $\sigma$  is the Cauchy stress at a current point;  $t$  is the traction across a point of the surface of the body;  $f$  is the body force per unit volume in the node;  $\delta u$  is the virtual velocity

field;  $\delta \varepsilon = \text{sym}(\partial \delta u / \partial x)$ ;  $q$  is the electric flux vector (electric “displacement” vector);  $q_s$  is the electric flux per unit area entering the body at a point on its surface;  $q_v$  is the electric flux entering the body per unit volume;  $\delta \varphi$  is the virtual potential and  $\delta E = -\partial \delta \varphi / \partial x$ .

Table 1. Material properties of PZT patch and concrete block (density in kg/m<sup>3</sup>)

Piezoelectric patch			
Density	Dielectric properties (CV <sup>-1</sup> /m)		
$\rho=7500$	$D_{11}=1.505$	$D_{22}=1.301$	$D_{33}=1.505$
Piezoelectric properties (F/m) · 10 <sup>-10</sup>			
$d_{112}=7.41, d_{211}=-2.74, d_{222}=5.93, d_{233}=-2.74,$ $d_{323}=7.41, d_{111}=d_{122}=d_{133}=d_{113}=d_{123}=d_{212}=0$ $d_{213}=d_{223}=d_{311}=d_{322}=d_{333}=d_{312}=d_{323}=0$			
Elastic properties (E and G in GPa)			
$E_1=E_3=60.61; E_2=48.31; G_{12}=G_{23}=23.0;$ $G_{13}=23.5; \nu_{12}=0.512; \nu_{13}=0.289; \nu_{23}=0.408;$			
Concrete block			
Young’s Modulus: $E=44.3\text{GPa}$			
Poisson’s ratio: $\nu=0.15$			
Mass density: $\rho=2400\text{kg/m}^3$			
Rayleigh damping			
$\alpha=2050.0$		$\beta=1.100 \cdot 10^{-8}$	

Electric potentials and displacement for the piezoelectric elements exist at the nodal locations and they are approximated with interpolation functions:

$$u = N^N u^N, \quad \varphi = N^N \varphi^N \quad (7)$$

where  $u^N$ ,  $\varphi^N$  are nodal quantities and  $N^N$  is the array of interpolation functions. The electrical potential gradient and strains are given with next equation:

$$E = -B_\varphi^N \varphi^N, \quad \varepsilon = B_u^N u^N \quad (8)$$

where  $B_u^N$  and  $B_\varphi^N$  are the spatial derivatives of  $N^N$ , defined in the current configuration for geometrically nonlinear analysis. The following system of equations is derived in terms of nodal quantities:

$$M^{MN} \ddot{u}^N + K_{uu}^{MN} u^N + K_{\varphi u}^{MN} \varphi^N = P^M \quad (9)$$

$$K_{\varphi u}^{MN} \varphi^N - K_{\varphi \varphi}^{MN} \varphi^N = -Q^M \quad (10)$$

with following notation:  $M^{MN}$  - mass matrix;  $K_{uu}^{MN}$  - displacement stiffness matrix;  $K_{\varphi \varphi}^{MN}$  - dielectric “stiffness” matrix;  $K_{\varphi u}^{MN}$  - piezoelectric coupling matrix;  $P^M$  - mechanical force vector;  $Q^M$  - electrical charge vector.

The surrounding concrete block is modeled as a linear elastic isotropic material with material characteristics defined in table 1. The contact between the patch and the concrete block is defined by surface based tie constraints, simulating a complete connection between these two parts. Piezoelectric contact surface was selected as a “master surface” and concrete contact surface was “slave surface”. Boundary condition on the concrete block are defined to external edge points by constrained all degrees of freedom. On one side of the PZT patch electric voltage equal to zero is fixed using the electric potential boundary condition, while on the other side is applied an electrical voltage having values ranging between 10V-100V with a step of 10V. The finite element mesh is made using the sweep technique of mesh generation with the approximate size of finite element of 0.03mm. The finite element used for modeling of the concrete block is the standard-linear-3D stress FE: C3D8R – 8-node linear brick with reduced integration and hourglass control. Whereas, for modeling of the PZT patch the standard-linear-piezoelectric FE: C3D8E – 8-node linear piezoelectric brick is used. Full analysis with multiple processors parallelization and single nodal output precision is performed. In the control points presented in Fig. 4, displacements in z-directions for all intermediate steps of the applied electric voltage are measured.

#### 4. RESULTS AND DISCUSSION

The results obtained based on the FEM analysis of PZT SA are presented in figures 4-6. In figures 5-6 displacements obtained in control points in the function of the applied electric voltage are presented. A clear linear dependence between the electric voltage and obtained displacements can be observed (Figure 5). Also, the highest displacements are obtained in the control point 1 and they reduce non-linearly towards the point 5, which can more clearly be seen in figure 6. Measured displacements on the non-deformed model is presented in figure 4 left, while in figure 4 right

are presented the same displacements on the deformed model.

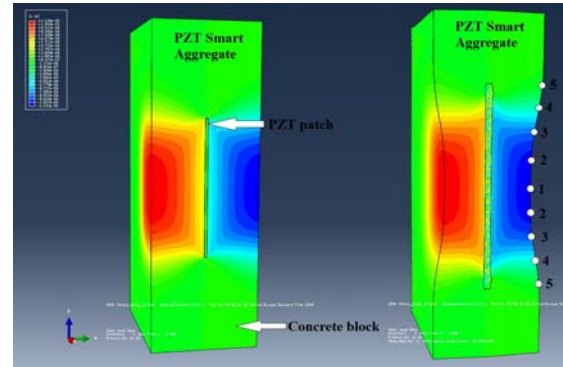


Figure 4. Left: Undeformed PZT SA model, Right: deformed PZT SA from ABAQUS/STANDARD

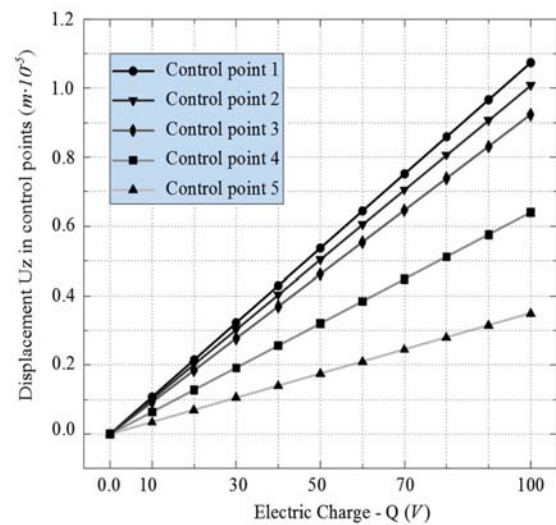


Figure 5. Results of displacement  $U_z$  in control points in function of electric charge (Q)

Displacements in the control points based on the FEM model done in the ABAQUS/STANDARD software is presented in cross-section of PZT SA (Figure 6). Displacements are displayed in the function of the electrical voltage. Based on this figure, it can be seen that with the increase of the electrical voltage, deformations of PZT SA also increase. The assumption is made that at the ends of the cross-section the deformations are equal to zero. The results obtained from this model can be used for modeling of wave propagation induced by a PZT SA actuators. Such method of modeling can be implemented because there are no piezoelectric finite elements in the explicit FEM analysis in ABAQUS, and it is impossible to model wave propagation in the standard FEM analysis because of the excessive size of the model. For that reason, instead of PZT SA actuator, in the modeling of wave propagation, displacement boundary conditions can be used [14].

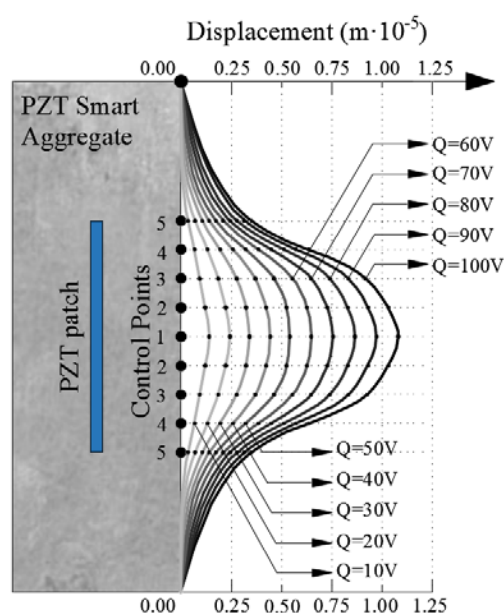


Figure 6. Displacement curves for different electric charge

## 5. CONCLUSION

Piezoelectric Smart Aggregates are multifunctional sensors/actuators having wide application in damage detection of reinforced concrete structures. Their application so far is based on performed experimental studies. Numerical models of PZT SA are very rarely analyzed and can be found in a small number of papers. This paper presents the numerical modeling procedure for PZT SA using the ABAQUS/STANDARD software package. Based on the FEM model, deformation-electric voltage curves were obtained for the analyzed voltages in the 10V-100V range with a step of 10V. A linear relationship between deformation and electrical voltage at control points was obtained, and nonlinear change of deformation through cross-sectional height. The presented results of displacement of PZT SA can be used for numerical modeling of wave propagation for damage detection purpose.

## REFERENCES

- [1] Liu, T., Zou, D., Du, C., and Wang, Y. (2017) „Influence of axial loads on the health monitoring of concrete structures using embedded piezoelectric transducers“, *Structural Health Monitoring*, Vol. 16(2), pp. 202-214.
- [2] Chalioris, C., et. al. (2016) „Applications of smart piezoelectric materials in a wireless admittance monitoring system (WiAMS) to Structures – Tests in RC elements“, *Case Studies in Construction Materials*, vol. 5, pp.1-18.
- [3] Mo, Y.L., Song, G., Moslehy, Y., Gu, H., Sanders, D.H. and Belarbi, D.J. (2011) „Damage Detection of Reinforced Concrete Columns Subjected to Combined Actions“, *NEESR Payload, Annual Report 2010-2011*, University of Houston.
- [4] Dumoulin, C., Karaiskos, G. and Deraemaeker, A. (2013) „Monitoring of crack propagation in reinforced concrete beams using embedded piezoelectric transducers“, VIII International Conference FraMCoS-8, 10-14 March 2013, Toledo, Spain.
- [5] Zhao, X., Li, H., Du, D. and Wang, J., (2008) „Concrete Structure Monitoring Based on Built-in Piezoelectric ceramics Transducers“, *Sensors and Smart Structures Technologies for Civil, Mechanical and Aerospace Systems – Proceedings of SPIE*, March 2008.
- [6] Song, G., Gu, H., Mo, Y.L., Hsu, T.T.C. and Dhonde, H. (2007) „Concrete structural health monitoring using embedded piezoceramics transducers“, *Smart Materials and Structures*, vol. 16(4), pp. 959-968.
- [7] Yan, S., et. al. (2009) „Health monitoring of reinforced concrete shear walls using smart aggregates“, *Smart Materials and Structures*, vol. 18, 047001 (6pp).
- [8] Gu, H., et.al. (2010) „Multi-functional smart aggregate-based structural health monitoring of circular reinforced concrete columns subjected to seismic excitations“, *Smart Materials and Structures*, vol. 19, 065026, (7pp).
- [9] Liao, W.I., et.al. (2011) „Structural health monitoring of concrete columns subjected to seismic excitations using piezoceramic-based sensors“, *Smart Materials and Structures*, vol. 20, 125015, (10pp).
- [10] Stojić, D., Nestorović, T., Marković, N., Marjanović, M., (2018) „Experimental and numerical research on damage localization in plate-like concrete structures using hybrid approach“, *Structural Control and Health Monitoring*, Vol. 25, Issue 9.
- [11] Zhang, H., Shuang, H., and Ou, J., (2018) „Validation of Finite Element Model by Smart Aggregate-Based Stress Monitoring“, *Sensors*, Vol. 18, 4062.
- [12] Marković, N., Nestorović, T., Stojić, N., (2015) „Numerical modeling of damage detection on concrete beams using piezoelectric patches“, *Mechanics Research Communications*, vol. 64, pp. 15-22.
- [13] Stojić, D., Nestorović, T., Marković, N., Cvetković, R. (2019) „Material defects localization in concrete plate-like structures – Experimental and numerical study“, *Mechanics Research Communications*, Vol. 98, pp. 9-15.
- [14] Marković, N., et.al.(2015) „Hybrid approach for two dimensional damage localization using piezoelectric smart aggregates“, *Mechanics Research Communications*, vol. 85, pp. 69-75.



## AUTHORS

### **Marko Radisic**

University of Belgrade  
Bulevar kralja Aleksandra 73, 11000 Belgrade  
mradisic@grf.bg.ac.rs

### **Mira Petronijevic**

University of Belgrade  
Bulevar kralja Aleksandra 73, 11000 Belgrade  
pmira@grf.bg.ac.rs

### **Gerhard Muller**

Technical University of Munich  
Arcisstr. 21, 80333 Munich  
gerhard.mueller@tum.de

# **VERTICAL VIBRATIONS OF RECTANGULAR FLEXIBLE FOUNDATION ON VISCOELASTIC HALFSPACE**

This paper presents a novel method, ITM-DSM, for the soil-foundation interaction problems analysis. It is a semi-numerical method based on the coupling of the Integral Transform Method (ITM) and the Dynamic Stiffness Method (DSM). The stiffness matrix of the soil-foundation system is obtained using the substructure technique. The ITM is used to obtain the solution of the wave propagation in the soil, while the DSM is used to calculate the dynamic stiffness matrix of the foundation. Both methods are operating in the frequency domain what makes them suitable for coupling. The number of numerical operations in the frequency domain is reduced by the application of the modal superposition technique. The analysis of vertical vibrations of flexible foundations resting on the viscoelastic half-space is presented. The formulation of the method could be generalized for horizontal and rocking vibrations. It could be also reduced to the problem of flexible strip foundations of infinite length.

**Keywords:** Integral Transform Method, Dynamic Stiffness Method, Fourier Transforms, Modal Superposition Method, Substructure Method

## **1. INTRODUCTION**

The effects of soil-structure interaction (SSI) are not negligible in general [1]. The soil is the integral part of the system and it has an influence on its response. Due to the different nature of the soil and the structure, the SSI problems are usually solved using the substructure technique: the substructures are modeled independently and then coupled applying available boundary conditions.

The modeling of the soil medium is complex in general, but especially in dynamic analysis. The soil must be presented as an unbounded medium so that the energy propagates from the source of vibrations towards the infinity. The traditional modeling techniques, such as the Finite Element Method, cannot address this problem well [2]. That led to the

development of new methods such as the Integral Transform Method (ITM) [3]. The ITM is based on solving Lamé's differential equations of motion, decoupling them using the Helmholtz decomposition and transforming them from partial to ordinary differential equations by a threefold Fourier Transform. The ordinary differential equations are solved in the transformed wavenumber-frequency domain by taking into account the boundary conditions of the system. The solution is transferred in the original space-time domain by threefold inverse Fourier Transform [4].

The SSI problems could be reduced to the soil-foundation interaction (SFI) problems. In the case of a surface, rigid foundation, the problem could be easily solved considering the foundation as a part of the soil surface, and applying kinematic transforms [5]. Since the foundation is always flexible up to a certain level, it is important to investigate the influence of the foundation stiffness on the response of the SFI system. The dynamic response of flexible foundations was investigated mainly by using the boundary element method [6] [7] [8] and finite element method [9] [10] [11]. In this paper a novel ITM-DSM [12] [13] [14] is used to solve that problem.

The DSM [6] is based on the exact solution of the governing differential equations of motion in the space-frequency domain. This results in the exact frequency dependent shape functions of a dynamic stiffness element. The dynamic stiffness matrices of elements are also frequency dependent and can be developed explicitly for one-dimensional beam elements and Levy-type plates. Only one element is sufficient to represent the dynamic behavior at any frequency. In the case of plates with arbitrary boundary conditions, the plate displacements are presented in infinite series form, and the boundary problem is solved using the Projection method [15].

Both ITM and DSM are operating in the frequency domain what makes them suitable for coupling. The coupling of the foundation and the soil is established using the dynamic modal stiffness matrix of the soil. The SFI problem is solved using the modal superposition technique [16].

This paper presents the formulation of the ITM-DSM for rectangular surface foundations. The proposed method is used for obtaining the response of the SFI system in terms of dimensionless displacements in characteristic points of the foundation. The results for

displacements have been validated against the existing data from the literature.

## 2. FORMULATION

The formulation is derived by observing vertical vibrations of a rectangular flexible foundation on the surface ( $z=0$ ) of an elastic, homogeneous and isotropic half-space. It is assumed that the foundation behaves as a Kirchhoff plate. The steady state analysis of the response of the foundation is performed in the frequency domain,  $(x, y, \omega)$ . The response of the soil medium is obtained in the wavenumber-frequency domain  $(k_x, k_y, z, \omega)$ . It is understood that all functions are  $\omega$  dependent, regarding the steady state analysis. Therefore, the  $\omega$  variable is omitted in the notation of the functions.

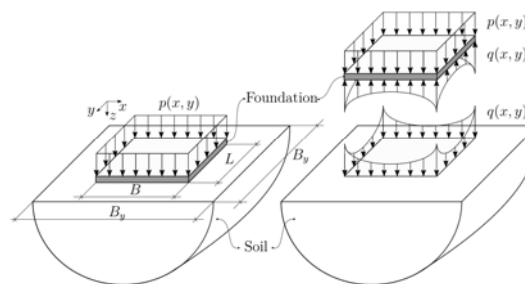


Figure 1. Disposition of the problem

The differential equation of the problem in  $(x, y, \omega)$  domain is given by

$$D \left( \frac{\partial^4 w(x, y)}{\partial x^4} + 2 \frac{\partial^4 w(x, y)}{\partial x^2 \partial y^2} + \frac{\partial^4 w(x, y)}{\partial y^4} \right) - \rho h \omega^2 w(x, y) = p(x, y) - q(x, y) \quad (1)$$

where  $D$  denotes the bending stiffness,  $w(x, y)$  is the displacement field,  $\rho$  is the material density and  $h$  is the thickness of the plate. The bending stiffness of the Kirchhoff plate is defined as

$$D = \frac{Eh^3}{12(1-\nu^2)} \quad (2)$$

where  $E$  is Young's modulus and  $\nu$  is Poisson's coefficient of the plate. The functions  $w(x, y)$ ,  $p(x, y)$  and  $q(x, y)$  are the transverse deflection of the foundation, the vertical load and the soil reaction, respectively. They can be expanded in a series of free vibration modes as follows:

$$w(x, y) = \sum_{n=0}^N Y_n \phi_n(x, y)$$

$$p(x, y) = \sum_{n=0}^N P_n \phi_n(x, y), \quad (3)$$

$$q(x, y) = \sum_{n=0}^N Q_n \phi_n(x, y)$$

where  $\phi_n(x)$  represents the orthonormalized mode shape of the foundation for the  $n^{th}$  mode and  $Y_n, P_n$  and  $Q_n$  are modal coefficients:

$$Y_n = \int_{x=0}^B \int_{y=0}^L w(x, y) \phi_n(x, y) dx dy$$

$$P_n = \int_{x=0}^B \int_{y=0}^L p(x, y) \phi_n(x, y) dx dy, \quad (4)$$

$$Q_n = \int_{x=0}^B \int_{y=0}^L q(x, y) \phi_n(x, y) dx dy$$

The mode shapes of the foundation are obtained for the case of free vibrations of the completely free plate, solving the eigenvalue problem by using the DSM [17]. The general solution of the problem is of the form

$$\phi_n(x, y) = e^{k_{xn}x} e^{k_{yn}y} \quad (5)$$

where  $k_{xn}$  and  $k_{yn}$  are wavenumbers in  $x$  and  $y$  direction, such that

$$k_{xn}^2 + k_{yn}^2 = \pm \omega_n \sqrt{\frac{\rho h}{D}} \quad (6)$$

The problem is solved by introducing an infinite series of base solution in the  $(k_x^2, k_y^2)$  plane [18]. Figure 2 shows the first eight mode shapes of a Kirchhoff plate. The first mode is a translational mode.

Substituting equations (3) and (5) into Eq. (1) gives

$$\sum_{n=0}^N (D(k_{xn}^4 + 2k_{xn}^2 k_{yn}^2 + k_{yn}^4) - \rho h \omega^2) \phi_n(x, y) Y_n =$$

$$= \sum_{n=0}^N \phi_n(x, y) P_n - \sum_{n=0}^N \phi_n(x, y) Q_n \quad (7)$$

Since mode shapes  $\phi_n(x)$  are orthonormal, for a uniform mass distribution, equation (7) can be decoupled into  $N$  equations by multiplying with mode shape  $\phi_m(x)$  and integrating over the area of the foundation. That gives the system of  $N$  equations, written in matrix form:

$$[D[\mathbf{k}^4] - \rho h \omega^2 [\mathbf{I}]] \{\mathbf{Y}\} = \{\mathbf{P}\} - \{\mathbf{Q}\} \quad (8)$$

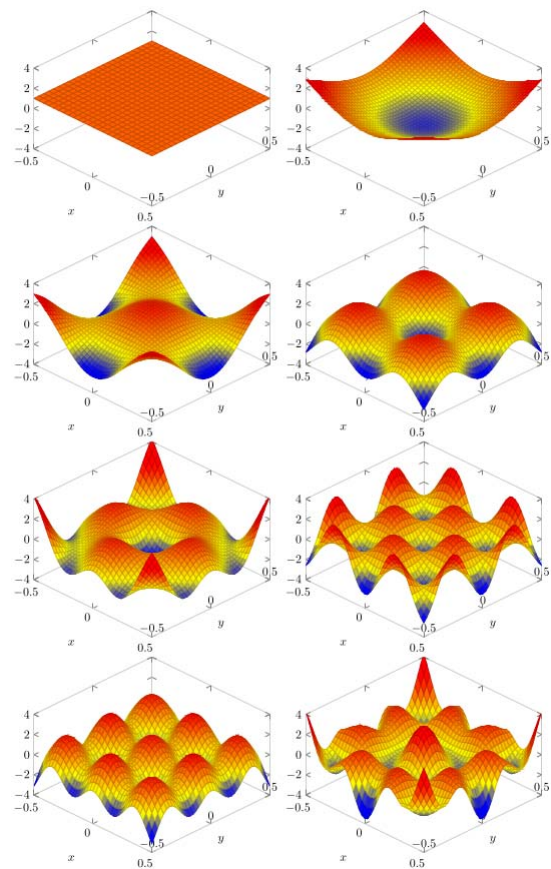


Figure 2. Free vibrations mode shapes of a rectangular foundation for  $n = 1-8$

where  $\{\mathbf{Y}\}, \{\mathbf{P}\}$  and  $\{\mathbf{Q}\}$  are coefficient vectors of the modal displacement, the load and the soil reaction, respectively,  $[\mathbf{I}]$  is identity matrix and  $[\mathbf{k}^4]$  is the pure bending wavenumber matrix of the plate

$$[\mathbf{k}^4] = \begin{bmatrix} 0 & 0 & \dots & 0 \\ 0 & \rho h \omega_1^2 & & \vdots \\ \vdots & & \ddots & 0 \\ 0 & \dots & 0 & \rho h \omega_N^2 \end{bmatrix} \quad (9)$$

In equation (9),  $\omega_n$  are natural frequencies of the plate, obtained using the DSM [19].

Relation between displacements and soil reaction coefficient vectors can be defined as follows

$$[\mathbf{K}_s] \{\mathbf{Y}\} = \{\mathbf{Q}\} \quad (10)$$

Substituting (10) into (8) the equation of motion becomes

$$[D[\mathbf{k}^4] - m_f \omega^2 [\mathbf{I}] + [\mathbf{K}_s]] \{\mathbf{Y}\} = \{\mathbf{P}\} \quad (11)$$

In equations 10 and 11  $[K_s]$  is the modal impedance matrix of the soil, obtained using ITM [14]. Once the modal impedance matrix of the soil is formed, the displacement coefficient vector  $\{Y\}$  is obtained by solving the system of equations (10) and finally the displacement field  $w(x,y)$  is obtained by using equation (3). To obtain the displacement field spectrum, the procedure should be repeated for every frequency in a desired frequency range.

A computer program based on this formulation is developed in MATLAB [20]. The results of the analysis are presented in terms of dimensionless displacements, in order to verify the response of the system with the results from the literature.

### 3. NUMERICAL EXAMPLE

In this section the vertical displacements of a square, massless, surface foundation excited by a uniformly distributed load are shown, see Figure 1. The damping mechanism is introduced by using a complex modulus with the damping coefficient  $\xi = 1\%$ . The analysis is performed by taking into account eight shape modes of the foundation shown in Figure 2. Since the problem is axi-symmetrical, only axi-symmetrical mode shapes are used.

The vertical displacement fields of the foundation obtained using the proposed method are compared with the results obtained by Whittaker and Christiano (W&C) [9]. They have modelled the foundation using thin plate finite elements. The displacements of a uniformly loaded plate are observed in three points: centre, edge midway and corner, Figure 3.

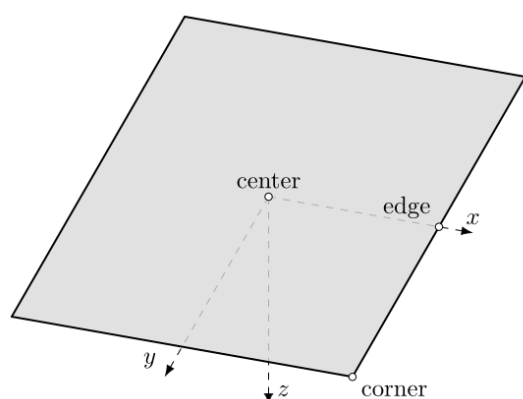


Figure 3. Characteristic points of the foundation

The results are presented in a dimensionless form,  $\Delta_i(a_0)$ , where  $\Delta_i$  is the dimensionless vertical displacement at the point  $i$

$$\Delta_i = \frac{wG_s B}{(1-\nu_s)\sum F_{ext}} \quad (11)$$

and  $a_0$  is the dimensionless frequency

$$a_0 = \frac{\omega B}{c_s} \quad (12)$$

In equations (11) and (12)  $w$  is the displacement,  $G_s$  is the shear modulus of the soil,  $\nu_s$  is Poisson's coefficient of the soil,  $\sum F_{ext}$  is the resultant of the external force in vertical direction, and  $c_s$  is the shear wave velocity in the soil.

The results are obtained for different foundation-soil stiffness ratios  $K$  introduced by Whittaker and Christiano

$$K = \frac{Eh^3(1-\nu_s^2)}{12(1-\nu_s^2)G_s\left(\frac{B}{2}\right)^3} \quad (13)$$

where  $E$  is Young's modulus and  $\nu$  is Poisson's coefficient of the plate.

Using the proposed method, the analysis is performed for  $K = 0, 0.004, 0.06, 3.3$  and the results are shown in Figures 4-7. The case of  $K=0$  corresponds to the analysis of the soil only (without foundation). For  $K \geq 3.3$  the foundation is considered rigid.

The results obtained by the proposed method are in a good agreement with the results from the literature. In general, with an increase of the relative stiffness  $K$  the displacements of the foundation become less spatially dependent. In the frequency range  $0 < a_0 < 4$ , for  $K=0$ , the proposed method gives lower amplitudes of the displacement at the centre of the foundation compared to the displacements from literature. For  $K > 0$ , the displacement amplitudes at the centre of the foundation tend to be higher than in literature, as opposed to the displacement amplitudes of the edge point and corner point. The differences between the results increase with the increase of  $K$  and  $a_0$ . In the frequency range  $a_0 > 4$ , the highest discrepancies between obtained results and results from literature are observed at the corner of the foundation. This is the point of significant stress concentration that is very difficult to model properly [21].



### 4. CONCLUSIONS

This paper presents an efficient semi-analytical method for obtaining the dynamic response of rectangular foundations resting on the surface of half-space. The method is based on the modal decomposition. The Dynamic Stiffness Method is used for obtaining mode shapes of the foundation. The impedance matrix of the soil is obtained by using the Integral Transform Method. The comparison of the results obtained using the proposed method with the results from the literature shows that the proposed method provides accurate results with low computational effort. The method could be easily reduced to problems of a strip foundation resting on a homogeneous or horizontally layered half-space as well as extended to the analysis of coupled horizontal and vertical vibrations problems.

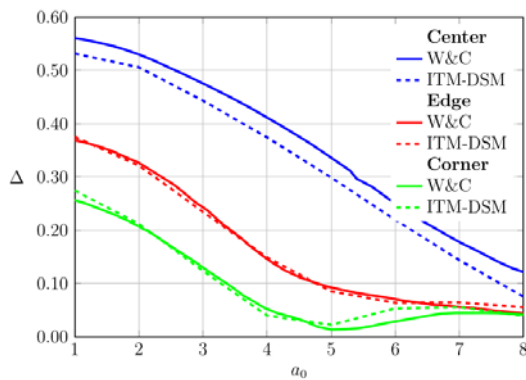


Figure 4. W&C - ITM-DSM comparison of the displacements of the characteristic points of the foundation,  $K = 0$

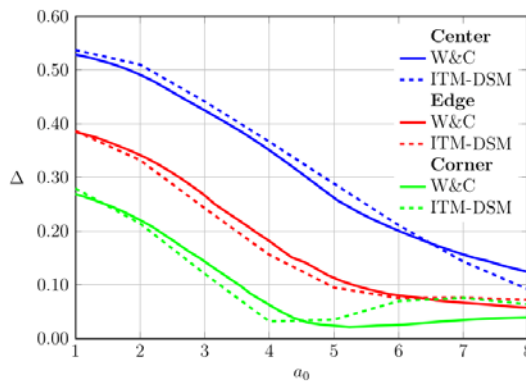


Figure 5. W&C - ITM-DSM comparison of the displacements of the characteristic points of the foundation,  $K = 0.004$

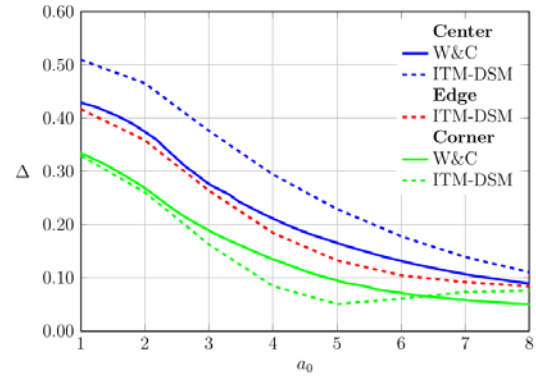


Figure 6. W&C - ITM-DSM comparison of the displacements of the characteristic points of the foundation,  $K = 0.06$

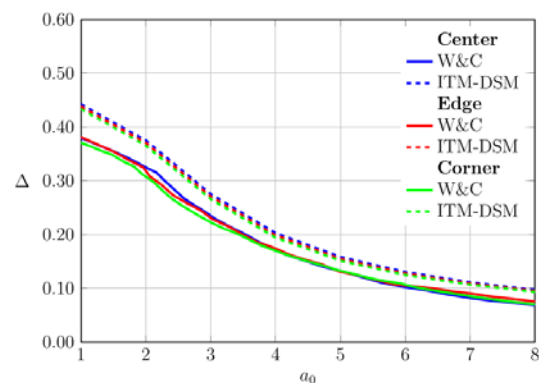


Figure 7. W&C - ITM-DSM comparison of the displacements of the characteristic points of the foundation,  $K = 3.3$

### Acknowledgements

This research is carried out within the Project TR36046 supported by the Ministry of Science and Technology, Republic of Serbia

### REFERENCES

- [1] G. Gazetas, "Analysis of machine foundation vibrations: State of the art," *Soil Dyn. Earthq. Eng.*, vol. 2, no. 1, pp. 2–42, 1983.
- [2] J. E. Luco, "Impedance functions for a rigid foundation on a layered medium," *Nucl. Eng. Des.*, vol. 31, no. 2, pp. 204–217, Jan. 1974.
- [3] J. I. Rastandi, "Modelization of Dynamic Soil-Structure Interaction Using Integral Transform-Finite Element Coupling," Technical University Munich, Munich, 2003.
- [4] M. Hackenberg, "A Coupled Integral Transform Method - Finite Element Method Approach to Model the Soil-Structure-Interaction," PhD Thesis, Technischen Universität München, Munich, Germany, 2016.

- [5] M. Radišić, G. Müller, and M. Petronijević, "Impedance Matrix for Four Adjacent Rigid Surface Foundations," in *IX International conference on structural dynamics - EUROODYN 2014*, Porto, Portugal, 2014, pp. 653–660.
- [6] F. T. Kokkinos and C. C. Spyrakos, "Dynamic Analysis of Flexible Strip-Foundations in the Frequency Domain," *Comput. Struct.*, vol. 39, no. 5, pp. 473–482, 1991.
- [7] C. C. Spyrakos and D. E. Beskos, "Dynamic response of flexible strip-foundations by boundary and finite elements," *Soil Dyn. Earthq. Eng.*, vol. 5, no. 2, pp. 84–96, Apr. 1986.
- [8] D. L. Karabalis and D. E. Beskos, "Dynamic response of 3-D flexible foundations by time domain BEM and FEM," *Int. J. Soil Dyn. Earthq. Eng.*, vol. 4, no. 2, pp. 91–101, Apr. 1985.
- [9] W. L. Whittaker and P. Christiano, "Dynamic Response of Plate on Elastic Half-Space," *J. Eng. Mech. Div.*, vol. 108, no. 1, pp. 133–154, 1982.
- [10] W. L. Whittaker and P. Christiano, "Response of a plate and elastic half-space to harmonic waves," *Earthq. Eng. Struct. Dyn.*, vol. 10, no. 2, pp. 255–266, Mar. 1982.
- [11] M. Iguchi, J. E. Luco, and O. N. An, "Dynamic response of flexible rectangular foundations on an elastic half-space," *Earthq. Eng. Struct. Dyn.*, vol. 9, no. 3, pp. 239–249, 1981.
- [12] M. Radišić, M. Petronijević, and G. Müller, "Vibrations of Flexible Strip on Viscoelastic Halfspace," *Procedia Eng.*, vol. 199, pp. 2420–2425, 2017.
- [13] M. Radišić, E. Damjanović, and M. Petronijević, "Vibrations of Massless Flexible Strip on Visco-Elastic Half-Space," in *7th International Congress of Serbian Society of Mechanics*, Sremski Karlovci, Serbia, 2019.
- [14] M. Radišić, "ITM-Based Dynamic Analysis of Foundations Resting on a Layered Halfspace," PhD Thesis, University of Belgrade, Belgrade, Serbia, 2018.
- [15] S. Kevorkian and M. Pascal, "An Accurate Method for Free Vibration Analysis of Structures with Application to Plates," *J. Sound Vib.*, vol. 246, no. 5, pp. 795–814, Oct. 2001.
- [16] S. S. Chen and J. G. Hou, "Modal analysis of circular flexible foundations under vertical vibration," *Soil Dyn. Earthq. Eng.*, vol. 29, no. 5, pp. 898–908, 2009.
- [17] M. Nefovska-Danilović, M. Petronijević, and M. Radišić, "Transverse vibration of plate with edge beams using spectral element method," in *Proceeding 4th International Congress of Serbian Society of Mechanics*, Vrnjačka Banja, Serbia, 2013, pp. 347–352.
- [18] P. H. Kulla, "High precision finite elements," *Finite Elem. Anal. Des.*, vol. 26, no. 2, pp. 97–114, Jun. 1997.
- [19] M. Nefovska-Danilović, "Dynamic analysis of soil-structure system using spectral element method," PhD Thesis, University of Belgrade, Belgrade, Serbia, 2012.
- [20] MathWorks, *MATLAB 2013a*. MathWorks Inc. The Language of Technical Computing, 2013.
- [21] M. Mohammadi and D. L. Karabalis, "3-D soil-structure interaction analysis by BEM: Comparison studies and computational aspects," *Soil Dyn. Earthq. Eng.*, vol. 9, no. 2, pp. 96–108, 1990.

## CLASSROOM ACOUSTICS ASSESSMENT

### AUTHORS

#### **Milica Jovanoska**

MSc, Assistant

Ss. Cyril and Methodius University  
Faculty of Civil Engineering - Skopje  
24, Partizanski odredi blvd, 1000  
m.jovanoska@gf.ukim.edu.mk

#### **Todorka Samardzioska**

PhD, Full Professor

Ss. Cyril and Methodius University  
Faculty of Civil Engineering - Skopje  
24, Partizanski odredi blvd, 1000  
samardzioska@gf.ukim.edu.mk

The concept of “good acoustics” is a combination of objective and subjective parameters. Real-time analysis allows the whole spectrum of a sound to be analyzed and to consider several parameters simultaneously in order to examine the acoustic quality of a classroom. Several measurements were performed to determine the sound fields and reverberation times in function of frequencies. Pink noise was generated from speakers and measurements were carried out using Cirrus 171b sound level meter. The sound source was located on the usual teacher's position, centrally in relation to the width of the room and 11 measurement positions were used to register the sound signals. To expand the information of the classroom acoustics, analytical and numerical analyses were carried out. Room modes were calculated using analytical relations and numerical FEM calculation. For the low frequencies, FEM Pressure Acoustics Analysis in Frequency Domain Module was performed, and for high frequencies, Geometric Acoustics - Ray Tracing method was used. Numerical analyses were conducted using the multi-physics software COMSOL. The acoustic parameters such as Clarity (C50) and Speech Transfer Index (STI) can be calculated out from the measured reverberation time, using the relations derived by Baron and Lee, [2]. The necessary acoustic parameters can be obtained also from the numerical analysis, from the Impulse Response and Energy Decay Curves for the modeled receiver position. The pronounced reflective nature of all constituent surfaces is the main problem in the room. This can be confirmed by the extremely large values of the reverberation time, T. To achieve satisfactory classroom acoustics, acoustic treatment using sound absorbing materials is required.

**Keywords:** classroom acoustics, room modes, pressure acoustics, ray tracing.

### 1. INTRODUCTION

Sound communication, which is the fundamental mechanism for perception, transmission and exchange of information, imposes the need for acoustic optimization of the rooms. Depending on the purpose of the room, various criteria for acoustic quality are

set, starting from elementary comfort to precisely defined acoustic needs in rooms with specific purpose, such as concert halls, theatres, recording studios, etc. Low quality of classroom acoustics leads to poor speech perception, poor listening comprehension, sound-induced disturbance and vocal fatigue in teachers. This emphasizes the importance of classroom acoustic quality.

Adapting the basement space of the Faculty of Civil Engineering in Skopje, an auxiliary classroom was built, Figure 1. The classroom has a rectangular shape with plane dimensions of 6.73 m x 13.76 m and height,  $h=3.00$  m up to the beam and  $h=3.30$  m up to the slab. The walls are built of plastered concrete, the ceiling is uncovered ribbed concrete slab and the floor is covered with linoleum. Painted plywood panels are hanged on the walls. These panels are used during the student exhibitions. The windows are double glazed with wooden frames. It is obvious that all of the interior surfaces of the considered classroom are hard and exclusively reflective. There is a lack of sound absorption surface and therefore, a long reverberation time (bad acoustics) in the classroom is expected.

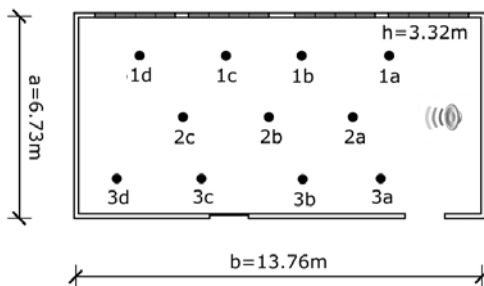
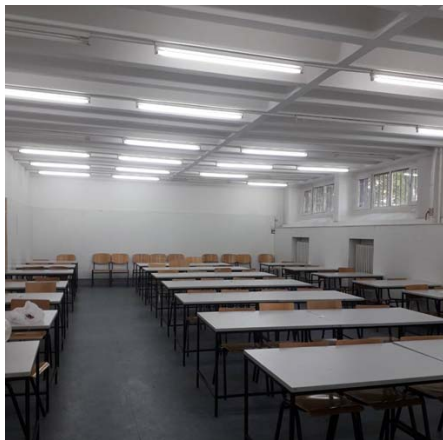


Figure 1. Interior and geometry of the classroom.

## 2. EXPERIMENTAL RESULTS

In order to examine the acoustic quality of the classroom, several measurements were

performed using the sound level meter Cirrus 171b (class 1 microphone, microphone pre-amplifier, 1:3 octave band filters). The sound source position and the pattern of the measurement positions are given in Figure 1. The sound level,  $L$ , is recorded with the sound level meter in 11 measuring positions in three levels ( $h_1 = 1.2$  m,  $h_2 = 1.5$  m,  $h_3 = 2$  m). For each measuring position and for each level, three measurements were performed, and then averaged. A total of 99 measurements were processed in 1/3 octave spectrum. Graphic representation of the sound field for  $f=250$  Hz and  $f=500$  Hz is shown in Figure 2.

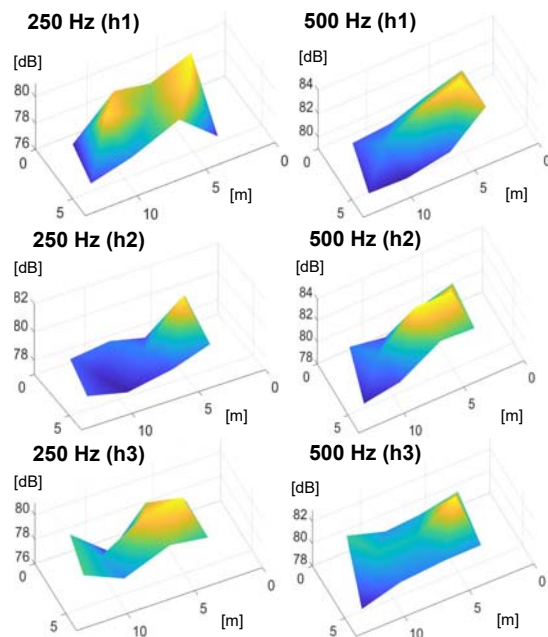


Figure 2. Sound field in the classroom for 250 Hz and 500 Hz.

For each measuring position, the reverberation time is obtained as the mean value of three measurements, as presented in Figure 3.

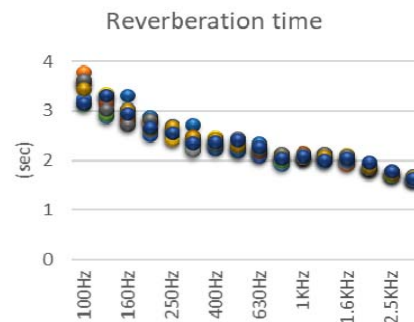


Figure 3. Reverberation time.

For low frequencies, the reverberation time has values between 2.5 sec and 3.5 sec, for middle frequencies between 2.1 sec and 2.5 sec and for high frequencies between 1.6 sec and 2.1 sec. The mean value for all frequencies is  $T=2.5$  sec.



### 3. ANALITICAL AND NUMERICAL MODELING

#### 3.1 ROOM MODES

The resonance frequencies in a room are called room modes or standing waves. The term regular room refers to a room that has three pairs of parallel walls connected at 90° angles. The room extends from  $x=0$  to  $x=L_x$  in the  $x$ -direction, and similarly from  $y=0$  to  $y=L_y$  and from  $z=0$  to  $z=L_z$ . It is assumed that all walls are rigid, which means that normal components of the velocity of particles disappear at the surface of the walls. Starting from the Helmholtz equation and setting the appropriate boundary conditions, the room modes can be obtained from the relations, [6]:

$$f_{n_x, n_y, n_z} = \frac{c}{2\pi} k_{n_x, n_y, n_z} \quad (1)$$

$$k_{n_x, n_y, n_z} = \pi \left[ \left( \frac{n_x}{L_x} \right)^2 + \left( \frac{n_y}{L_y} \right)^2 + \left( \frac{n_z}{L_z} \right)^2 \right] \quad (2)$$

where  $n_x$ ,  $n_y$  and  $n_z$  are positive integers that identify the room mode,  $c$  is the speed of sound in the air and  $k$  is the wave number.

Most of the sound energy is stored in the axial, then tangential modes, while the oblique modes are negligible. Above the Schroeder frequency ( $f_s$ ), the room acts as a reverberant room, while under the Schroeder frequency the influences of discrete modes dominate (modal region). For the room under consideration, the average reverberation time is  $T=2.5$  sec, while the volume is equal to  $V=13.76 \times 6.73 \times 3.15 = 291.7 \text{ m}^3$ , hence:

$$f_s = 2000 \sqrt{\frac{T}{V}} = 185 \text{ Hz} \quad (3)$$

If we adopt regular form for the classroom, from the Equation 1 and Equation 2, the axial, tangential and spatial room modes can be calculated under the Schroeder frequency.

Table 1. Several room modes.

12.46 Hz	1-0-0	ax	147.74 Hz	6-5-0	tan
24.93 Hz	2-0-0	ax	149.15 Hz	0-4-2	tan
25.48 Hz	0-1-0	ax	149.56 Hz	12-0-0	ax
28.37 Hz	1-1-0	tan	151.57 Hz	9-4-0	tan
35.65 Hz	2-1-0	tan	151.72 Hz	12-1-0	tan
37.39 Hz	3-0-0	ax	152.9 Hz	0-6-0	ax

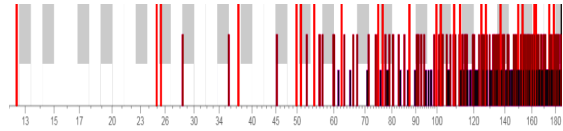


Figure 4. Distribution of the room modes under Schroeder frequency.

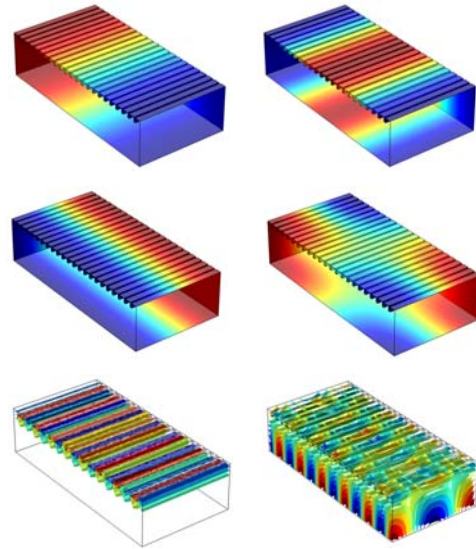


Figure 5. Room modes from COMSOL.

This simulation in Pressure Acoustics interface in COMSOL predicts eigenmodes that for the low frequency strongly resemble with the analytical solution, Figure 5, a-d. The higher the frequency, the more the geometry details matters, in this case the concrete ribs interfere, Figure 5, e-f.

#### 3.2 PRESSURE ACOUSTICS – FREQUENCY DOMAIN

The behaviour of rooms at low frequencies is analysed solving Helmholtz equation using the finite element method. In order to resolve the wave, the mesh size should be less than  $\lambda/6$ , where  $\lambda$  is wavelength. FEM method can be used optimally up to 2-3 kHz, after this region, the number of the degrees of freedom is too high and the computational effort is non-reasonable.

The model assumes that all boundaries are hard (rigid) boundaries. This can be easily changed and adapt to the real characteristics. The membranes of the speakers are modelled with normal acceleration boundary condition.

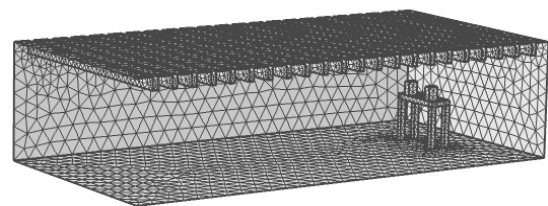


Figure 6. – Model mesh.

The distribution of the sound pressure level for  $f=250$  Hz is presented in the Figure 7. The plots for h1, h2 and h3 levels are also given.

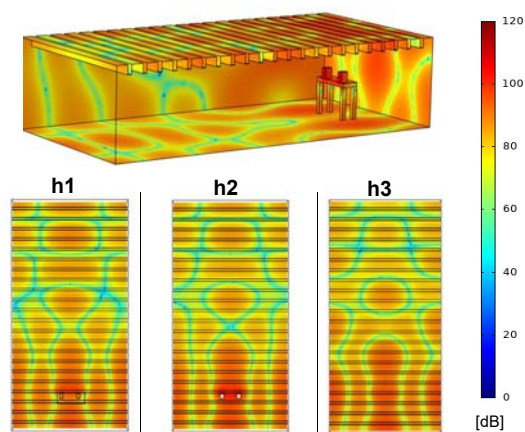


Figure 7. – Sound pressure level,  $f=250$  Hz.

For the higher frequencies, the absorption coefficients of the boundaries should be included for more realistic modelling.

### 3.3 RAY TRACING

For large geometries or/and high frequencies, the Geometry acoustics (Ray Tracing, Acoustic Diffusion) gives the more optimal results. The big advance for this method is that only coarse meshing of boundaries is needed. With Ray Tracing, the trajectories, phase, and intensity of acoustic rays can be computed, and also the impulse response.

The boundaries are modeled as concrete with recommended absorption coefficient with specular reflection and the source is modeled with spherical radiation. Specular reflection is a mirror-like reflection. The ray trajectories for different time sequences are given in Figure 8.

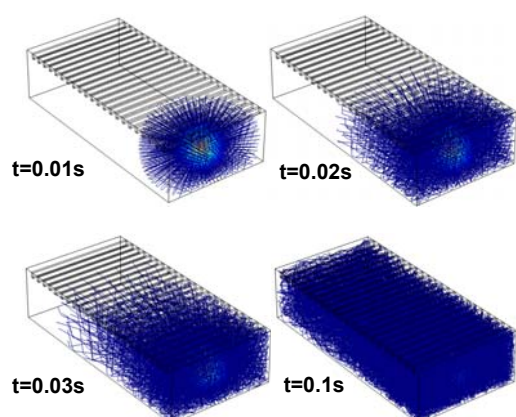


Figure 8. – Ray trajectories.

In order to obtain the impulse response, it is necessary to model the sound power and intensity through the rays. The propagation in

the unmeshed domains is defined with the material properties of the fluid - air.

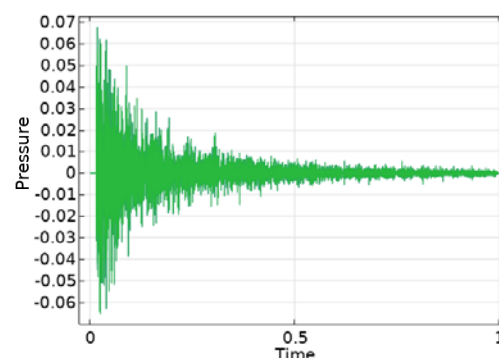


Figure 9. – Impulse response.

From the impulse response, with additional post-processing, relevant acoustic parameters can be obtained, such as C50, EDT, STI etc.

## 4. CONCLUSION

In classrooms and lecture halls, it is necessary to ensure clear perception of speech. The main problem in the analyzed classroom is the pronounced reflective nature of all surfaces. This is shown by the large values of the reverberation time. Regarding Sabine's equation, [6], to achieve an optimal reverberation time of 0.5 sec, an equivalent absorption area  $A=93.93$  m<sup>2</sup> is required. According to the mean measured value  $T=2.5$  sec,  $A=18.79$  m<sup>2</sup>, which is five times less than the required absorption area. As the classroom falls into medium-volume rooms, by installing sufficient absorption surface, the Schroeder frequency will be shifted towards lower region, avoiding the modal region problem.

Numerical methods can simulate virtual measurements and/or expand all the necessary data, which is difficult to obtain with measurements regarding the fact that one microphone is one measuring point.

## REFERENCES

- [1] Ballou Glen, Handbook for Sound Engineers, Elsevier, Burlington, 2008.
- [2] Barron M., Lee L. J., Energy relations in concert auditoriums, J Acoust Soc Am, vol 84, 1988.
- [3] Everest F.Alton, Pohlmann Ken C., Master Handbook of Acoustics, New York, 2009.
- [4] Heutschi Kurt, Lecture notes on Acoustics, ETH, Zurich, 2016.
- [5] Khrystoslavenko O., Grubliauskas R., Simulation of Room Acoustics Using Comsol Multiphysics, Environmental protection engineering, ISSN 2029-7157, 2017.
- [6] Kuttruff Heinrich, Room Acoustics, Spon Press, Oxon, 2009.

## AUTHORS

### **Kristina Milkova**

Assistant  
Ss. Cyril and Methodius University  
Faculty of Civil Engineering – Skopje  
milkova@gf.ukim.edu.mk

### **Elena Dumova-Jovanoska**

PhD, Full Professor  
University “Ss. Cyril and Methodius”  
Faculty of Civil Engineering – Skopje  
dumova@gf.ukim.edu.mk

### **Franco Vaccari**

Research fellow  
Department of Mathematics and Geosciences  
University of Trieste, Italy  
vaccari@units.it

### **Fabio Romanelli**

Researcher, Department of Mathematics and  
Geosciences  
University of Trieste, Italy  
romanel@units.it

### **Giuliano F. PANZA**

Olim Professor,  
Accademia Nazionale dei Lincei  
Via della Lungara, 10 – Roma, Italy  
giulianofpanza@fastwebnet.it

## **APPLICATION OF NEO- DETERMINISTIC ANALYSIS FOR NORTH MACEDONIA**

In this paper, a scenario-based neo-deterministic approach for seismic hazard assessment (NDSHA) giving a realistic description of the seismic ground motion due to an earthquake of a given distance and magnitude is applied to the territory of North Macedonia and the hazard maps are obtained. A comprehensive understanding of both the seismic source process and the propagation of seismic waves is a prerequisite in the process of the application of NDSA on a specific region. The procedure is based on the integration of the existing geological, seismotectonic and geotechnical databases relevant to the selected region. In the definition of scenario earthquakes, the available seismic data, as well as information for the geological active faults in North Macedonia are used. This multi scenario-based analysis simultaneously incorporates the known databases and with use of advanced physical modeling techniques provides the required ground motion data set.

The results are based on the computation of realistic synthetic seismogram. A reliable hazard map at regional scale, for the complete territory of North Macedonia are shown.

As a final result, Maximum Credible Seismic Input – MCSI is computed for various locations in North Macedonia and valuable response spectra for the selected locations are obtained.

These data (spectra and time histories) are set to be used as seismic input for the nonlinear analysis of the existing structures in North Macedonia in the process of seismic risk analysis on a regional scale.

**Keywords:** Seismic hazard; Neo-deterministic seismic hazard assessment; Hazard maps; Maximum Credible Seismic Input

## **1. INTRODUCTION**

The ground shakings that occur repeatedly remains as of the importance of the continues research in the field of hazard estimation on a region, as an input in the process of seismic

design of buildings and a crucial requirement for performing the seismic risk analysis of a given characteristic building class.

Two approaches, probabilistic seismic hazard analysis (PSHA) and deterministic seismic hazard analysis (DSHA), are commonly used in the process of seismic hazard assessment.

The most frequently used method is the Probabilistic Seismic Hazard Assessment (PSHA). Eurocode defines the seismic design parameters in terms of PGA and probabilities of exceedance needed to satisfy the two fundamental requirements: (1) No-collapse and (2) Damage limitation for which the seismic action shall be associated with reference probability of exceedance (10%) in 10 and 50 years reference period [6]. In the deterministic approach (DSHA) seismic hazard assessment is done in terms of a fixed ground motion measure, given the magnitude and the location of a scenario event. In the neo-deterministic approach, NDSHA, the integration of all known information from seismological, geological, geophysical, and geotechnical databases for the site of interest are used [7]. Neo-deterministic seismic hazard (NDSHA) maps for the region of Kosovo-North Macedonia have been elaborated, based on the obtained ground motion parameters maximum values for frequencies up to 1Hz. [2].

## 2. NEO-DETERMINISTIC SEISMIC HAZARD ASSESSMENT AT REGIONAL SCALE

### 2.1 STRUCTURAL MODEL DEFINITION

For the purpose of structural model definition, the zoning proposed by Arsovski [1] was used. The map of geotectonic zoning from Arsovski was utilized for the definition of the structural polygons required by NDSHA. Each polygon is associated with a structural model, composed of a stack of flat anelastic layers, representing the average properties down to a depth of about 1000km. All of the defined polygons are characterized with the thickness of each layer, the density, P and S wave velocities and their attenuation factors. The results from the TRANSMED project were used, where the geology of the Mediterranean realm is represented in 9 sections across the tectonic structures. Of a great importance for the definition of the layers' properties [9] was the fact that the longest section crosses the whole territory North Macedonia.

### 2.2 HISTORICAL SEISMICITY AND SEISMIC ZONATION

The location of the North Macedonia, as part of the Balkan Peninsula is a territory characterized by relatively high seismic hazard and has been struck by a number of strong earthquakes during the past centuries. The earthquake catalogue that is used consists of all of the significant events registered from year 518 until 2015. For the earthquakes occurred before 1904 only the epicenters and the magnitudes are provided. The fault plane mechanism for all of the other events is calculated at the Seismological Observatory of the Faculty of Natural Sciences and Mathematics, Ss. Cyril and Methodius University, Skopje.

Having in mind the earthquake data only from the last century, in lacking information it can be reasonably concluded that more severe seismic events may have happened on this territory.

### 2.3 THE PROCEDURE

NDSHA at regional scale [7-8] incorporates together the knowledge of tectonic style of the considered region, the active fault characterization, the earth crust model and the historical seismicity. The modal summation techniques are used for wave propagation modeling. Synthetic seismograms are generated at all of the predefined grid points distributed over the region of interest. The calculated maximum values of ground horizontal velocity, horizontal displacement and design ground acceleration are used as seismic hazard parameters.

The region is divided into  $0.2^{\circ} \times 0.2^{\circ}$  grid cells and at every node in the grid is given the maximum value of the magnitudes reported in the earthquake catalogue (Figure 1). The smoothing procedure defined by NDSHA is then applied in order to account for the uncertainties connected with the exact location of the epicenters, for the fault dimensions and for the location of possible future events within the seismically active areas. The smoothing procedure consists of several steps [7]. First, a running window with radius of 3 cells is defined. Second, all of the points in the window are assigned with the magnitude of the central cell, if their magnitude is lower than the magnitude of the central cell. The seismicity obtained after the smoothing procedure (Figure 2) is then cut within the seismogenic zones that represent the seismically active regions (Figure 3). Each dot



inside a seismogenic zone represents a source. The characteristic focal mechanisms from the dominant earthquake of each seismogenic zone are assigned to each source belonging to the zone itself.

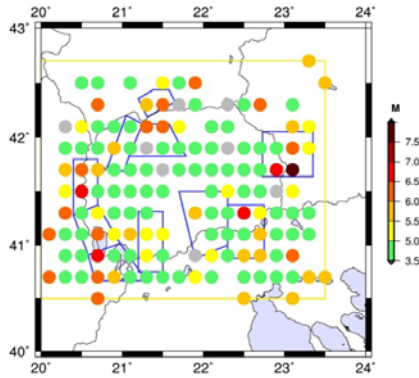


Figure 1. Discretization of seismicity.

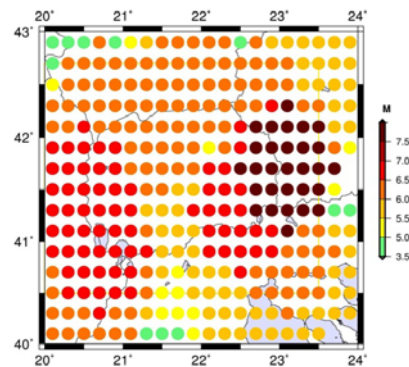


Figure 2. Smoothing.

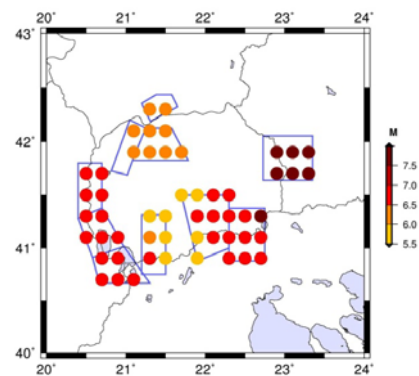


Figure 3. Seismogenic zones with sources.

### 3. MAXIMUM CREDIBLE SEISMIC INPUT – MCSI

Maximum Credible Seismic Input (MCSI) [3-4] is a procedure that calculates the response spectra at a selected site, taking into account the uncertainties of the rupturing process on the fault. Several ground shaking scenarios are modeled [4] at the site of interest by

making the variations in the nucleation point of the rupture, in the rupture velocity pattern and in the distribution of the slip on the fault, taking account also the directivity effects. Additionally, the methodology has been implemented in such a way that it allows to take into account scenarios obtained varying any parameter that defines the model, like focal mechanism of the sources, hypocentral depth, layering of the lithosphere etc.

Maximum Credible Seismic Input (MCSI) is obtained as the envelope of the response spectra computed at each site. By applying this procedure to the six cities of interest in North Macedonia, the response spectra are computed. MCSI is calculated for 5% damping of the response spectra. Six families of scenarios are taken into account: bilateral rupturing style with 0° directivity, bilateral rupturing style with 90° directivity, bilateral rupturing style with 180° directivity, unilateral rupturing style with 0° directivity, unilateral rupturing style with 90° directivity and unilateral rupturing style with 180° directivity. For each family 50 realizations of the rupturing process have been modeled. Response spectra are obtained separately for each scenario event, and then properly merged to have a comprehensive estimate of the seismic input.

### 4. RESULTS

On Figure 4 the results from a single execution (source realization) of the NDSHA analysis for the maximum ground shaking for the horizontal directions acceleration are shown.

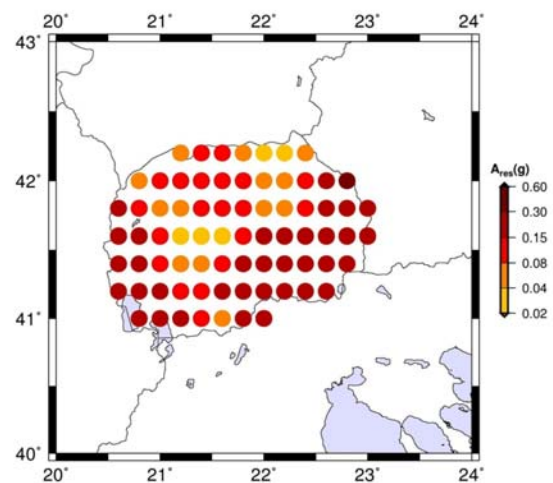


Figure 4. Peak horizontal acceleration.

As a result from MCSI, Two components can be considered when combining the results,



shown in Figure 5 as Max and Res. Both of them represent the amplitude of the calculated spectra: the plot Max considers the maximum horizontal component, while the plot Res takes into account the resultant of the two horizontal components, and therefore provides a more conservative hazard estimate. In the plots of Figure 5, each colored curve represents the median response spectrum of 50 realizations of the rupturing process for one scenario that contributes to the envelope. The six scenarios listed for MCSI Max correspond to three sources located at different azimuth and/or distance with respect to the site (*sre* and *edi* parameters). In the MCSI Res plot only one source contributes to MCSI, with three different directivity effects. In each plot, the shaded areas represent the spectral accelerations comprised, at each period, between the median and the 95th percentile of the distribution.

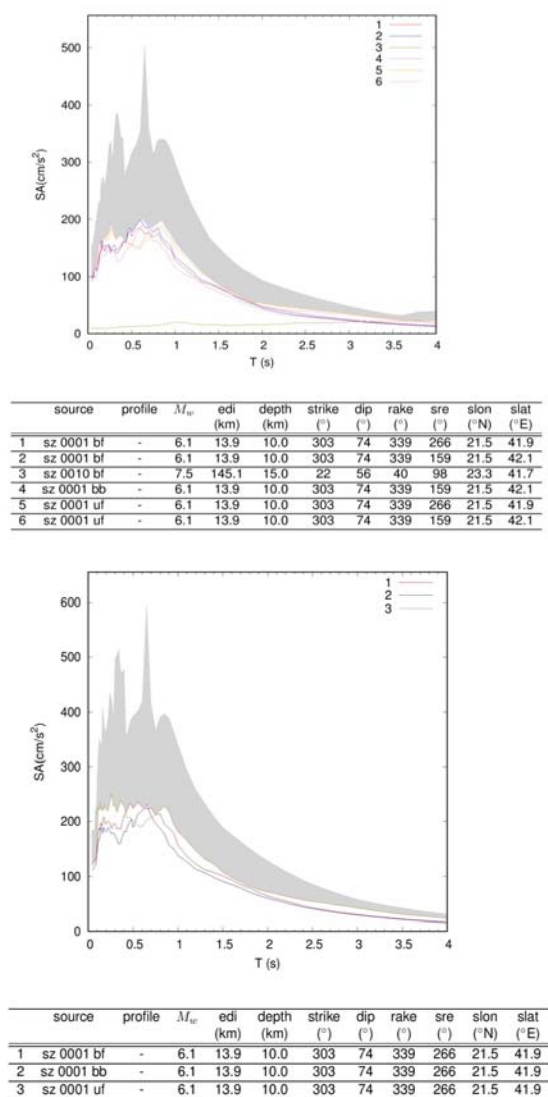


Figure 5. MCSI obtained at one selected site of interest. Maximum (top) and Resultant (bottom) horizontal components are considered.

In the source label, *bf* indicates bilateral rupture with forward directivity, *bb* bilateral rupture with backward directivity, *uf* unilateral rupture with forward directivity. At this site, no part of the MCSI spectrum is associated with the scenarios generated with neutral directivity (*bn* or *un*), or unilateral rupture with backward directivity (*ub*).

## REFERENCES

- [1] Arsovski M. (1997). Tectonics of Macedonia, *Ph.D. Thesis*, Faculty of Geology and Mining, Stip. 306 p. (in Macedonian).
- [2] Dojcinovski, D., Pekevski, L., Hasi, N., Olumceva, T., Panza, G.F., Vaccari, F., Romanelli, F. (2013). Re-Evaluation of Seismic Hazard for the Territory of Republic of Macedonia and Kosovo: Neodeterministic Approach”, International SE-50EEE Conference to mark 50 years of Skopje Earthquake, May 28-31, 2013, Skopje, R. Macedonia.
- [3] Fasan, M., Magrin, A., Amadio, C., Romanelli, F., Vaccari, F., Panza, G.F. (2016). A seismological and engineering perspective on the 2016 Central Italy earthquakes, *Int. J. Earthquake and Impact Engineering*, Vol. 1, No. 4, 395-420.
- [4] Fasan, M., Magrin, A., Amadio, C., Panza, G.F., Romanelli, F., Vaccari, F., Noè, S. (2017). A possible revision of the current seismic design process, *16th World Conference on Earthquake Engineering*, 16WCEE 2017, Santiago Chile.
- [5] Gusev, A.A. (2011). Broadband kinematic stochastic simulation of an earthquake source: a refined procedure for application in seismic hazard studies, *Pure and Applied Geophysics* 168, 155–200. doi:10.1007/s00024-010-0156-3.
- [6] Milutinovic, Z., Salic, R. (2015), An Overview on Earthquake Hazard and Seismic Risk Management Policies of Macedonia, *International SE-50EEE Conference to mark 50 years of Skopje Earthquake*, May 28-31, 2013, Skopje, R. Macedonia.
- [7] Panza, G.F., Romanelli, F., Vaccari, F. (2001). Seismic wave propagation in laterally heterogeneous anelastic media: theory and applications to seismic zonation, *Advances in Geophysics*, Vol. 43, pp.1–95.
- [8] Panza, G.F., La Mura, C., Peresan, A., Romanelli, F., Vaccari, F. (2012). Seismic hazard scenarios as preventive tools for a disaster resilient society, *Advances in Geophysics*, Vol. 53, pp.93–165.
- [9] Zagorchev, I., Dabovski, C., Dumurdzhanov, N. (2008). Tectonic structure of Bulgaria and Macedonia based on transmed Transect iii, *First Congress of Macedonian geologists*, Ohrid, Macedonia.

#### AUTHORS

##### **Marija Docevska**

M.Sc.

Ss. Cyril and Methodius University  
Faculty of Civil Engineering – Skopje  
Bul. Partizanski Odredi 24, 1000  
docevska@gf.ukim.edu.mk

##### **Goran Markovski**

PhD, Full Professor

Ss. Cyril and Methodius University  
Faculty of Civil Engineering – Skopje  
markovski@gf.ukim.edu.mk

##### **Peter Mark**

PhD, Full Professor

Ruhr University Bochum, Germany  
Institute of Concrete Structures  
peter.mark@rub.de

## **CREEPING EFFECTS OF CONCRETE UNDER TIME- VARYING STRESS HISTORIES**

Certain concrete structures during their service life are exposed to variable repeated loads with significant magnitude and duration. Typical examples are bridges, parking garages and storage buildings where besides permanent, variable loads can also affect the long-term concrete behavior. Currently, this concrete phenomenon to creep under variable loads is well-recognized in the codes and considered through the so-called quasi-permanent load. However, the creep and the recovery property under these load types are still far from clear.

This paper is concerned with a study of the effects of variable repeated stresses on the creep and creep recovery of concrete. For that purpose, two separate experiments were performed in which concrete specimens were exposed to time-variable uniaxial compressive stresses. The first experiment aims at assessing the influence of different service stress levels at loading (30% and 45% of  $f_c$ ) as well as different level of unloading (full and partial unloading). The second one focusses on the influence of different drying conditions of the specimens (sealed and unsealed condition).

The results indicate that regardless of the stress level, the creep becomes fully recoverable after a sufficient number of loading and unloading cycles. On the other hand, the drying conditions show remarkable influence on the irreversible proportion of the creep in each loading cycle. Moreover, the absolute value of the creep recovery seems unaffected by the hygral exchange conditions of the specimens.

The obtained results demonstrate that the creep behavior under repeating stresses in a large scale differs from the ones under just sustained stresses.

**Keywords:** time-variable load, creep, creep recovery, drying conditions, quasi-permanent load.

## 1. INTRODUCTION

The influence of the sustained service loads on the time-dependent concrete behavior is widely researched. In the last decades, large research efforts have been also dedicated to understand the influence of other load types (variable, cyclic) on the long-term behavior of concrete structures. Among them are experimental studies conducted at FCE Skopje [1,3,4] which focusses on repeating load types applied on beam elements. The results from these studies clearly indicate that the concrete creep does not appear only under constant sustained load. The intensity [3], as well as the duration [1] of the variable loads can significantly influence the time-dependent behavior of reinforced concrete structures.

Time-dependent deformations caused by the application and removal of a load (like in repeated variable load histories) referred to as creep and creep recovery.

This study intends to give a detailed insight into these properties under repeating loads by testing concrete specimens under different loading and drying conditions. To replicate the real field conditions, the study involves different loading and unloading levels (test series 1) as well as different hygral states of concrete (test series 2), considered within two independent experiments.

The complete experimental program along with the most relevant findings are going to be outlined in the following sections.

## 2. DECOMPOSITION OF TIME-DEPENDENT STRAINS

At a time  $t$ , under constant stress and temperature, the total concrete strain  $\epsilon_c(t)$  consists of: instantaneous strain  $\epsilon_i(t_0)$ , creep strain  $\epsilon_{cc}(t, t_0)$  and shrinkage strain  $\epsilon_{cs}(t, t_s)$ .

At the removal of applied loads, a distinction should be made between instantaneous recovery  $\epsilon_e(t_e)$ , generally very close in absolute value to the instantaneous strain at the same age, and the total recovery  $\epsilon_{rec.tot.}$ , which is defined by the difference between the strain measured after unloading  $\epsilon_{res}$  and the strain that would have been recorded at the same age if there had been no unloading  $\epsilon_c(t)$  [2] (Fig.1):

$$\epsilon_{rec.tot.} = \epsilon_e + \epsilon_{cr.rec.} = \epsilon_c - \epsilon_{res} = \epsilon_c - \epsilon_{cs} - \epsilon_{cr.f} \quad (1)$$

The creep recovery  $\epsilon_{cr.rec.}$  can accordingly be defined as:

$$\epsilon_{cr.rec.} = \epsilon_c - \epsilon_e - \epsilon_{cs} - \epsilon_{cr.f} \quad (2)$$

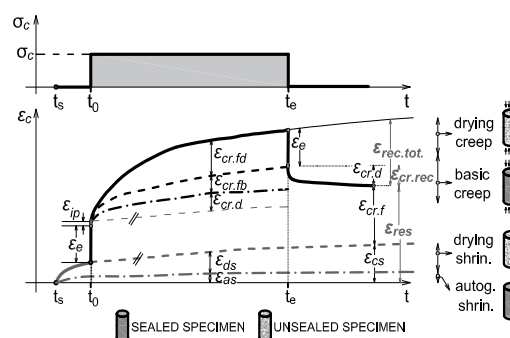


Figure 1. Time-dependent strain components.

The recoverable part of creep is often ascribed to the delayed elastic strain  $\epsilon_{cr.d}(t)$ .

The major share of the creep strain is irreversible and often referred to as the flow  $\epsilon_{cr.f}(t)$ . The flow component of creep is subdivided into rapid initial flow  $\epsilon_{cr.fi}(t)$  and remaining flow  $\epsilon_{cr.f}(t)$ . The remaining flow can be further divided into basic flow  $\epsilon_{cr.fb}(t)$  and drying flow  $\epsilon_{cr.fd}(t)$  (Fig.1) [2].

Concrete creep within an element of a cross-section is non-uniform with respect to moisture. For instance, at the initial state when the load is applied for the first time, the concrete has not yet lost much of its initial moisture and therefore, creeps in sealed conditions (so-called basic creep) [5]. Later and near the surface of a member, creep takes place in a drying environment and develops different from the creep in the regions remote from a drying surface. In this case, additional creep share occurs known as drying creep.

The total longitudinal strain in sealed conditions  $\epsilon_{sealed}^{tot}$  consists of the instantaneous elastic strain  $\epsilon_e$ , the rapid initial strain  $\epsilon_{cr.fi}$ , the basic creep strain  $\epsilon_{cr.fb}$  and the autogenous shrinkage strain  $\epsilon_{as}$ . The load-induced strain is:

$$\epsilon_{sealed}^{tot} - \epsilon_{as} = \epsilon_e + \epsilon_{cr.fi} + \epsilon_{cr.fb} \quad (3)$$

In case of unsealed conditions, the total longitudinal strain  $\epsilon_{unsealed}^{tot}$  consists of two shares more, namely the drying creep strain  $\epsilon_{cr.fd}$  and the drying shrinkage  $\epsilon_{ds}$ . The load-induced strains can then be obtained as:

$$\epsilon_{unsealed}^{tot} - \epsilon_{as} - \epsilon_{ds} = \epsilon_e + \epsilon_{cr.fi} + \epsilon_{cr.fb} + \epsilon_{cr.fd} \quad (4)$$

### 3. EXPERIMENTAL PROGRAM

Two independent experiments were organized to provide a better understanding of the creep components under different repeating stress histories and drying conditions. They are performed in the Structural Testing Laboratory at Ruhr University Bochum (Germany). Table 1 gives an overview on the test setups, curing conditions, stress to strength ratios and loading histories to yield the specific aims.

Variables in the first test series were stress to strength ratios at loading  $R_L$  and unloading  $R_U$ . Conversely, variables within the second test series were drying conditions as well as the type of a stress history.

The stress levels in both experiments were chosen between 30% and 45% of the compressive concrete strength. The duration of the loading to unloading cycles (8h/16h and 12h/12h) was chosen to replicate typical live load variations in daily used concrete structures.

The studied concrete in both experiments was chosen to a standard C30/37 with no additives.

#### 3.1 TEST SERIES 1

Five standard cylinders in total were involved in this series. Two of them (SH1) were tested under repeated stresses consisting of cycles of 8 hours loading followed by 16 hours of full unloading. One of them (SH1\_1) was subjected to a ratio  $R_L$  of 45% of  $f_c$ , while the other (SH1\_2) was subjected to 30% of  $f_c$ . Another two specimens (Series SH2) exhibit a partial unloading. The level of unloading was chosen to the half of the corresponding loading level. The pattern of cycling and the loading stress level remained the same. The last specimen (SH0) was used as a companion specimen to observe the load-free strains of concrete.

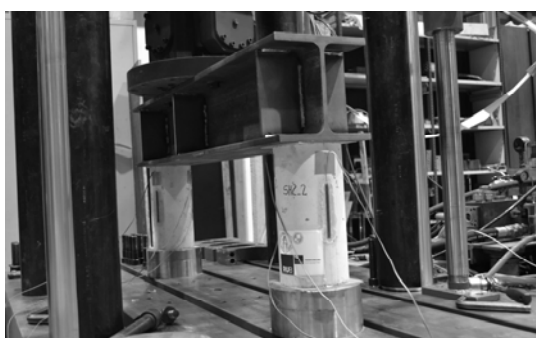


Figure 2. Setup for Series SH2.

For SH2, a special test setup (Fig.2) was developed to allow for a simultaneous testing of two specimens with different stress to strength ratios. Introducing a single span steel girder and adjusting the lever arms to the stress ratio, the required stress level in both specimens was achieved.

#### 3.2 TEST SERIES 2

Series 2 involved eight creep and shrinkage specimens. Two of them belong to series A (A1-sealed; A2-unsealed) and were simultaneously subjected to identical repeated stress pattern (Fig.3). The stress pattern consisted of cycles of 12h of loading ( $R_L=0.40$ ) followed by 12h of full ( $R_U=0$ ) and partial ( $R_U=0.20$ ) unloading. Two other specimens (B1-sealed; B2-unsealed) with identical drying conditions as those in series A, were exposed to sustained stress with a ratio  $R_L$  of 0.40.

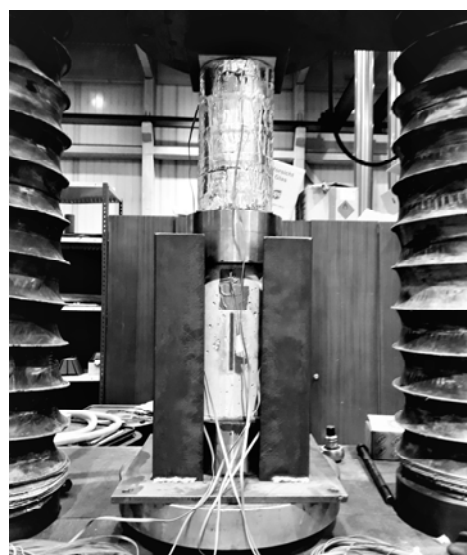


Figure 3. Setup for Series A.

Series C and D consist of unstressed sealed and unsealed specimens, respectively. They were used to establish the autogenous and drying shrinkage strains under identical atmospheric conditions.

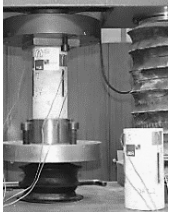
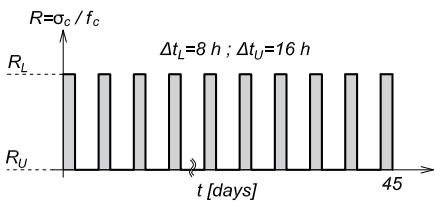

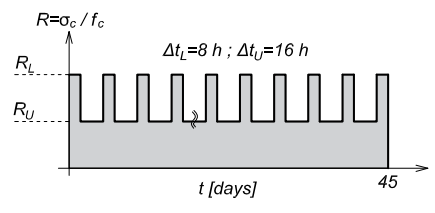

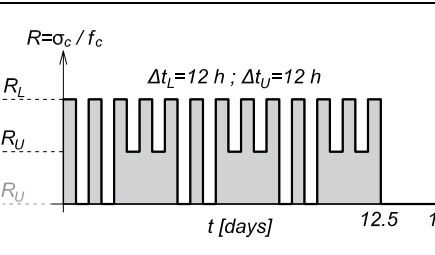
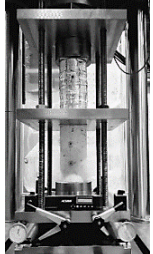
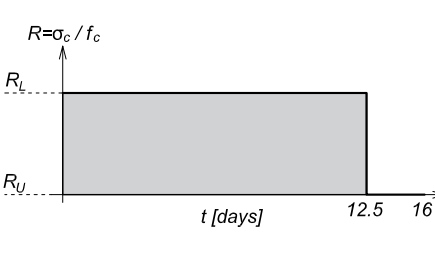
## 4. RESULTS AND DISCUSSION

### 4.1 INFLUENCE OF STRESS HISTORY UNDER UNIFORM DRYING CONDITIONS

The experimental results of test series 1 are summarized in Figs. 4 and 5. They include the stress-induced strain evolution over time for the specimens SH1 and SH2 as well as the stress-free strains recorded on the companion specimen SH0.



Table 1. Overview of the experimental program.

Series 1						
Setup	Specimen		DC	Variables		aim
				$R=\sigma_c/f_c$	Stress history	
/1/	/2/		/3/	/4/	/5/	/6/
	SH1	SH1_1	U	$R_L=0.45$ $R_U=0$		$\epsilon_{cr.f}$ $\epsilon_{asds}$
		SH1_2		$R_L=0.30$ $R_U=0$		
	SH2	SH2_1		$R_L=0.45$ $R_U=0.22$		$\epsilon_{cr.f}$ $\epsilon_{asds}$
		SH2_2		$R_L=0.30$ $R_U=0.15$		
/	SH0			/	/	$\epsilon_{asds}$
Series 2						
Setup	Specimen		DC	Variables		aim
				$R=\sigma_c/f_c$	Stress history	
	A	A1	S	$R_L=0.40$ $R_U=0$ $R_U=0.20$		$\epsilon_{cr.fb}$ $\epsilon_{as}$
		A2				U
	B	B1	S	$R_L=0.40$ $R_U=0$		$\epsilon_{cr.fb}$ $\epsilon_{as}$
		B2				U
/	C	C1/C2	S	/	/	$\epsilon_{as}$
	D	D1/D2	U	/		$\epsilon_{asds}$
DC - Drying Condition; S - Sealed; U - Unsealed; $R_L$ -stress/strength ratio at loading; $R_U$ -stress/strength ratio at unloading; $\Delta t_L$ -duration of loading sequence; $\Delta t_U$ -duration of unloading sequence						

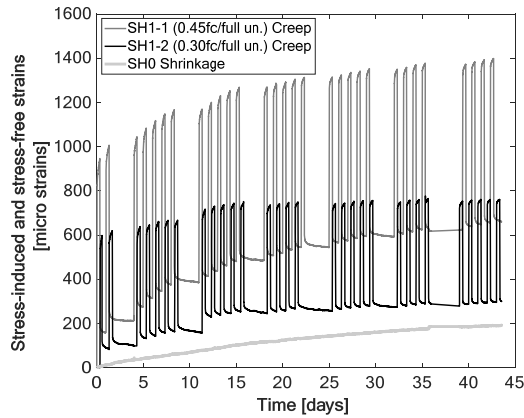


Figure 4. Stress-induced and stress-free strain evolutions vs. time for the specimens SH1 and SH0.

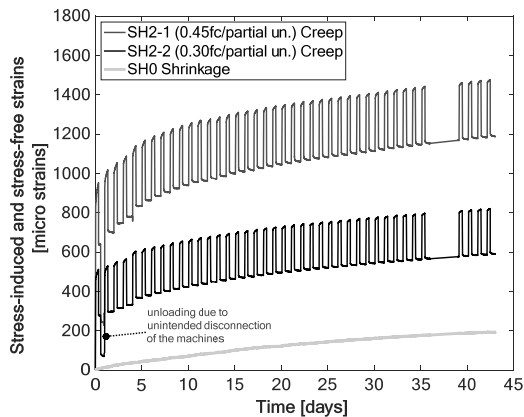


Figure 5. Stress-induced and stress-free strain evolutions vs. time for the specimens SH2 and SH0.

The creep (black dots) and the recovery increments (grey dots) in each loading/unloading cycle of SH1\_1 and SH1\_2 are plotted in Figs. 6 and 7, respectively. For both stress levels, the results demonstrate a reduction in the creep response in each subsequent loading cycle. The reduction is especially pronounced within the first cycles and gradually stabilizes in the later ones.

It is remarkable to note that the reduction of the recovery within the loading cycles is not as pronounced as in the case of creep, especially for the first few cycles (Figs.6 and 7).

The insets in the Figs. 6 and 7 present the creep-recovery/creep ratio in each loading/unloading cycle over the considered time. Regardless of the stress level, this ratio increases over time with a tendency to approach unity. It means that after a sufficient number of loading/unloading cycles, the whole creep share in the loading cycle will be fully recovered in the following unloading one.

The creep-recovery/creep ratio for the specimens subjected to partial unloading is plotted over time in Fig.8. It should be

emphasized that it does not present a ratio between the total creep recovery and the creep, as it was the case with the specimens exhibiting complete unloading (SH1). Here, a pronounced residual stress persists.

At the end of the test, it reaches a maximum value of 0.80 regardless of the stress level.

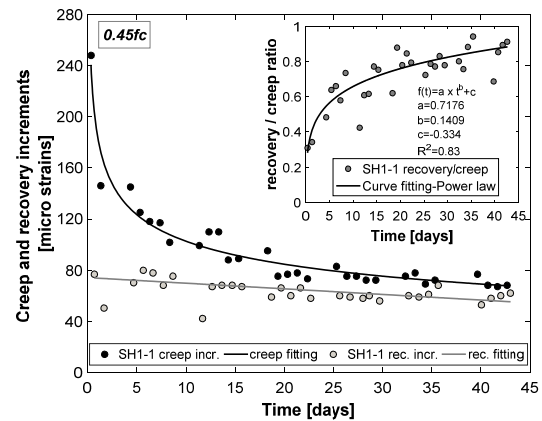


Figure 6. Creep increments (black dots) and recovery increments (grey dots) for SH1\_1 (0.45fc).

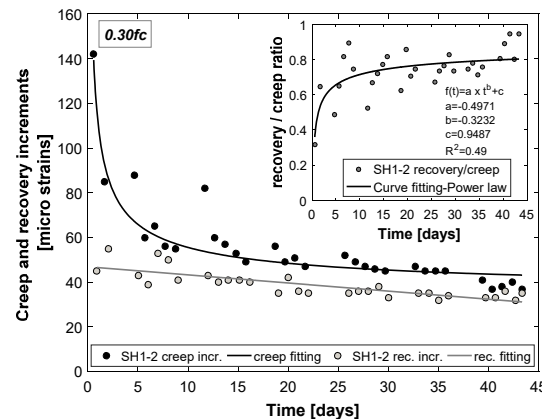


Figure 7. Creep increments (black dots) and recovery increments (grey dots) for SH1\_2 (0.30fc).

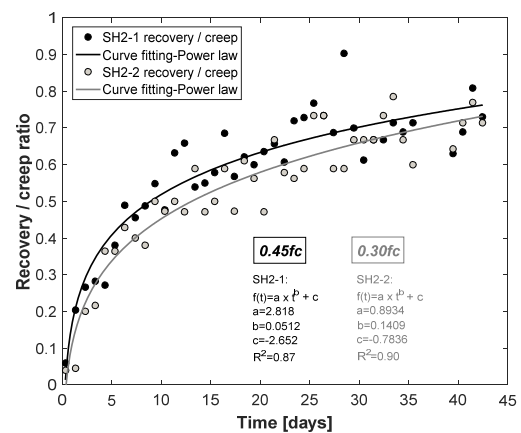


Figure 8. Creep-recovery/creep ratio for SH2\_1 (0.45fc) and SH2\_2 (0.30fc).

## 4.2 INFLUENCE OF STRESS HISTORY UNDER DIFFERENT DRYING CONDITIONS

The stress-induced (specimens A and B) and the stress-free strain evolutions (specimens C and D) over time are summarized in Fig.9.

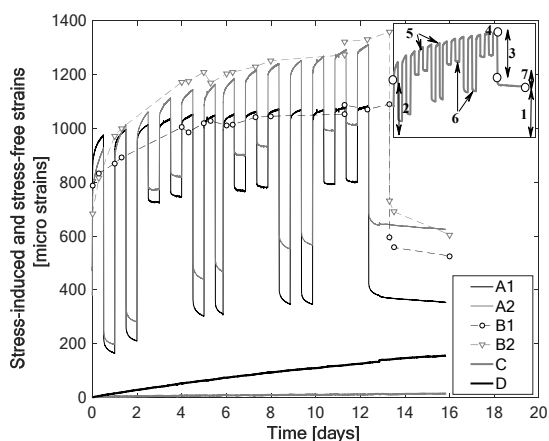


Figure 9. Stress-induced and stress-free strain evolutions vs. time for the specimens A, B, C and D.

For all specimens involved in the tests, comparisons between different strain components are tabularly arranged in Table 2.

Table 2. Comparison of the stress-induced strain components [ $\mu\epsilon$ ] of series A and B.

Strain component	A		B	
	A1	A2	B1	B2
1. Final strain	353	625	526	605
2. Instantaneous strain	786	683	786	683
3. Instantaneous recovery	634	602	494	630
4. Total stress-induced strain	1084	1312	1090	1360
5. Sum of creep increments $\Delta\epsilon_{rec}$	792	1219	304	676
6. Sum of rec. increments $\Delta\epsilon_{cr}$	666	716	/	/
7. Final recovery	97	85	70	125
$\sum\Delta\epsilon_{rec} / \sum\Delta\epsilon_{cr}$	0.84	0.59	0.23	0.19

Larger final residual strains (1) recorded at the end of the tests were observed for the specimens allowed to dry during the loading (A2 and B2). The reason is evident. In unsealed specimens, the basic creep component is accompanied by additional drying creep which - according to results in the literature [5] - participates with more than 50% in the total recorded creep.

Under repeated stresses, the influence of the drying conditions on the creep behavior is evidently large, while in the case of recovery it is less pronounced. The sum of all creep increments within the repeated stress history is 35% bigger for the unsealed (A2) than for the sealed (A1) specimen. On the other hand, both specimens show similar amounts of recoverable creep (difference of 7%).

The creep-recovery/creep ratio shows that concrete exhibits higher reversibility in sealed conditions regardless of the type of stress history.

## 5. CONCLUSIONS

Based on the results from the conducted experiments, the authors arrived at the following conclusions:

- Under repeating loading followed by full unloading, the creep response in the loading cycle continuously reduces. Unlike the creep, the recovery reduces in a less pronounced way.
- After a sufficient number of loading/unloading cycles, the creep becomes fully recoverable regardless of the stress level.
- The creep recovery seems unaffected by the hygral exchange conditions of the specimens. On the other hand, the influence of the drying conditions on the irreversible proportion of the creep in each cycle is of remarkable extent.

## REFERENCES

- [1] Arangjelovski, T. (2010), "Time-dependent behavior of reinforced high-strength concrete elements under action of variable loads", Doctoral dissertation, FCE Skopje.
- [2] Gilbert, R. I., Ranzi, G. (2010), "Time-dependent behaviour of concrete structures" CRC Press, London.
- [3] Markovski, G. (2003), "Influence of variable loads on time-dependent behavior of prestressed concrete elements", Doctoral dissertation, FCE Skopje.
- [4] Nakov, D. (2014), "Time-dependent behaviour of SFRC elements under sustained and repeated variable loads", Doctoral dissertation, FCE Skopje.
- [5] Rusch, H., Jungwirth, D., Hilsdorf, H.K. (1983), "Creep and shrinkage-Their effect on the behavior of concrete structures" Springer, New York.

**SEEFORM Generation I**



Toni  
Arangjelovski



Borko  
Bulajic



Kemal  
Edip



Igor  
Gjorgiev



Florim  
Grajevci



Josif  
Josifovski



Marija  
Nefovska-Danilovic



Merima  
Sahinagic-Isovic



Anina  
Sarkic



Azra  
Spago



Marina  
Trajkovic



Vladimir  
Vitanov



## MODEL CALIBRATION OF WELDED SHS-TO-SHS T-JOINTS UNDER MOMENT LOADING

### AUTHORS

#### **Mile Partikov**

MSc, Assistant

Ss. Cyril and Methodius University  
Faculty of Civil Engineering – Skopje  
partikov@gf.ukim.edu.mk

#### **Petar Cvetanovski**

PhD, Full Professor

University “Ss. Cyril and Methodius”  
Faculty of Civil Engineering – Skopje  
cvetanovski@gf.ukim.edu.mk

The behaviour of the semi-rigid joints can be obtained by laboratory tests or by an appropriate finite element analysis. This paper describes the process of modelling joints in the SOFISTIK software package and their calibration method.

The verification of the results obtained from the 3D models is performed with values obtained from laboratory tests. In the framework of the modelling and calibration process of the models, all parameters that influence the accuracy of the results are being reviewed.

Analyses performed with well-calibrated mathematical models including finite elements based on experimental research within certain parameters allow a large number of parametric analyses to be faster and more economical if performed exclusively by laboratory tests.

**Keywords:** joint, hollow section, rotational stiffness.

### 1. TESTING OF T JOINTS

A total of twelve joints (shown in Table 1), were examined for the purposes of the experimental research. The joints were divided into three series depending on the  $2\gamma$  parameter, such as: J3, J4 and J5.

The parameter  $2\gamma$  was selected according to Eurocode 3, Part 1-8 and CIDECT Design Guide 3's recommendations for this type of joints, where the lower limit of this parameter was set to 20 in order to enable the joint to fall into the group of semi-rigid joints ( $2\gamma > 16$ ). Furthermore, the maximum allowable value for hollow section joints was selected as the upper limit, which is 33.3 for S235.

Each of the aforementioned series consists of four samples that vary the parameter  $0.4 \leq \beta \leq 0.7$ .

The thickness ratio parameter  $\tau$  of the chord and brace walls is not varied and remains constant throughout the research paper.

The  $\alpha$  parameter also remains constant for all examined samples and is 20.

Table 1. Tested Joints

Joint	$\alpha$	$\beta$	$2\gamma$	$\tau$
J3_40	20	0.4	33.3	1
J3_50	20	0.5	33.3	1
J3_60	20	0.6	33.3	1
J3_70	20	0.7	33.3	1
J4_40	20	0.4	25	1
J4_50	20	0.5	25	1
J4_60	20	0.6	25	1
J4_70	20	0.7	25	1
J5_40	20	0.4	20	0.8
J5_50	20	0.5	20	1
J5_60	20	0.6	20	1
J5_70	20	0.7	20	0.8

SHS 100x100 hollow sections with a length of 1000mm are being used for the chords, while SHS40x40 to SHS70x70 sections with a length of 400mm are being used for the brace.

Figure 1 shows the joint testing method and the positioning of the testing equipment.



Figure 1. Test layout

## 2. MODELLING OF T JOINTS

Three-dimensional solid elements (BRIC) (Figure 2) defined by the use of eight points in space and a 1:1 ratio of the sides, were used for modelling the geometry of the joint. Each of the points defining the geometry of the finite element has six degrees of freedom (DoF). This type of finite element was selected according to the recommendations by current studies on all

types of hollow section joints which indicate that it gives more accurate results than a four-node quadrilateral finite element (QUAD).

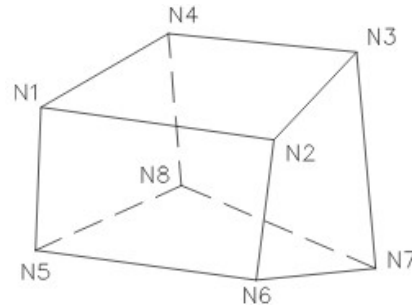


Figure 2. Three-dimensional Solid Element (BRIC)

### 2.1 MATERIAL MODELLING

What is typical for the hollow sections, within the unreinforced semi-rigid “T” joints, is that they quickly reach the yielding strength before reaching the design resistance given in Eurocode 3, Part 1-8 (Table 7.14).

The modelling method of the material and its nonlinear behaviour are given in Eurocode 3 Part 1-5 Annex C.

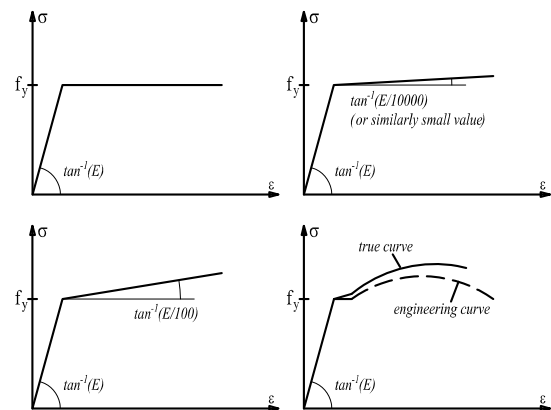


Figure 3. Material model

Material quality tests have been carried out for the purposes of the research paper, thus, the engineering stress-strain curve and the true curve is shown in Figure 4.

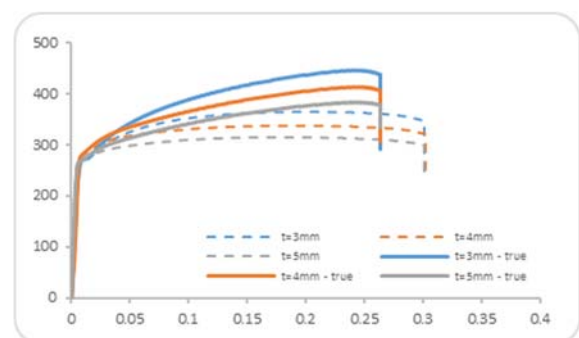


Figure 4. Stress-Strain curves for tested materials

The correction of the stresses and strains of the engineering curve is being performed with the following equations:

$$\varepsilon_T = \int_1^{1+\Delta l} \frac{dx}{x} = \ln \frac{1+\Delta l}{1} = \ln(1 + \varepsilon_E) \quad (1)$$

$$\sigma_T = \frac{A}{A_U} \sigma_E = \frac{A}{\frac{A}{1 + \varepsilon_E}} \sigma_E = \sigma_E (1 + \varepsilon_E) \quad (2)$$

Where,

- $l$  is original gage length
- $A$  is original cross-section area
- $A_u$  is true cross section area
- $\varepsilon_E$  is engineering strain
- $\varepsilon_T$  is true strain
- $\sigma_E$  is engineering stress
- $\sigma_T$  is true stress

Due to the process of cold-forming, the yielding strength in the bending zones of the material has been increased. This additional material correction is made in accordance with the Eurocode 3 formula, as given below:

$$f_{ya} = f_y + k * n * \frac{t^2}{A} * (f_u - f_y) \quad (3)$$

Where,

- $f_y$  is yielding strength of the material
- $f_u$  is ultimate strength of the material
- $t$  is the material thickness
- $A$  is cross-section area
- $k$  is coefficient depending on type of forming ( $k=7$  for cold rolling)
- $n$  is the number of  $90^\circ$  bends in the section with internal radius  $<5t$
- $f_{ya}$  should not exceed  $f_u$  or  $1.2f_y$

In order to examine the material model influence for each of the joint series, a selection of one joint is made, which is solved with each of the four proposed models (Figures 5, 6 and 7).

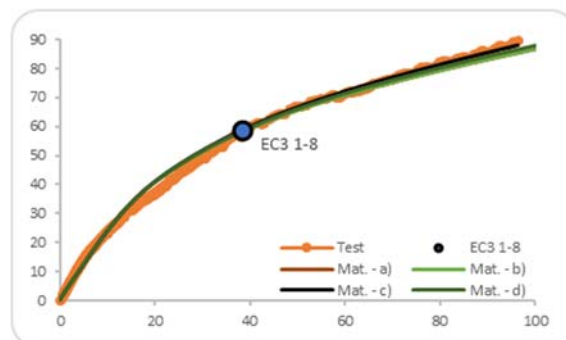


Figure 5. Influence of material model for „J3“

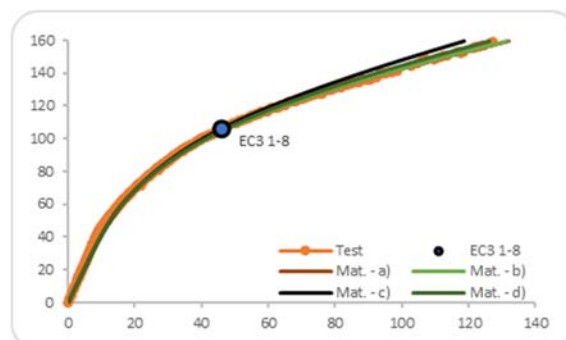


Figure 6. Influence of material model for „J4“

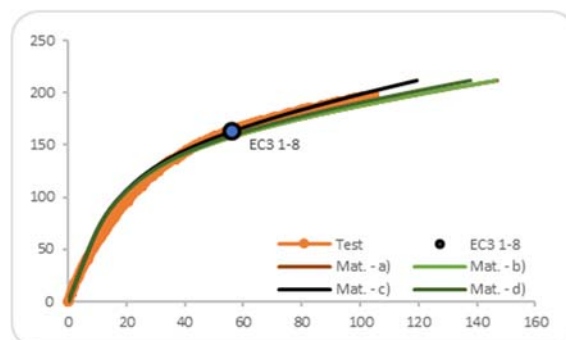


Figure 7. Influence of material model for „J5“

The diagrams show that all material models are very compliant with the tested values. However, material model with linear strain-hardening will be used for the further analysis, since it contributes to better convergence of solutions i.e., the residual forces from the analysis are quite small and within the limits of the required accuracy of the analysis.

## 2.2 FE MESH SIZE

The analytical study requires a test to find a balance between the finite element mesh density, the results obtained and the time required to complete the analysis. On one hand, too low density “rough” mesh may lead to unreliable results, but on the other, too high density “fine” mesh may increase the required time for analysis.

According to research recommendations so far, the dimensions of the finite elements for smaller cross-sections are 3x3mm, and for larger cross-sections up to 10x10mm. The discretization of the section thicknesses generally depends on the value of the  $2\gamma$  parameter, for example, for “thick-walled” sections with  $2\gamma \leq 20$ , up to four divisions of thickness, and for “thin-walled” sections with  $20 < 2\gamma \leq 33$ , up to two divisions of thickness. Based on these recommendations, an analysis of all  $2\gamma$  parameter values covered by the laboratory tests was performed, with the models varying the size of the finite elements and the number of wall thickness divisions.

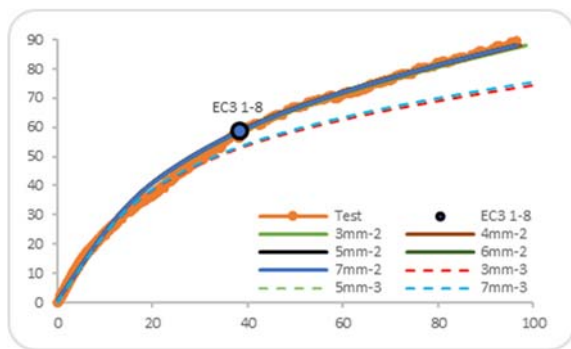


Figure 5. Influence of material model for „J3“

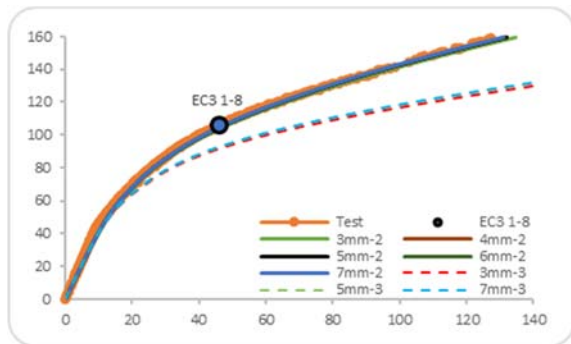


Figure 6. Influence of material model for „J4“

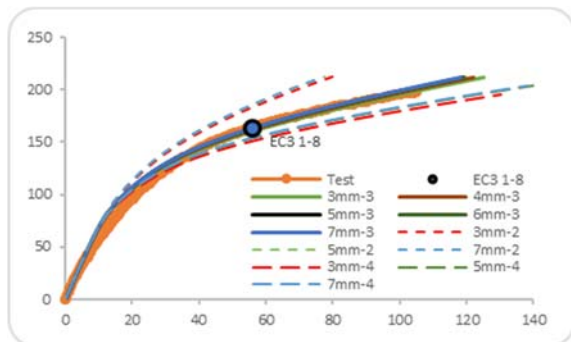


Figure 7. Influence of material model for „J5“

A total of three joints with five different dimensions of the finite elements were considered, i.e. finite elements with 3, 4, 5, 6

and 7mm. In terms of wall thickness, the “J3” and “J4” joint series have been treated with two or three divisions and the “J5” joint series with two, three and four wall thickness divisions.

It can be clearly seen from the diagrams that the models for “J3” and “J4” joint series give excellent results for two wall thickness divisions, while in the “J5” joint series this is repeated with three wall thickness divisions. These values for wall thickness divisions are adopted for further analysis.

As presented in Figure 8, the decreasing trend of the time required for analysis observed in terms of finite element size occurs for values of 3mm to 5mm, thus, it can be noted that further increase in dimensions do not have much effect on time.

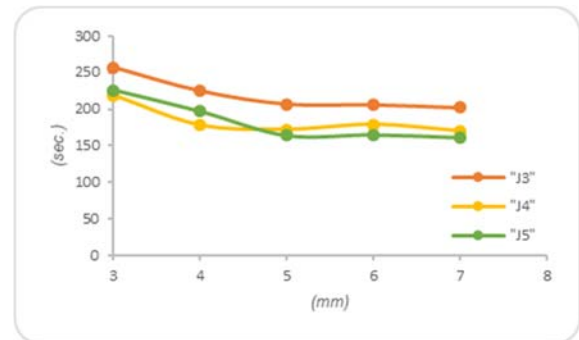


Figure 8. Influence of material model for „J5“

Considering the results of the convergence of the mathematical model, the following finite element values have been adopted:

- Top and bottom part of chord – 10mm
- Contact wall/side of chord – 5mm
- Remaining chord walls – 8mm
- Brace – 5mm
- Sections radiuses – 6 segments
- Weld – 2 segments

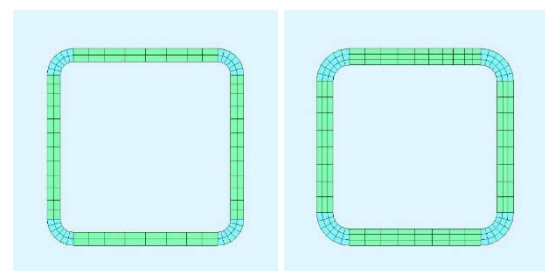


Figure 9. Cross sections



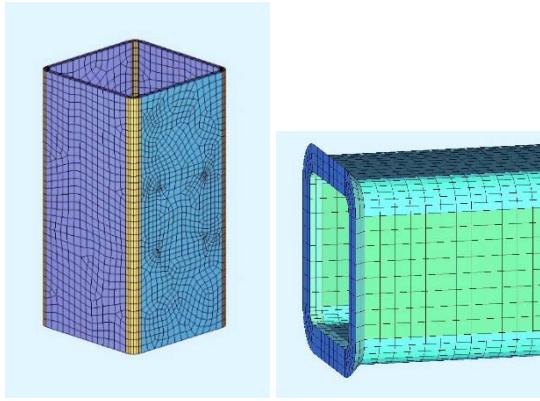


Figure 10. FE Mesh for chord and brace members

## 2.4 WELD MODELLING

The joints between the bracing and the chord are constructed with arc welding in protective atmosphere of CO<sub>2</sub> gas. In accordance with the CIDECT recommendations, fillet weld details have been used for all joints as shown in Figure 11.

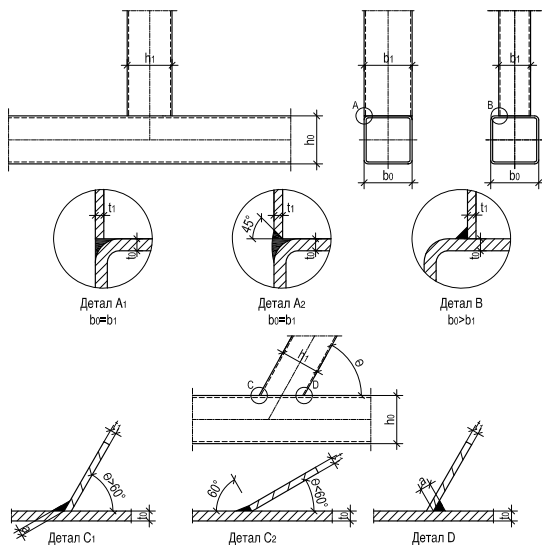


Figure 11. Weld details

Welds for three-dimensional solid elements (BRIC) models can be modelled in three ways as shown in Figure 12.

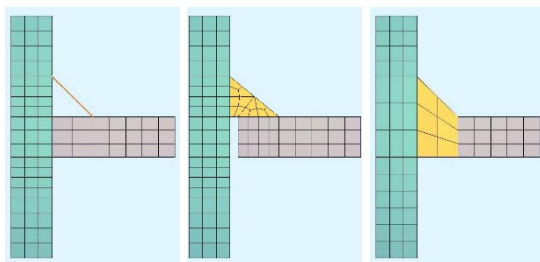


Figure 12. Weld models

The first model represents a “hybrid” model proposed by van der Vegte. He suggests the weld to be fastened to the chord using a rigid connection and the weld to be modelled with shell elements to form a ring throughout the section.

In the second model, the weld has been modelled by using three-dimensional solid elements (BRIC) in full scale thus, the brace has no contact with the chord. According to the recommendations, the distance must not exceed 2mm.

The third model used to model the welds for this research paper, suggests that the weld must be modelled by using three-dimensional solid elements (BRIC) with a full rigid connection between the weld and the chord. This model was selected as a result of the type of welding performed on the tested models (welding with full penetration). For modelling the material properties of the weld, the same properties were used as those of the braces.

Figures 13, 14 and 15 show the results for three joints with different values of the  $2\gamma$  parameter showing the weld influence on the moment-rotation.

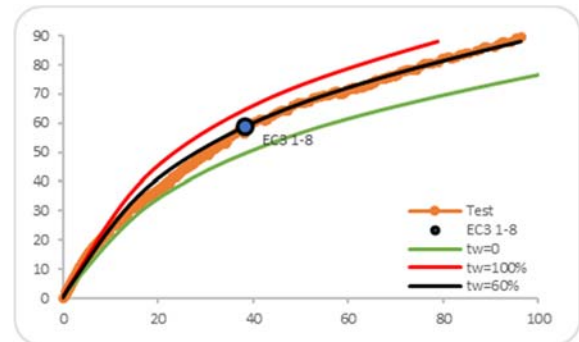


Figure 13. Influence of weld size for „J3“

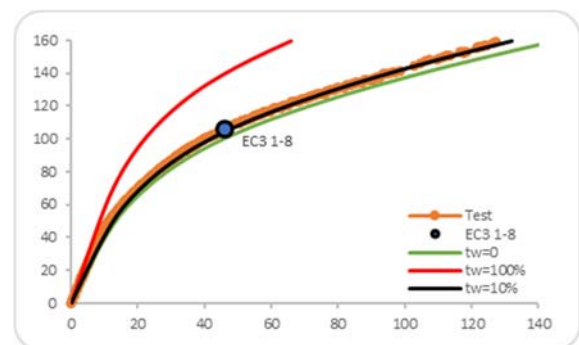


Figure 14. Influence of weld size for „J4“

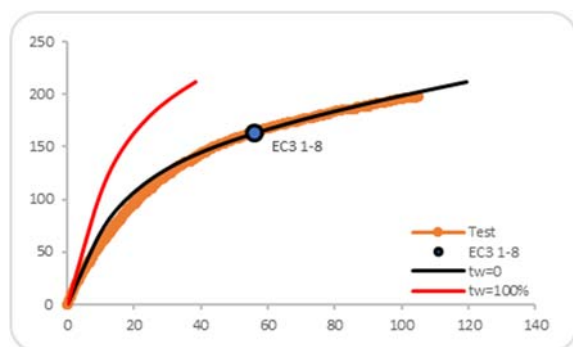


Figure 15. Influence of weld size for „J5“

## 2.5 ANALYSIS

The SOFISTIK software package for solving these models by using three-dimensional solid elements (BRIC) offers two analysis types such as: first order elastic-plastic analysis which includes only the effects of the nonlinear material behaviour and second or third order elastic-plastic analysis. For this case with three-dimensional solid elements (BRIC), a third order analysis (TH3) has been used, which takes into account geometrical nonlinearity in addition to material nonlinearity.

Both analysis express relatively good results overlapping until reaching the design resistance. The differences are larger for lower values of  $2\gamma$ , so for the value of the bending moment equal to the design resistance according to Eurocode 3 it can be noted that for the joint with  $2\gamma = 33.3$  the third order analysis gives a 7.7% lower rotation, however, for the joint with  $2\gamma = 25$ , that difference is 9.8% and for the joint with  $2\gamma = 20$  the difference is 13.4%.

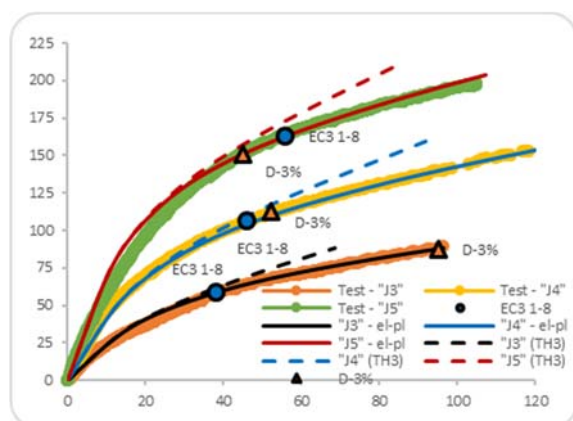


Figure 15. Influence of analysis type

## 3. CONCLUSION

The solutions of the mathematical models for the tested joints by including all previously described variables that influence their behaviour give results that are largely consistent with the results obtained from laboratory tests. The models developed and calibrated with the methods and analysis types presented in this paper, illustrate the behavior of hollow sections “T” joints and can be used in further parametric studies within the ranges of the parameters considered,  $0.4 \leq \beta \leq 0.7$ ,  $20 \leq 2\gamma \leq 33$  and  $0.8 \leq \tau \leq 1.0$ .

## REFERENCES

- [1] EN 1991-1-1: Eurocode 3: Design of steel structures – Part 1-1: General rules and rules for buildings, CEN 2005.
- [2] EN 1991-1-5: Eurocode 3: Design of steel structures – Part 1-5: Plated structural elements, CEN 2005.
- [3] EN 1991-1-8: Eurocode 3: Design of steel structures – Part 1-8: Design of joints, CEN 2005.
- [4] J.A. Packer, J. Wardinier, X.-L. Zhao, G.J. van der Vegte and Y. Kurobane, Design Guide 3 for rectangular hollow section (RHS) joints under predominantly static loading, CIDECT 2008
- [5] Y. Kurobane, J.A. Packer, J. Wardinier, N. Yeomans, Design Guide 9 for structural hollow section column connections, CIDECT 2004

AUTHOR

**Ana Grupcheva**

Civil Engineer

St." Dimitar Vlahov" no.47, 6000 Ohrid

anagrupceva@gmail.com

**Goce Taseski**

Assistant Professor

Ss. Cyril and Methodius University

Faculty of Civil Engineering – Skopje

taseski@gf.ukim.edu.mk

## HYDRAULIC MODEL OF STORMWATER DRAINAGE SYSTEM USING DIFFERENT METHODS FOR DEFINING THE CATCHMENT AREA

The stormwater drainage system is an infrastructure facility that accumulates the rainwater, protecting the urban areas from flooding. An important parameter for stormwater drainage systems in urban areas is the size, shape and type of the catchment area. According to current practice the catchment area can be determined by several methods: classical methods where the catchment area can be defined using a roof symmetry by links or by distributing it in equal parts at all nodal points of the hydraulic model and modern methods in which the definition of the catchment area is made by taking into account additional parameters such as the slope of the terrain, the position of node points, the distance of the connection points to the future sewage, the size of the catchment area, etc.

Subject of this hydraulic analysis is to apply the classical and modern methods for defining the catchment area in order to show the advantages and disadvantages of the methods with a further comparison and recommendations for designing the stormwater drainage system.

**Keywords:** hydraulic analysis, stormwater drainage systems, catchment areas.

### 1. INTRODUCTION

The amount of water flow that appears in the stormwater drainage system is highly variable throughout the year. During dry periods it is equal to zero, while during heavy rains its value can be quite high. The maximum flow which occurs as surface runoff, depends on: hydrometeorological conditions, urban surface relief, slope, type and size of the catchment area, hydrogeological composition of the soil, groundwater etc. The stormwater drainage system collects the water flows from the natural water processes such as: rainfalls, melting snow, ground water, etc [1].

According to previously stated, the water flow in the stormwater drainage system depends on various parameters, giving a lead role to the

size and type of the catchment area due to creating a hydraulic model and its analysis.

## 2. RATIONAL METHOD

A hydrograph is a graph showing the rate of flow (discharge) versus time past a specific point in a river, channel, or conduit carrying flow. The maximum, or peak, of the hydrograph is sufficient for design and analysis of the hydraulic model of the stormwater drainage system, which can be easily calculated using the Rational method [1,2,3].

The rational method is based on a simple formula that relates runoff-producing potential of the catchment area, the average intensity of rainfall for particular length of time (time of concentration) and the catchment area. This method is applied when the size of the catchment area is less than 13 km<sup>2</sup>. The equation is:

$$Q = C \cdot i \cdot A \quad (1)$$

The runoff coefficient  $C$ , is a dimensionless ratio intended to indicate the amount of runoff generated by the catchment area, given an average intensity of precipitation for a storm. The value of this coefficient varies between 0.05-0.95, depending on the type of the catchment area.

Storm intensity  $i$ , is a function of geographic location and design exceedence frequency (or return interval). The relation between the three components- storm duration, storm intensity, and storm return interval, is presented by a family of curves called the intensity-duration-frequency curves, or IDF curves. They can be determined by analysis of storms for a particular site [4].

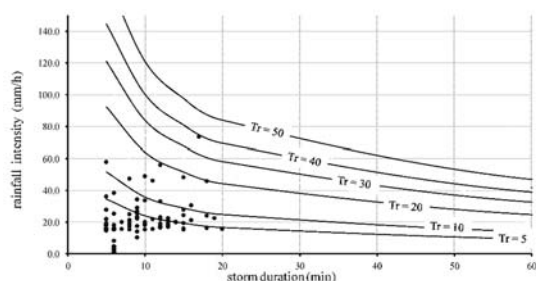


Figure 1. Example for IDF-curves

Time of concentration of a catchment area is often defined to be the time required a parcel of runoff to travel from the most hydraulically distant part of a watershed to the outlet. This

parameter also depends of the size and type of the catchment area.

## 3. CATCHMENT AREA

Catchment areas are hydrologic units of land whose topography and drainage system elements direct surface runoff to a single discharge point. They are divided into pervious and impervious subareas. Surface runoff can infiltrate into the upper soil zone of the pervious subarea, but not through the impervious subarea. Runoff flow from one subarea in a catchment area can be routed to the other subarea, or both subareas can drain to the catchment outlet. The other principal input parameters for catchment areas include: assigned rain gage (using an IDF-curve); outlet node (subarea); assigned land uses; area size; imperviousness; slope; characteristic catchment width; Manning's  $n$  for overland flow on both pervious and impervious areas, etc.

While making a hydraulic model, the size of the catchment area and its parameters can be defined using the two methods:

- classical method - where the catchment area can be defined using a roof symmetry by links or by distributing it in equal parts at all nodal points of the hydraulic model
- modern methods - where the definition of the catchment area is made by taking into account additional parameters such as the slope of the terrain, the position of node points, the distance of the connection points to the future sewage, the size of the catchment area, etc.

## 4. CLASSICAL METHOD

To define the catchment area using the classical method mean that the boundary conditions will be determined by the method of roof symmetry by links or by distributing it in equal parts at all nodal points of points of the hydraulic model, also named as a method of Thiessen polygon [4].

In the areas of hydraulics and hydrology, the measurement of rainfall is one of the most important elements in modelling or dimensioning of storm water drainage, as well as the amount of rainfall that fell on a particular surface.

The Thiessen polygon method is created by American scientist Alfred H. Thiessen (1872-1956). For distribution of the water (fecal, storm water, etc.), Thiessen's polygon in modeling is



used to quickly and clearly define the catchment areas on the nodes of a system, individually. There are two types of defining the Thiessen polygon method:

- Method for determining of Thiessen polygons with circles
- Method for determining Thiessen polygons with triangulation

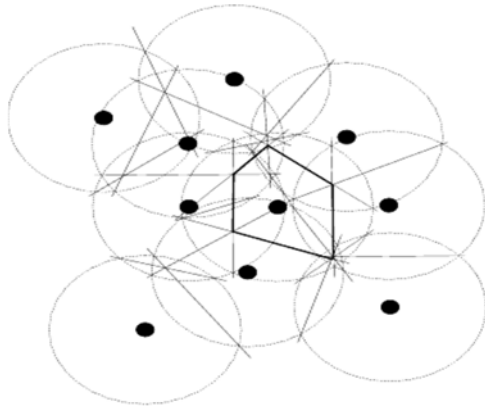


Figure 2. Method for determining of Thiessen polygons with circles

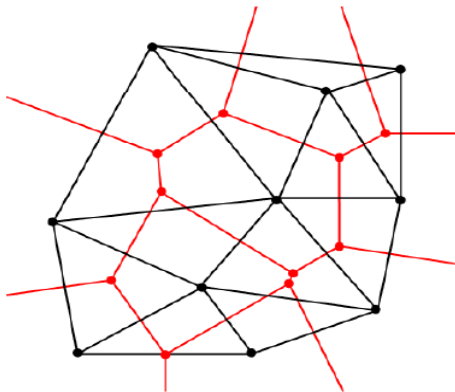


Figure 3. Method for determining Thiessen polygons with triangulation

In Figure 2. and Figure 3. are given the graphical presentation of the two methods of the Thiessen polygon, where the boundaries and size of the catchment area are presented.

In order to obtain greater accuracy in the determination of catchment areas, a so-called method is used that is named "Roof symmetry method". This method makes a two-dimensional distribution of rain amounts depending on the length of the links and the location of the nodes in the system. Graphically this method is executed as presented on Figure 4.

Combining the Thiessen polygon method and the Roof symmetry method, the Classical method of defining the catchment area size and boundaries is defined.

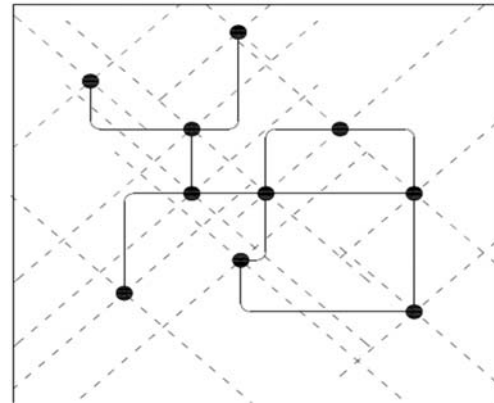


Figure 4. Roof symmetry method

## 5. MODERN METHOD

Defining the catchment areas using the Modern Method generates the topography of the terrain, with a main note on its: slope, groundwater, its use, elevation, geometric change, embankments, etc.

Once the boundary of the urban area has been defined, it is necessary to define the catchment areas separately. 2D modeling of stormwater drainage systems begins with 2D modeling of catchment areas. The amount of rainfall that the systems generates in 2D modeling by modern methods depends largely on the size of the catchment areas. Each of the created 2D catchments must belong to the already defined boundary of the urban surface. 2D catchments serve to control surface runoff and direct that flow to the final drainage point - realistic as the field or to the next closest drainage point. (Figure 5.)

### 5.1 BREAK LINES

The boundary elements defining these surfaces are called "break lines" (or break points). They are plotted in places where the 3D model of the terrain has significant topographies and geographical variations or in places where there are significant elements. Also, they can be placed as bisector lines on the links that connect the nodes. They are placed at each location where there is a break (barrier) to the free flow.

Connecting the break lines, within them self they create a polygon in the already defined

urban boundary area, which represent the 2D catchment areas.

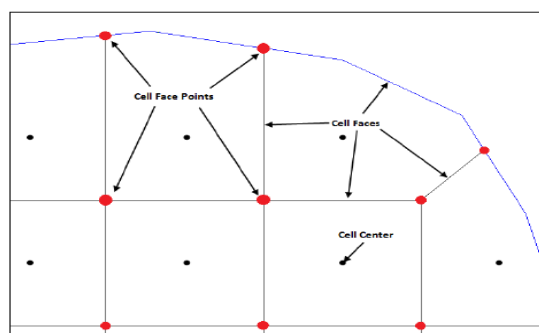


Figure 5. 2D catchment areas and their properties

## 5.2 CHARACTERISTIC CATCHMENT WIDTH

An initial estimate of the characteristic width is given by the catchment area divided by the average maximum overland flow length. The maximum overland flow length is the length of the flow path from the outlet to the furthest drainage point of the subcatchment. Maximum lengths from several different possible flow paths should be averaged. These paths should reflect slow flow, such as over pervious surfaces. Adjustments should be made to the width parameter to produce good fits to measured runoff hydrographs.

## 6. HYDRAULIC MODEL

In the modelling of stormwater drainage systems, defining the catchments is considered as a key element for the output data. Due to the hydraulic analysis, the main parameters of the elements are predefined, so the accuracy and operation of the system is ascertained by defining the catchment areas. Depending on the boundaries of the urban surface from where the runoff is drawn, the dimensions of the catchment areas play big role on the peak flow from where the system is designed. The rainfall is governed by the intensity of the rain (IDF-curves), with a note that a bigger catchment area generates greater amount of flow (rainfall concentration), and vice versa smaller catchment area- less amount of flow.

For the purpose of the hydraulic analysis, a hydraulic model has been developed that will simulate the runoff conditions of the stormwater drainage system, using the SWMM (Storm Water Management Model) software package. While developing the model, first the parameters of the main elements are

examined, such as: manholes and catch basins; channels; links (pipes); outfalls; main collector; urban surface border and catchment areas.

Furthermore, for the developing of the hydraulic model analysis, a certain calibration needs to be done for the input: terrain and elevation points, maximum flow, flow velocity, links diameters, IDF-curves, concentration time and catchment areas. By varying this input data, the hydraulic model is generated, where the peak flow of the hydrogram is used as a corrective output parameter to validate the model.

Using the SWMM software package, the creation of different scenarios for a case study for the variable parameters was simplified. The return period from the inserted IDF-curves was chosen for 2 years to be in accordance with the designing law for stormwater drainage systems. The study of this hydraulic model is validated with a real situation for the two already created methods of defining catchment areas – the classical and the modern method. The analysis works on the principle of the “Rational Method”, with already defined runoff coefficient  $C=0.450$ , the impervious percent of the surface is 25%, the impervious coefficient is 0.011, and the pervious is 0.03 (Manning's). Infiltration was calculated experimentally by Horton's method.

The purpose of this hydraulic model is to prove the accuracy and functionality of a stormwater drainage system in hydraulic analysis, by defining the catchment area sizes at different calculated characteristic catchment widths including two different analysis for the both methods (classical and modern).

## 7. RESULTS

To make a comparison between the accuracy of the two analysis of the hydraulic model, one can see the difference in the flow rate of the links, depending on the amount of water they receive from the catchment areas. This is further illustrated by means of hydrograms that are examining the dependence between the  $Q$  flow and the  $T$  time. The flow  $Q$  is expressed in [l/s], and the time  $T$  is expressed in [min].

The following hydrograms provide a detailed overview of the maximum peak flow that occurs after a certain time: at the upstream links, at the intermediate collecting links and at the downstream links at the outlets, which occurs a separation in to three groups.

### 7.1 UPSTREAM LINKS

On Figure 6. are presented the hydrograms for the upstream link shown on Figure 7. and Figure 8., with total length of 208.8 m, which includes 6 manholes and 5 pipes. According to the classical method, one catchment area is defined for this link and six catchment areas according to the modern method. Because of the separation of the catchment areas due to using the modern method, is enabled to make an optimization of the diameter of the pipes that generate less peak flow according to its hydrograms. The maximum peak flow is  $Q=162.9$  l/s.

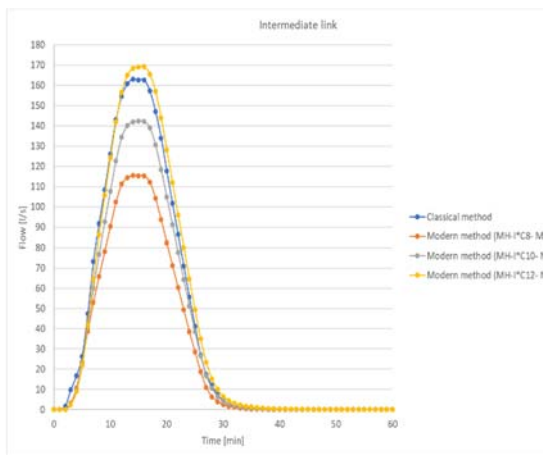


Figure 6. Hydrograms for upstream link

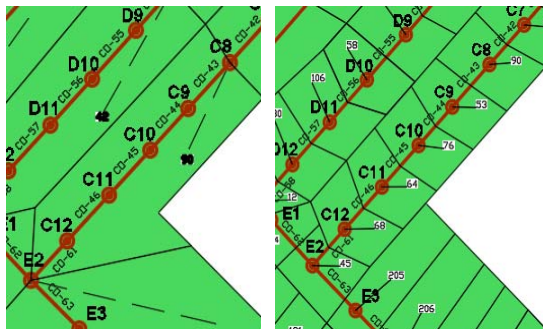


Figure 7. Classical method

Figure 8. Modern method

### 7.2 INTERMEDIATE LINKS

On Figure 9. are presented the hydrograms for intermediate link shown on Figure 10. and Figure 11., with total length of 212.45 m, including 6 manholes and 5 pipes. According to the hydrograms of the classical and modern method, their peak flows are almost equivalent. With the classical method only one catchment

area is defined and using the modern method – for each manhole there are six catchment areas. In this case scenario both, the classical and modern method of defining the catchment areas can be used for analysis and designing the stormwater drainage system. The difference between the peak flows is  $Q=52.25$  l/s.

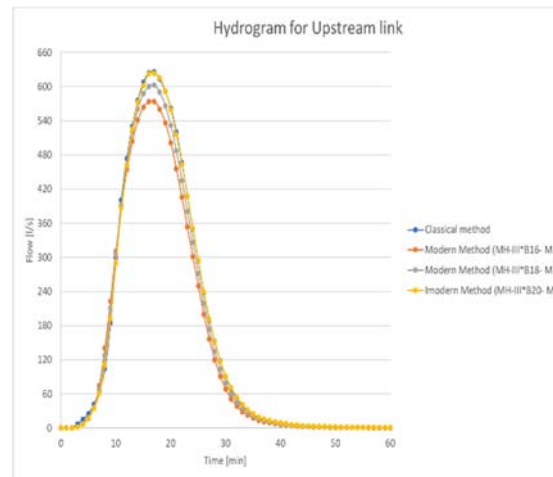


Figure 9. Hydrograms for intermediate link

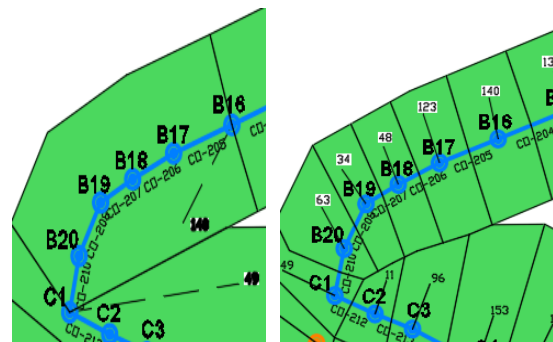


Figure 10. Classical method

Figure 11. Modern method

### 7.3 DOWNSTREAM LINKS

On Figure 12. are presented the hydrograms for the downstream link shown on Figure 13. and Figure 14., with total length of 172.8m, including 1 manhole, 1 outfall and a pipe between them. Using the classical and modern method it can be concluded that using the classical method there is a bigger peak flow because of the larger catchment area defined. According to the hydrogram from the modern method, the peak flow is less than the other, due to smaller catchment area size, with difference of  $Q=57.81$  l/s. In this case scenario it can be concluded that both of the methods can be used for its analysis and designing, with a note

that the modern method generates a smaller peak flow.

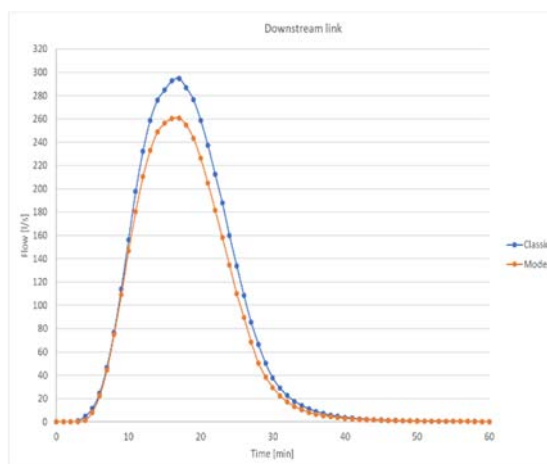


Figure 12. Hydrograms for downstream link

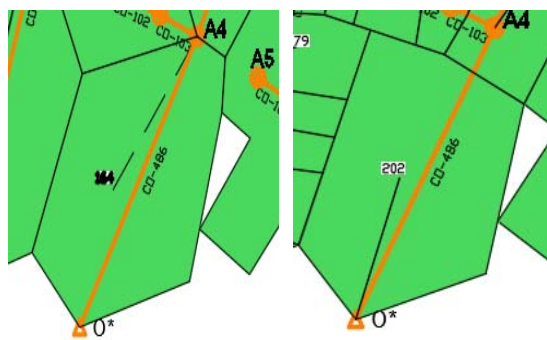


Figure 13. Classical method

Figure 14. Modern method

## 8. CONCLUSION

The different approaches to defining catchment areas at the upstream links of the system give a larger difference in the peak flows of the hydrograms. When analyzing a stormwater drainage systems, the second method of defining the catchment areas - the modern method (distribution of rainfalls on catchment areas depending on the topography of the terrain, with a main note on its: slope, groundwater, terrain use, elevation, geometric change of terrain, embankments, etc.) can be said to be better for upstream parts of these kind of systems because they allow optimization of the pipe diameters (due to its peak flows). With the help of diametric optimization, lower economic cost of current projects would be obtained. In the case of the intermediate and downstream parts of

stormwater drainage systems, it can be said that both the classical and modern methods are suitable for the use of catchment area definitions, as the difference in hydrograms is minimal, thus proving their validity. These recommendations would apply to urban, predominantly plain areas.

## REFERENCES

- [1] Ana Grupcheva' "Hydraulic Model of Stormwater Drainage System Using Different Methods for Defining the Catchment Area", Master thesis, Skopje, North Macedonia, 2019
- [2] Cvetanka Poposka, Violeta Gjesovska "Hydrology", Publisher Civil Engineering Faculty, University Ss. Cyril and Methodius, ISBN 978-608-4510-11-6
- [3] Thewodros K. Gebermariam Ph.D., P.E., D. WRE. "Urban Drainage Infrastructure Design Model Calibration and Output Uncertainty Minimization", 2014, New York University Polytechnic School of Engineering, Department of Civil & Urban Engineering, NY 11201, USA, 2347-3878
- [4] David B. Thompson "The Rational Method", September, 2006, Civil Engineering Department, Texas Tech University (in PDF)
- [5] National Highway Institute, "URBAN DRAINAGE DESIGN MANUAL", August, 2001, U.S. Department of Transportation, Publication No. FHWA-NHI-01-021
- [6] SewerGEMS, Bentley, V8i Edition "User's guide", October, 2017
- [7] S.T. DAYARATNE, B.J.C. PERERA "Calibration of urban stormwater drainage models using modelling", December, 2004, Urban Water Journal, Vol.1, 283-297
- [8] HEC-RAS River Analysis System "2D Modelling User's Manual", Version 5.0, February, 2016, US Army Corps of Engineers, Hydrologic Engineering Center
- [9] L. Davis Mackenzie and Susan J. Masten, "Principles of Environmental Engineering and Science", 2004, Prentice hall